Julius-Maximilians-Universität Würzburg
Fakultät für Physik und Astronomie

Nonequilibrium phase transitions and surface growth

Andre Cardoso Barato

Betreuer: Prof. Dr. Haye Hinrichsen

Dissertation zur Erlangung des
naturwissenschaftlichen
Doktorgrades
der Julius-Maximilians-Universität
Würzburg

Würzburg
2010

Eingereicht am:
bei der Fakultät für Physik und Astronomie

1. Gutachter: Prof. Dr. H. Hinrichsen
2. Gutachter: Prof. Dr. W. Kinzel
der Dissertation.

1. Prüfer: Prof. Dr. H. Hinrichsen
2. Prüfer: Prof. Dr. W. Kinzel
3. Prüfer: Prof. dr. J. Geurts
im Promotionskolloquium.

Tag des Promotionskolloquiums: 16. Juli 2010

Doktorkunde ausgehändigt am:

Erklärung an Eides Statt

Hiermit erkläre ich, Andre Cardoso Barato geboren am 20. April 1982 in São Paulo, mit meiner Unterschrift an Eides Statt, dass ich die vorliegende Arbeit selbständig sowie ohne unzulässige Hilfe Dritter angefertigt habe und außer den angegebenen keine weiteren Hilfsmittel zur direkten und indirekten Erstellung dieser Arbeit (Nonequilibrium phase transitions and surface growth) verwendet habe. Sämtliche verwendeten Quellen befinden sich in der Literaturangabe.

Andre Cardoso Barato

Acknowledgments

Deutsche Forschungsgemeinschaft (DFG) is gratefully acknowledge for financial support.
For scientific collaboration I acknowledge Dietrich Wolf, Juan A Bonachela, Carlos E Fiore, Miguel A Muñoz, Raphael Chetrite and David Mukamel.
I would like to thank Mário José de Oliveira and Haye Hinrichsen for excellent orientation during my masters and PhD, respectively. They introduced me to nonequilibrium statistical physics.
I am thankful to my parents Ana Maria Cardoso Barato and Jarbas Novelino Barato for many things.

Abstract

This thesis is concerned with the statistical physics of various systems far from thermal equilibrium, focusing on universal critical properties, scaling laws and the role of fluctuations. To this end we study several models which serve as paradigmatic examples, such as surface growth and non-equilibrium wetting as well as phase transitions into absorbing states. As a particular interesting example of a model with a non-conventional scaling behavior, we study a simplified model for pulsed laser deposition by rate equations and Monte Carlo simulations. We consider a set of equations, where islands are assumed to be point-like, as well as an improved one that takes the size of the islands into account. The first set of equations is solved exactly but its predictive power is restricted to the first few pulses. The improved set of equations is integrated numerically, is in excellent agreement with simulations, and fully accounts for the crossover from continuous to pulsed deposition. Moreover, we analyze the scaling of the nucleation density and show numerical results indicating that a previously observed logarithmic scaling does not apply.

In order to understand the impact of boundaries on critical phenomena, we introduce particle models displaying a boundary-induced absorbing state phase transition. These are one-dimensional systems consisting of a single site (the boundary) where creation and annihilation of particles occur, while particles move diffusively in the bulk. We study different versions of these models and confirm that, except for one exactly solvable bosonic variant exhibiting a discontinuous transition with trivial exponents, all the others display a non-trivial behavior, with critical exponents differing from their mean-field values, representing a universality class. We show that these systems are related to a $(0+1)$-dimensional non-Markovian model, meaning that in nonequilibrium a phase transition can take place even in zero dimensions, if time long-range interactions are considered. We argue that these models constitute the simplest universality class of phase transition into an absorbing state, because the transition is induced by the dynamics of a single site. Moreover, this universality class has a simple field theory, corresponding to a zero dimensional limit of direct percolation with Lévy flights in time.

Another boundary phenomena occurs if a nonequilibrium growing interface is exposed to a substrate, in this case a nonequilibrium wetting transition may take place. This transition can be studied through Langevin equations or discrete growth models. In the first case, the Kardar-Parisi-Zhang equation, which defines a very robust universality class for nonequilibrium moving interfaces, is combined with a soft-wall potential. While in the second, microscopic models, in the corresponding universality class, with evaporation and deposition of particles in the presence of hard-wall are studied. Equilibrium wetting is related to a particular case of the problem, corresponding to the Edwards-Wilkinson equation with a potential in the continuum approach or to the fulfillment of detailed balance in the microscopic models. In this thesis we present the analytical and numerical methods used to investigate the problem and the very rich behavior that is observed with them.

The entropy production for a Markov process with a nonequilibrium stationary state is expected to give a quantitative measure of the distance form equilibrium. In the final chapter of this thesis, we consider a Kardar-Parisi-Zhang interface and investigate how entropy production varies with the interface velocity and its dependence on the interface slope, which are quantities that characterize how far the stationary state of the interface is away from equilibrium. We obtain results in agreement with the idea that the entropy production gives a measure of the distance from equilibrium. Moreover we use the same model to study fluctuation relations. The fluctuation relation is a symmetry in the large deviation function associated to the probability of the variation of entropy during a fixed time interval. We argue that the entropy and height are similar quantities within the model we consider and we calculate the Legendre transform of the large deviation function associated to the height for small systems. We observe that there is no fluctuation relation for the height, nevertheless its large deviation function is still symmetric.

Zusammenfassung

Diese Dissertationsschrift befasst sich mit der statistischen Physik verschiedener Systeme fernab vom thermischen Gleichgewicht. Im Mittelpunkt stehen dabei die kritischen Eigenschaften, Skalierungsgesetze sowie die Rolle von Fluktuation. Dazu werden als paradigmatische Beispiele verschiedene Modellsysteme untersucht, unter anderem Wachstumsprozesse, Benetzungsphänomene fernab vom Gleichgewicht sowie Phasenübergänge in absorbierende Zustände.

Als ein besonders interessantes Beispiel mit einem unkonventionellen Skalierungsverhalten wird zunächst ein Modell für gepulste Laserdeposition sowohl numerisch als auch mit Ratengleichungen untersucht. Wir betrachten dazu eine Approximation, das auf der Annahme punktförmiger Teilchen beruht, sowie ein verbessertes Gleichungssystem, das die Ausdehnung der deponierten Inseln mit berücksichtigt. Die numerisch integrierten Lösungen dieses verbesserten Systems stimmen mit den Simulationsresultaten hervorragend überein und reproduzieren ebenfalls den Crossover von kontinuierlicher zu gepulster Deposition. Darüber hinaus wird das Skalierungsverhalten der Nukleationsdichte im Detail untersucht und eine kürzlich eingeführte Hypothese logarithmischer Skalengesetze in Frage gestellt.

Um den Einfluss von Randtermen auf kritische Phänomene unter Nichtgleichgewichtsbedingungen besser zu verstehen, wird ein Modell mit einem randinduzierten Phasenübergang eingeführt. Der Rand besteht aus hier einem einzigen Gitterplatz, an dem Teilchen erzeugt und vernichtet werden können, während die Teilchen im Innern des Systems lediglich diffundieren können. Es werden verschiedene Varianten dieses Modells

untersucht, die mit Ausnahme einer bestimmten bosonischen Variante zu einer neuen Universalitätsklasse mit einem nichttrivialen kritischen Verhalten gehören. In der Arbeit wird gezeigt, dass diese Systeme effektiv auf ein 0+1-dimensionales Modell mit einer zeitlich nichtlokalen Dynamik reduziert werden können, dass also Phasenübergänge in nicht-Markovschen Nichtgleichgewichtssystemen sogar in 0 räumlichen Dimensionen, d.h. einem einzigen Punkt möglich sind. Es handelt sich wahrscheinlich um den einfachsten nichttrivialen Phasenübergang dieser Art, der formal dem nulldimensionalen Limes der sogenannten gerichteten Perkolation mit zeitlichen Levy-Flügen entspricht.

Eine andere Art von Randeffekten tritt auf, wenn ein Wachstumsprozess fernab vom Gleichgewicht auf einem inerten Substrat stattfindet, wobei es zu einem Benetzungsphasenübergang kommen kann. Solche Systeme können anhand ihrer Langevin-Gleichung, z.B. der Kardar-Parisi-Zhang (KPZ)-Gleichung in einem geeigneten Potential, oder auf der Basis diskreter Wachstumsprozesse mit Deposition und Verdampfung von Teilchen auf einem Substrat untersucht werden. Benetzungsübergänge im thermischen Gleichgewicht stellen sich als Spezialfall heraus, der durch die Edwards-Wilkinson-Gleichung bzw. detaillierte Balance beschrieben wird. Die vorliegende Arbeit stellt analytische und numerische Methoden vor und demonstriert die reichhaltige Phänomenologie solcher Modelle.

Das letzte Kapitel befasst sich mit der Rolle von Fluktuationen und der Entropieproduktion von Nichtgleichgewichtssystemen. Um zu überprüfen, ob sich die Entropieproduktion als ein Maßfür den Abstand vom Gleichgewicht eignet, wird wiederum ein einfacher Wachstumsprozess untersucht, der diese Hypothese bestätigt. Das gleiche Modell wird benutzt, um verschiedene Fluktuationsrelationen zu testen, die auf Symmetrien in der Wahrscheinlichkeitsverteilung extremer Fluktionationen beruhen. Obwohl die Entropie und die Höhe der deponierten Schicht im stationären Zustand formal ähnliche Eigenschaften besitzen, gelingt es nicht, ein

Fluktuationstheorem für die Höhenvariablen zu formulieren, obwohl die entsprechende Wahrscheinlichkeitsverteilung symmetrisch ist. Dies legt den Schluss nahe, dass Fluktuationstheoreme grundsätzlich nur auf der Basis von Wahrscheinlichkeitsströmen konstruiert werden können.

Contents

1 Introduction **5**

1.1 Equilibrium and nonequilibrium statistical physics 5
1.2 Stochastic Processes 7
1.3 Contents of this thesis 10

2 Pulsed laser depostion **15**

2.1 Introduction 15
2.2 Models for MBE and PLD 18
2.3 Relevant quantities and scaling 19
2.4 Rate equations 24
2.5 Improved rate equations 28
2.6 Scaling properties of pulsed laser deposition 32
2.7 Conclusion 36

3 Simplest phase transition into an absorbing state **38**

3.1 Introduction 38
3.2 Basic concepts 40
  3.2.1 Percolation and directed percolation 40
  3.2.2 The contact process 43
  3.2.3 Field theoretical approach for DP 48
  3.2.4 Algebraically distributed waiting times 57
3.3 Boundary induced phase transition into an absorbing state . . 58
  3.3.1 Basic model definition and simulations 58

3.3.2 Order parameters 60
3.3.3 Mean field approximation 66
3.3.4 Related models and field theoretical approaches 68
3.3.5 Relation to a $(0+1)$-dimensional non-Markovian process 74
3.4 The timeline spreading process 76
3.4.1 Model definition 76
3.4.2 Field theoretical approach for the TSP 78
3.4.3 Numerical results 84
3.5 Conclusion 92

4 Nonequilibrium wetting 94
4.1 Introduction 94
4.2 Definition of the problem 98
4.2.1 Continuum model 98
4.2.2 Microscopic models 100
4.2.3 Observables and related exponents 105
4.3 Exact results 112
4.3.1 Transfer matrix formalism 113
4.3.2 Calculation of the critical exponents 115
4.3.3 Attractive wall: the case $q_0 \neq q$ 117
4.3.4 Exact calculation of the velocity of a free interface . . . 119
4.4 Numerical simulations 121
4.4.1 The exponents of bKPZ– universality class 122
4.4.2 Scaling picture and differences between the bKPZ universality classes 123
4.4.3 Wetting as a Contact Process with an external field . . 126
4.4.4 Numerical integration of the bKPZ equation 128
4.4.5 Numerical results for the attractive substrate case . . . 130
4.4.6 Extensions of the problem 132
4.5 Mean Field Approximations for microscopic models 134
4.5.1 Master equation 134

4.5.2 The RSOSW model 136
4.5.3 The SSW model 142
4.6 Nonequilibrium wetting in higher dimensions 146
4.6.1 Mean field for the continuum model 146
4.6.2 Scaling analysis 149
4.7 Final remarks 151

5 Entropy production and fluctuation relations 153
5.1 Introduction 153
5.2 Entropy production 156
5.3 Fluctuation relations 158
5.3.1 Finite time fluctuation relation 160
5.3.2 Asymptotic fluctuation relation 162
5.4 The RSOS model 164
5.5 Calculation of the entropy production 168
5.5.1 Solving the RSOS model 168
5.5.2 Exact results 172
5.5.3 Approximative results 174
5.5.4 Different transition rates 176
5.6 Fluctuation relation for a KPZ interface 177
5.6.1 Finite size effects on the asymptotic fluctuation relation 177
5.6.2 Fluctuation relations for the height 178
5.6.3 Small systems 181
5.7 Conclusion 183

6 Conclusion and perspectives 186

Chapter 1

Introduction

1.1 Equilibrium and nonequilibrium statistical physics

The systems studied in (equilibrium) statistical mechanics [1, 2] are macroscopic systems, i.e., systems constituted of a very large number of particles. In principle, one could consider the individual trajectory of all the constituents of a macroscopic system and obtain information about it using classical mechanics [3]. However, in practice, this is not possible because the number of degrees of freedom is too large. In statistical mechanics this problem is overcome by the use of probability theory [4].

An statistical ensemble is a theoretical concept, where one considers a a large number of identical systems: by identical we mean with the same state space (in a system of N particles, for example, an state is determined by the position and momenta of the N particles) and under the same macroscopic conditions. The microcanonical ensemble describes an isolated system with N particles, volume V and energy E. From Liouville's theorem follows that the distribution of states is uniform, that is, all states are equally probable. On the other hand, the canonical ensemble describes a system in contact with a thermal reservoir at temperature T. From the knowledge of the microcanonical distribution one can easily find that, in the canonical ensemble, an state C has the following probability distribution,

$$P(C) = Z^{-1} \exp(-\beta H(C)), \tag{1.1}$$

where β is the inverse of the temperature T, $H(C)$ is the Hamiltonian of the system and Z is the partition function that normalizes the probability distribution. The physical observables of interest in statistical mechanics are macroscopic quantities that are calculated in the following way. If one considers some function of the states $f(C)$, its average value, denoted by $\langle f \rangle$, is given by:

$$\langle f \rangle = \sum_{C} f(C) P(C). \tag{1.2}$$

Macroscopic quantities are given by the average of some state function $f(C)$ and, therefore, they can be calculated with the knowledge of the probability distribution $P(C)$.

As an example we consider the well-known Ising model. In this case one considers a system of spins, that can be up or down. At a site i, one associates a variable s_i such that $s_i = 1$ ($s_i = -1$) represents spin up (down). A state C is characterized by the configurations of spins: in a system with N spins we have 2^N states. The hamiltonian of the Ising model is given by

$$H = J \sum_{<ij>} s_i s_j, \tag{1.3}$$

where $\sum_{<ij>}$ runs over all nearest neighbors. Therefore, within the canonical ensemble, the probability distribution of a configuration $\{s\}$ is

$$P(\{s\}) = Z^{-1} \exp(-\beta J \sum_{<ij>} s_i s_j). \tag{1.4}$$

An important macroscopic quantity of the Ising model is the magnetization m, which is the average of $f(\{s\}) = \sum_i s_i$. Therefore the magnetization can be written in the form,

$$m = Z^{-1} \sum_{\{s\}} \exp(-\beta J \sum_{<ij>} s_i s_j) f(\{s\}). \tag{1.5}$$

As shown in [5] the explicit calculation of the magnetization is possible for some specific lattices, which may be a very complicated task. The point we want to make is that in equilibrium statistical physics the probability distribution of states is known and macroscopic quantities can be calculated form this knowledge.

Consider a system that is put into contact with a thermal reservoir at temperature T. After waiting some time the system and the reservoir (which is much bigger than the system) will equilibrate, the system will have the temperature T and the distribution of states will be given by (1.1). One may be interested in the behavior of the system before it relaxes to equilibrium, in this case the probability distribution of states $P(C,t)$ is time-dependent and in general not known. This is a specific case of nonequilibrium statistical physics. It is specific in the sense that although $P(C,t)$ is not known, the stationary state probability distribution, $P(C) = \lim_{t\to\infty} P(C,t)$ is known and given by (1.1). More generally, in a nonequilibrium system also the stationary state probability distribution, if it exists, is not known. In this thesis we are interested in such systems.

1.2 Stochastic Processes

If one tosses a coin one time there are two possible (and equally probable) outcomes: head or tail. These two possible outcomes form the sample space and each of them takes place with probability 1/2. More generally, a sample space is a set of events such that to each event a number between zero and one is related. This number interpreted as the probability of the event and summing the probabilities over all sample space gives 1. A random variable is a function defined in the sample space, in the coin tossing problem one can consider the random variable s, such that $s = 0$ ($s = 1$) is associated to head (tail). The probability distribution $P(s)$ is given by $P(0) = P(1) = 1/2$. In this thesis, we will consider the sample space as a set of states (or configurations) denoted by $\{C\}$, and each state has a certain probability $P(C)$.

A stochastic process [6, 7] is a collection of random variables that are indexed by time. Let

$$T(C_n, \tau_n | C_1, \tau_1; C_2, \tau_2; ...; C_{n-1}, \tau_{n-1}) \tag{1.6}$$

be the conditional probability of being in the state C_n at time τ_n given that the system was in the state C_1 at time τ_1, C_2 at time τ_2,..., and C_{n-1} at time τ_{n-1}. The stochastic process is said to be Markovian if

$$T(C_n, \tau_n | C_1, \tau_1; C_2, \tau_2; ...; C_{n-1}, \tau_{n-1}) = T(C_n, \tau_n | C_{n-1}, \tau_{n-1}), \tag{1.7}$$

i. e., a Markovian process has no memory, since the state at the next time step depends only on the present state. An important equality, that holds for Markov processes, is the Chapman-Kolmogorov equation, which reads

$$T(C_2, \tau_2 | C_1, \tau_1) = \sum_C T(C_2, \tau_2 | C, \tau) T(C, \tau | C_1, \tau_1). \tag{1.8}$$

It says that the probability of being in an state C_2 at time τ_2 given that the system was in C_1 at time τ_1 is the sum over all possible states C of the probability of being at C_2 at time τ_2 given that the system was in C at τ multiplied by the probability of being in C at time τ given that the system was in C_1 at time τ_1, with $\tau_1 \leq \tau \leq \tau_2$. In the continuous time limit (see [4, 6] for details) the Chapman-Kolmogorov equality leads to the master equation, given by

$$\partial_t P(C, t) = \sum_{C' \neq C} \Big(P(C', t) w_{C' \to C} - P(C, t) w_{C \to C'} \Big), \tag{1.9}$$

where $P(C, t)$ is the probability of being in state C at time t and $w_{C' \to C}$ is the transition rate (transition probability per unit of time) of state C' to state C. The master equation is a balance equation, the first term on the right hand side takes into account all possibilities of entering the state C and the second term of leaving the state C.

Admitting continuous time Markov process with an unique stationary state solution $P(C) = \lim_{t\to\infty} P(C,t)$ we have, from (1.9),

$$\sum_{C'\neq C} \Big(P(C')w_{C'\to C} - P(C)w_{C\to C'} \Big) = 0. \tag{1.10}$$

If all the terms in the above sum are zero then detailed balance holds, i.e., the detailed balance condition reads

$$P(C')w_{C'\to C} = P(C)w_{C\to C'}. \tag{1.11}$$

In this case the stationary probability distribution is the canonical equilibrium distribution, which can be written in the form $P(C) = \exp(-H(C))$, where

$$H(C) - H(C') = \ln \frac{w_{C'\to C}}{w_{C\to C'}}. \tag{1.12}$$

If detailed balance does not hold, then we have a nonequilibrium stationary state and $P(C)$ is generally not known. Therefore, in the context of continuous time Markov processes, equilibrium means that the detailed balance condition (1.11) is fulfilled. For the physical systems studied in this thesis, detailed balance may hold only for very specific choices of the parameters controlling them, but in general we will consider genuine nonequilibrium systems in the sense explained above.

Let us consider a Markov process with its states being labeled by some continuous variable x. The Fokker-Planck equation for it reads

$$\partial_t P(x,t) = -\partial_x[a(x)P(x,t)] + \frac{1}{2}\partial_x^2[b(x)P(x,t)]. \tag{1.13}$$

The Fokker-Planck is a specific type of master equation (both are linear in P), it can be derived from the master equation if some assumptions on the probability distribution of states and the transition rates hold (see [6] for details). Associated to the Fokker-Planck equation there is a Langevin equation, which reads

$$\frac{d}{dt}x = a(x) + b(x)\eta(t) \tag{1.14}$$

where the above Langevin equation is interpreted in the Ito sense (see [7]) and $\eta(t)$ is the noise. The stochastic character of the Langevin equation comes from the noise term $\eta(t)$, which has zero average and correlations of the form $\langle\eta(t)\eta(t')\rangle = \delta(t-t')$, where $\langle\rangle$ stands for the ensemble average. A noise with these two properties is called a white gaussian noise. A master equation is associated with any continuos time Markov processes while the Langevin equation applies only to some continuous time Markov processes, therefore the master equation is more general.

Within physical systems that are appropriately described by a stochastic process we may have to deal with a master equation or with a Langevin equation. In order to write down the master equation one needs to know all the transition rates between states, therefore we call this a microscopic description of the physical system. A Langevin equation can be written down from the knowledge of some properties of the physical system, a detailed knowledge about all transition rates is not necessary. In principle, the Langevin equation can be derived from the master equation, however in some cases we may have a Langevin equation and microscopic models that describe the same physics and a way of formally deriving the Langevin equation from one of the microscopic models is not known. We note that, while the master equation is more general in the sense explained above, the same physical phenomena may be captured by one Langevin equation and several microscopic models (master equations), in this sense the Langevin description of this physical phenomena is said to be more general.

1.3 Contents of this thesis

In the following chapters, we consider systems that are described by a master equation or by a Langevin equation. In order to analyze them, we use several numerical and analytical methods, including: Monte Carlo simulations, numerical integration of Langevin equations, mean field approximations, renormalization group approach and exact solutions. More specifically, we will deal with: the submonolayer regime of Pulsed Laser Depositon (PLD); phase transitions into an absorbing state; nonequilibrium wetting; entropy production and fluctuation relations for a nonequilibrium growing interface. Below we give a short explanation of these topics, pointing out our work on them.

Pulsed Laser Deposition: PLD is a technique for the growth of thin films and multilayers. It differs from Molecular Beam Epitaxy (MBE), the most prominent among such techniques, in the way particles are deposited. In MBE atoms are randomly deposited on a substrate continuously. These atoms diffuse on the substrate until they coalesce with an island (cluster of atoms) or another atom (forming a new island). The processes taking place in PLD are also deposition, diffusion and coalescence. Nevertheless, differently than in MBE, intense and short pulses are deposited on the target in PLD, making the deposition of particles approximately discontinuous. That is, a certain quantity of atoms (a pulse) is deposited almost instantaneously, then they diffuse on the substrate during some fixed time interval. In chapter 2, we study the submonolayer regime of PLD using a simplified stochastic model. The coverage is defined as the total number of deposited atoms divided by the area of the substrate: the submonolayer regime corresponds to coverages smaller than one. The relevance in analyzing the size and format of the islands in this regime, lies in the fact that it has great influence in the subsequent growth kinetics. Various results of Chapter 2 are published in [8], where we studied rate equations and scaling in PLD.

Phase transitions into an absorbing state: An absorbing state is a state that can be accessed by the dynamics but cannot be left. Systems with an absorbing state have a transition in the following sense: depending on some control parameter, in the long time limit, the system certainly reaches the absorbing state (where the order parameter of the transition is zero) or it stays in an active state (where the order parameter has an non-zero fluctuating value). A classical example for this transition is a toy model for the propagation of a disease, where a infected individual can infect a healthy neighbor or get healthy spontaneously. The control parameter is the infection rate and the absorbing state corresponds to the annihilation of the disease (all individuals healthy). Hence, if the infection rate is bigger than some threshold, in the long time limit the number of infected individuals (the order parameter) will be a finite fluctuating value. On the other hand, if the infection rate is smaller than the threshold, after some time all individuals will be healthy, ceasing the dynamics. It turns out that such phase transitions can be characterized by a set of critical exponents that are universal. If two different models have the same set of critical exponents we say that they belong to the same universality class. The most robust universality class of systems with absorbing states is the directed percolation (DP) universality class. The subject of chapter 3 is special type of boundary-induced phase transitions that corresponds to a new universality class of phase transitions into an absorbing state. We introduced this new universality class in [9] and further studied in [10, 11]. As we will show this is the simplest universality class of phase transitions into an absorbing state, corresponding to a zero-dimensional limit of DP with algebraically distributed waiting times. Moreover, we demonstrate that in nonequilibrium a phase transition can take place even in zero dimensions.

Nonequilibrium wetting: Chapter 4 is a topical review about nonequilibrium wetting, as published in [12]. In this chapter, we consider surface growth models in the presence of a hard-core wall. Depending on the control parameters these growth models can be in two phases: the moving phase, where the interface detaches form the wall and grows linearly in time, or the bound phase, where it stays pinned to the wall. By varying the control parameters the system goes form the bound phase to the moving phase undergoing a wetting transition. In chapter 4 we explain the analytical and numerical methods that are used to study the very rich phenomena of nonequilibrium wetting. Other contributions that we did in this field are [13, 14]: They are related to mean-field approximations for a microscopic model with a nonequilibrium wetting transition and a detailed numerical study of the same model, respectively.

Entropy production and fluctuation relations: Finally, in chapter 5 we consider entropy production and fluctuation relations for a Kardar-Parisi-Zahng (KPZ) interface. The entropy production is a quantity that is naively expected to give a measure of the distance of a nonequilibrium stationary state from equilibrium. The nonequilibrium stationary state of a KPZ interface is characterized by the interface velocity and by how the interface velocity depends on the interface slope. We calculate these quantities analytically (exactly and with approximations) to analyze how the entropy production quantifies the distance from equilibrium. As we will show, for a KPZ interface the entropy and the height are closely related, hence we also investigate the possibility of finding a fluctuation relation (that holds for the entropy) for the height. The results of chapter 5 are still unpublished.

Although the topics are closely related, we organized the chapters in such a way that they can be read autonomously. In the following we explain how the different topics are related. Considering nonequilibrium wetting, in the moving phase the growth of the interface is described by the KPZ equation which is also the kind of growing interface studied in chapter 5. More precisely, the growth model we use to study entropy production and fluctuations relations in chapter 5 is also one of the microscopic models considered in chapter 4 to study nonequilibrium wetting. The relation between Chapters 3 and 4 is that both are about nonequilibrium phase transitions. Different from the phase transitions studied in chapter 3, the nonequilibrium wetting transition is not a phase transition into an absorbing state. Nevertheless, as we show in chapter 4, there are situations where a crossover form the DP universality class to the universality class characterizing wetting takes place. In chapter 2, as in chapter 4 and 5, we study nonequilibrium growing interfaces. However, when we consider PLD we study the submonolayer regime (short time) and we are interested in the detailed structure of the interface. On the other hand, when dealing with a KPZ interface we study average properties of the interface in the long time limit. Therefore, the methods we use and the questions we investigate in chapter 2 are completely different from the methods and investigations of chapters 4 and 5.

Chapter 2

Pulsed laser depostion

2.1 Introduction

Among the techniques for the growth of thin films and multilayers Molecular Beam Epitaxy (MBE) and Pulsed Laser Deposition (PLD) [15] play an important role. Compared to MBE, PLD has several advantages. For example, pulsed laser deposition is a widely used technique which allows one to control the stoichiometry of multilayers more efficiently and leads in some situations to a better layer-by-layer growth [16]. The essential difference between these two techniques lies in the way how particles are deposited and the kinetic energy of the arriving particles. While in MBE the flux of particles is continuous, in PLD intense and short pulses are deposited on the target, making the flux of incoming particles approximately discontinuous. Also, in PLD the kinetic energy of the deposited particles is typically higher than in MBE.

During the growth of thin films, particles are deposited onto a two-dimensional substrate, where they diffuse until they find other particles, to which they attach. Therefore, agglomerates of particles, islands, are formed and if the attachment is irreversible (no diffusion at the edge of the islands) they have the form of a diffusion limited aggregation (DLA) fractal [17, 18]. In DLA, initially, a seed particle is placed at the origin. Then a particle is

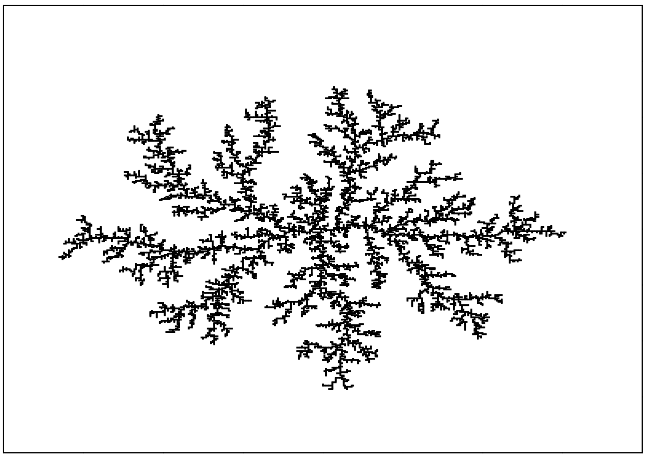

Figure 2.1: DLA cluster with 10^4 particles.

released at a position far from the origin an it diffuses until it meets the seed particle, forming a cluster of two particles, that remains immobile. After that, another particle is released far from the origin and it diffuses until it meets the two-particle cluster, forming a three particle cluster. Repeating the process Z times we have a DLA cluster of size $Z + 1$. In Fig.2.1 we show a DLA-like cluster with 10^4 particles, it is a fractal object with fractal dimension $d_f \approx 1.72$ [19]. The importance of DLA fractals stems from the fact that they are observed in several experiments (see [18, 20]).

In this Chapter we study a stochastic model for PLD introduced in [21], where particles are deposited in pulses, diffuse on the surface and nucleate. If a particle meets another particle it sticks irreversibly, therefore, during this deposition and diffusion process, DLA-like islands are generated. The coverage θ of a system is defined as the total number of deposited particles (multiplied by the area that a particle occupies) divided by the area of the substrate. Here we analyze the surface morphology in the submonolayer regime, where the coverage $\theta \leq 1$. It turns out that the dynamical processes at the bottom layer determine the growth process at the following layers to a large extent [22].

There is already a great amount of theoretical work on MBE (see [20] for a review), while there are less theoretical studies on PLD [21, 23, 24, 25, 26, 27, 28]. Here we apply to PLD a theoretical method that proved to be very useful in MBE, namely, the rate equations approach [29]. By integrating a set of rate equations for the island density one can make predictions about the experimentally relevant quantities characterizing the system. We use two sets of rate equations: In the first and more simple one, we consider the islands as point-like objects, while in the second approach, introduced for MBE in Ref. [30], we improve the equations by considering the competition of islands of different sizes for the arriving and diffusing monomers. The first approach has the advantage that the rate equations can be solved exactly. The improved set of rate equations can only be integrated numerically but it shows excellent agreement with simulations.

A nucleation event occurs when a diffusing monomer encounters another monomer. A quantity of interest in the study of PLD and MBE is the nucleation density n, which is defined as the number of nucleation events divided by the system area. In Ref. [21] it was suggested that for PLD this quantity follows an unusual logarithmic scaling. Later this type of scaling behavior was explained in the framework of scaling laws with continuously varying exponents [31]. Opposed to these early conjectures, we present numerical evidence that such logarithmic scaling laws do not hold asymptotically, although they may be used as a good approximation.

This Chapter is organized in the following way. In the next section we define the model for PLD to be investigated (we also define the corresponding model for MBE). The properties of the model and the observables that we are going to calculate are discussed in Section 3. The fourth section is dedicated to the rate equations, where islands are approximated as point-like objects. In section 5 we introduce and analyze the improved set of rate equations, which account for the way islands (of different sizes) compete for the diffusing monomers. Section 6 is concerned with a critical analysis of scaling laws for

PLD. Finally, our conclusions are summarized in section 7.

2.2 Models for MBE and PLD

In what follows we compare PLD with MBE. When we consider MBE, the model we have in mind is the following [32]. It is defined on a two-dimensional discrete lattice with $L \times L$ sites. Two events can take place, namelly: deposition of a new monomer, with rate F (the flux of particles), and diffusion of an monomer with rate D. If a monomer is deposited at a site that already has a particle the diffusion rate is also D, including diffusion across terraces (there is no Ehrlich-Schwoebel barrier [33, 34]). If a diffusing monomer finds another monomer or the edge of an island at a neighboring site, it sticks to it irreversibly. In the first case we have a nucleation event and a new island is formed. In order to perform an efficient simulation one should keep track of the number of monomers and their positions on the lattice. With probability $q = F/(F + N_1 D)$ a new monomer is deposited at a random position on the lattice and with probability $1 - q$ one of the monomers is chosen and moved randomly to one of the four nearest-neighbor sites. The coverage θ is equal to the total number of deposited atoms divided by L^2.

The PLD model, introduced in [21], deposition and diffusion take place in the following way.

- In each pulse $I \cdot L^2$ monomers, where $0 < I \leq 1$ is the pulse intensity, are randomly deposited on the lattice.

- During a time interval between two pulses of length $\tau = I/F$, where F is the time-averaged influx of particles, the monomers diffuse on the surface with rate D.

- When a monomer encounters another monomer or the border of an agglomerate of particles, it sticks irreversibly.

The model does not take into account that the arriving particles in PLD have a high kinetic energy, leading to transient effects such as an enhanced mobility. In fact, the transient mobility was shown to have a great influence on the growth kinetics [26, 27, 28]. However, Vasco et al. [28], analyzing a set of rate equations, found out that the way particles are deposited already leads to differences in the film roughness. More specifically, they found that continuous deposition leads generally to rougher films while the additional transient mobility in the case of continuous (discontinuous) deposition makes the film rougher (smoother). Other simplifications assumed in the model are the irreversibility of aggregation and the immobility of nucleated islands. For instance, the assumption of irreversible aggregation suppresses Ostwald ripening, which was recently proposed to be the key mechanism ruling the PLD growth kinetics in monomer-depleted regimes [28]. Here we want to study the difference in the island morphology for continuous and discontinuous deposition and the corresponding crossover in the limit of low energies, assuming that transient mobility effects lead to corrections that can be neglected.

2.3 Relevant quantities and scaling

Depending on the pulse intensity I and the ratio $R = D/F$ the model for PLD defined above displays different features. For very small pulse intensities and a finite value of R, it exhibits essentially the same behavior as MBE. More specifically, for intensities much smaller than a typical value I_c, which depends on R, the model is effectively in the MBE regime. Then, increasing the pulse intensity to a value much larger than I_c, the model crosses over to a different regime, the so-called PLD regime. The two regimes differ in so far as they are characterized by different surface morphologies, that is, the number and size of islands are distributed differently. However, as edge diffusion is not included in the model, the islands are DLA-like fractals (when diffusion

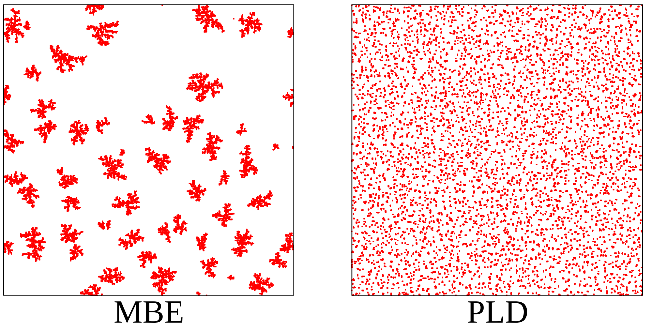

Figure 2.2: Comparison between the island morphologies of the MBE (left) and PLD (right) models. In both cases $\theta = 0.05$ and $D/F = 10^{10}$ and for the PLD model $I = 0.01$. For PLD there are more islands and their average size is smaller.

of atoms along the edges of islands is also permitted the islands may become compact [24, 30].). In Fig. 2.2 we show typical surface morphologies for the MBE and PLD (with $I > I_c$), which are very different for the same values of coverage and average flux of particles. In the PLD case there are more islands and the average island size is smaller.

The two regimes are also different with respect to the scaling of the average distance between islands l_D. In the MBE limit $I \ll I_c$ the average distance between islands grows as [20]

$$l_D \sim R^{\gamma}, \tag{2.1}$$

where

$$\gamma = \frac{1}{d_f + 4}, \tag{2.2}$$

while in the PLD limit $I \gg I_c$ one has [21]

$$l_D \sim I^{-\nu}, \tag{2.3}$$

where

$$\nu = \gamma/(1 - 2\gamma). \tag{2.4}$$

Hence, the crossover takes place if

$$I_c \approx R^{-\gamma/\nu} = R^{2\gamma-1}. \tag{2.5}$$

Relations (2.1) and (2.3) can be combined in the following scaling form [21]

$$l_D \sim R^\gamma \, h(I/R^{-\gamma/\nu}), \tag{2.6}$$

where $h(x)$ is a scaling function which is constant for $x \ll 1$ and scales as $h(x) \sim x^{-\nu}$ for $x \gg 1$. The same type of scaling behavior is also expected to hold when considering other typical length scales as, for example, the mean distance that a monomer travels before being captured by an island or another monomer, the square root of the mean island size, and the inverse of the square root of the nucleation density. In numerical simulations the scaling relations (2.1), (2.3) and (2.6) were observed to hold for small coverages before coalescence of islands sets in (see below).

In the PLD limit the model is independent of R, the time interval between two pulses is big enough to make the density of monomers equal to zero. Hence, taking the PLD limit means that diffusion of monomers occurs until the density of them is zero, and in principle such a limit can be taken for any value of I. The smallest value of I by which we perform simulations is 0.0001. This value is much lower than typical experimental pulse intensities, which are of order 0.1 [35, 36]. We use low values for the pulse intensity because we are interested in the scaling behavior of the model in the limit $I \to 0$.

The probability that an occupied site belongs to a cluster of size s is given by

$$p_s = \frac{sN_s}{\theta}, \tag{2.7}$$

where N_s is the number-density of islands of size s and

$$\theta = Ft = \sum_{s=1}^{\infty} sN_s \tag{2.8}$$

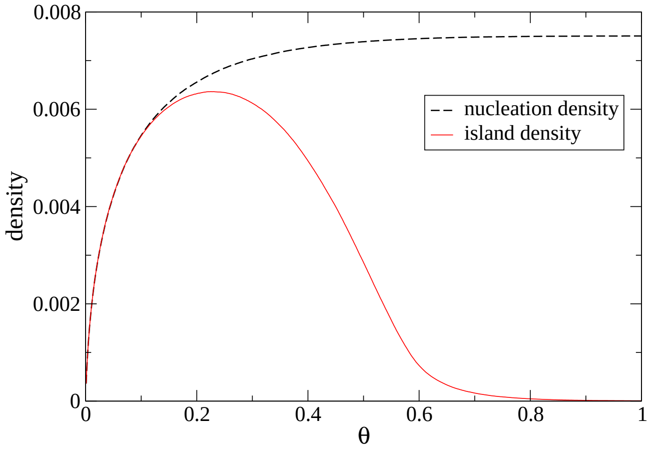

Figure 2.3: Nucleation density $n(t)$ and island density $N(t)$ obtained from simulations in the PLD limit for $I = 0.001$.

is the coverage. Therefore, the mean island size is given by

$$\langle s \rangle = \frac{1}{\theta} \sum_{s=1}^{\infty} s^2 N_s . \tag{2.9}$$

The nucleation density n is defined as the number of nucleation events (when a monomer meets another monomer) in the bottom layer per unit area. Initially, when freshly nucleated islands do not yet touch each other, it is equal to the island density, given by

$$N = \sum_{s=2}^{\infty} N_s \, . \tag{2.10}$$

However, as the coverage increases, more and more islands coalesce, forming bigger islands. Consequently their number decreases so that the island density becomes smaller than the nucleation density, as is shown in Fig.2.3. As can be seen, coalescence – indicated by a difference between n and N – sets in already before the island density reaches its maximum. At this maximum the island density begins to decrease because coalescence events become more frequent than nucleation events.

As for the scaling of the nucleation density in the PLD regime, the following relations were observed in Ref. [21]: After the first pulse, where $\theta = I$, the nucleation density scales as

$$n(I, I) \sim I\,. \tag{2.11}$$

Upon completion of the bottom layer ($\theta = 1$) the nucleation density was found to scale as

$$n(I, 1) \sim I^{2\nu}. \tag{2.12}$$

These two scaling laws determine the terminal points of the curves $n(I, \theta)$ for different intensities I. However, these curves were found to have a different shape in a double-logarithmic representation, making it impossible to perform an ordinary data collapse. This suggested that the model does not exhibit ordinary power-law scaling.

As a possible way out, a logarithmic scaling form was proposed [21]. Starting point was the observation that by squeezing and stretching the curves the terminal points collapse, in such a way that the entire curves for different intensities seem to collapse as well. This led to the conjectured scaling form

$$\ln M(I, \theta) = (\ln I)\, g\left(\frac{\ln \theta}{\ln I}\right), \tag{2.13}$$

where

$$M(I, \theta) = \frac{n(I, \theta)}{n(I, 1)}\,. \tag{2.14}$$

Here $g(x)$ is a universal function, and this scaling is supposed to be valid in the full range $0 < \theta \leq 1$. In a subsequent work, this type of scaling behavior was backed up by a theoretical framework which involves continuouslly varying exponents [31], where the scaling exponents are continuous functions of the control parameters. One of the purposes of this paper is to show that this logarithmic scaling does probably not apply to PLD in a strict sense.

Throughout this Chapter all numerical simulations were performed in 2+1 dimensions on a 400 × 400 lattice with periodic boundary conditions.

For average quantities such as the island and nucleation densities or the mean island size, the number of independent runs was 100 while, when calculating the probability distribution (2.7), we used 10000 runs.

2.4 Rate equations

In this and the following sections we study the model introduced above by mean-field approximations on different levels. Before starting let us emphasize that these approaches are based on the same assumptions (e.g. irreversible aggregation, immobile aggregates) as the full model defined in the introduction, extended by additional mean-field type approximations such as the homogeneity of densities and the neglect of correlations.

We start with a simple set of rate equations for the island density N and the monomer density N_1 (see Ref. [20, 30, 32])

$$\frac{dN_1}{dt} = F(t) - 2DN_1^2 - DNN_1, \tag{2.15}$$

$$\frac{dN}{dt} = DN_1^2 \,. \tag{2.16}$$

The first term on the right hand side of Eq. (2.15) describes the flux of particles while the second and third terms are related to nucleation of two monomers and attachment of monomers at existing islands, respectively. In Eq. (2.16) the term on the right hand side describes the increase of the island density by nucleation of two diffusing monomers. For MBE the flux is constant, while for PLD the flux is modeled by a discontinuous sequence of spikes

$$F(t) = I \sum_{l=0}^{\infty} \delta(t - \tau l), \tag{2.17}$$

where τ is the time interval between two pulses.

In this set of rate equations coalescence is not taken into account, hence within this theory the nucleation density and the island density are identical. Moreover, the approach does not take into account how islands of different sizes compete for the diffusing and arriving monomers since islands are treated as point-like objects. Therefore, this approximation is expected to be valid (when compared with simulations) just for the first few pulses.

The MBE limit corresponds to taking $\tau \to 0$ and $I \to 0$ with $I/\tau = F$, since this renders a constant flux F. In the MBE regime it was found that initially, when $N \ll N_1$, the island density grows as $N \sim t^3$. However, when $N \gg N_1$, the growth of the island density becomes slower, crossing over to the power law $N \sim t^{1/3}$ (see Ref. [20]).

In order to solve the equations in the PLD limit, let us first consider the evolution between two pulses l and $l+1$:

$$\frac{dN_1}{dt} = -2N_1^2 - NN_1, \tag{2.18}$$

$$\frac{dN}{dt} = N_1^2, \tag{2.19}$$

where, without loss of generality, we set $D = 1$. In order to make the above equations linear one introduces a modified time variable [37, 38]

$$T = \int_0^t N_1(t')dt'. \tag{2.20}$$

Because of $dT = N_1(t)dt$, Eqs. (2.18) and (2.19) turn into

$$\frac{dN_1}{dT} = -2N_1 - N, \tag{2.21}$$

$$\frac{dN}{dT} = N_1. \tag{2.22}$$

With the initial conditions $N_1(0) = I$ and $N(0) = N^{(l)}$, where $N^{(l)}$ is the island density after l pulses, one is led to the solutions

$$N_1(T) = [I - (I + N^{(l)})T] \exp(-T), \tag{2.23}$$

$$N(T) = [N^{(l)} + (I + N^{(l)})T] \exp(-T). \tag{2.24}$$

In the PLD limit the pulses are so strongly separated in time that all diffusing monomers have nucleated or attached to existing islands before the next pulse arrives. The diffusion process ends at the final (modified) time T_f when

$$N_1(T_f) = 0 \tag{2.25}$$

and the corresponding island density $N(T_f) = N^{(l+1)}$ stays constant until the next pulse arrives. Because of Eq. (2.23) the modified final time T_f is given by $T_f = I/(I + N^{(l)})$, hence with Eq. (2.24) we obtain the recurrence relation

$$N^{(l+1)} = (I + N^{(l)}) \exp\left(\frac{-I}{I + N^{(l)}}\right), \tag{2.26}$$

with the initial condition $N^{(0)} = 0$. Rewriting the island density as

$$N^{(l)} = A_l I \tag{2.27}$$

with

$$A_0 = 0 \tag{2.28}$$

this recurrence relation turns into

$$A_{l+1} = (1 + A_l) \exp\left(\frac{-1}{1 + A_l}\right), \tag{2.29}$$

which is independent of I. This means that within this mean field approximation the island density is proportional to the pulse intensity. As shown in Fig. 2.4, where relations (2.27), (2.28) and (2.29) are compared with simulations, this is indeed the case for the first few pulses. For the predicted slope, however, we see a better agreement for the first pulse and also for smaller values of the pulse intensity.

This approximation reproduces another important feature of the full model, namely, after the first pulse, for a fixed value of I, the nucleation density in the PLD limit is considerably larger than the nucleation density in the MBE limit $R \ll I^{1/(2\gamma-1)}$ (see Fig. 2.5, where the rate equations and simulation results are compared in both limits). However, the nucleation density in the MBE limit grows faster and eventually exceeds the nucleation density in the PLD limit such that the two curves in Fig. 2.5 cross each other.

The rate equations used here assume islands to be point-like objects. Obviously, this approach works only for very small values of the coverage (much smaller than the value at which coalescence starts) and thus it is

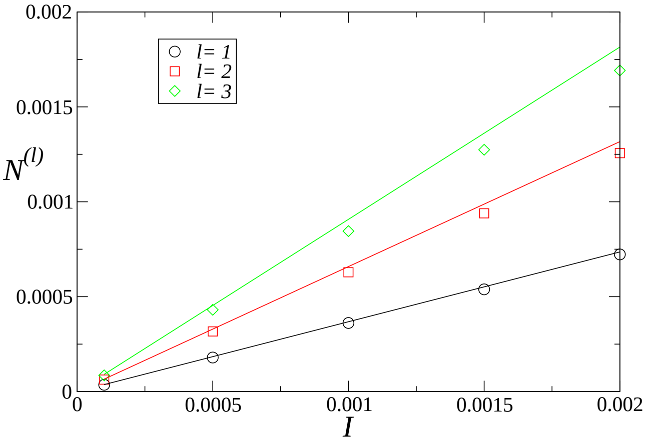

Figure 2.4: Island density in the PLD limit as a function of I for the first three pulses $l = 1, 2, 3$ obtained from simulations (points) and from relations (2.27), (2.28), and (2.29) (lines).

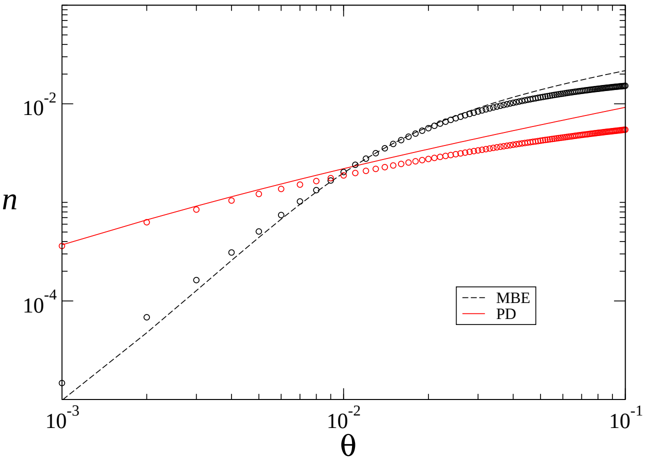

Figure 2.5: Comparison of the nucleation density obtained by simulations (points) and the rate equations (2.15) and (2.16) (lines) with $I = 0.001$ and, in the MBE limit, $R = 10^4$. Note that for comparing the two cases for given I, R has to be chosen such that $R \ll I^{1/(2\gamma-1)}$.

inadequate to fully account for the crossover from PLD to MBE. In particular, it does not allow one to confirm the scaling relation (2.6). In the next section we consider improved rate equations that overcome these problems.

2.5 Improved rate equations

In order to improve the rate equations for the model defined in the introduction let us now consider the dynamics of islands with different sizes separately and study how they compete for the diffusing monomers and how other adatoms are deposited on top of these islands.

A set of rate equations for MBE that takes these features into account is [30]

$$\begin{aligned} \frac{dN_s}{d\theta} &= (D/F)N_1\left(\sigma_{s-1}N_{s-1} - \sigma_s N_s\right) \\ &\qquad + k_{s-1}N_{s-1} - k_s N_s, \qquad (2.30) \\ \frac{dN_1}{d\theta} &= 1 - (D/F)N_1(2\sigma_1 N_1 + \sum_{s=2}^{\infty}\sigma_s N_s) \\ &\qquad - k_1 N_1 - \sum_{s=1}^{\infty} k_s N_s, \qquad (2.31) \end{aligned}$$

where the constants σ_s are effective rates describing how an island of size s competes for the diffusing monomers while the constants k_s are related to the capture of the incident monomers. These quantities are given by [30]

$$k_s = s^{2/d_f} \qquad (2.32)$$

and

$$\sigma_s = 2\pi(R_s/\xi)\frac{K_1(R_s/\xi)}{K_0(R_s/\xi)}\,, \qquad (2.33)$$

where K_0 and K_1 are modified Bessel functions, R_s is the island radius, and ξ is the average distance a monomer travels before being captured by an island or another monomer, given by

$$\xi^{-2} = 2\sigma_1 N_1 + \sum_{s=2}^{\infty}\sigma_s N_s + (F/D)k_1 N_1\,. \qquad (2.34)$$

These improved relations assume that the islands are circular. However, in reality and simulations the islands resemble fractal objects. The fractal morphology of the islands is taken into account in an effective way by assuming that the island radius grows with its size by [30]

$$R_s = \alpha\, s^{1/d_f}, \tag{2.35}$$

where α is a fit parameter, to be determined by the comparison of the results arising from numerical integration of the rate equations and simulations, and $d_f \approx 1.72$ is the fractal dimension of DLA-like clusters [19].

In order to generalize the above rate equations to pulsed laser deposition we use, as in the former case, a discontinuous flux of incoming monomers, obtaining the differential equations

$$\begin{aligned} \frac{dN_1}{d\theta} = \sum_l \left(1 - k_1 N_1 - \sum_{s=1}^{\infty} k_s N_s\right) I\delta(\theta - lI) \\ -2D\sigma_1 N_1^2 - DN_1 \sum_{s=2}^{\infty} \sigma_s N_s, \end{aligned} \tag{2.36}$$

$$\begin{aligned} \frac{dN_s}{d\theta} = \sum_l [k_{s-1}N_{s-1} - k_s N_s] I\delta(\theta - lI) \\ +DN_1[\sigma_{s-1}N_{s-1} - \sigma_s N_s], \end{aligned} \tag{2.37}$$

where the δ-functions couple to the terms proportional to k_s since those terms are related to the capture of arriving monomers, an event that takes place during deposition. As in the previous case, the improved equations predict that the nucleation density n and island density N are identical since coalescence is not taken into account. Since coalescence influences directly only the island density, we find it more appropriate to compare the results coming from numerical integration of these equations with the nucleation density obtained by simulations.

The rate equations (2.36) and (2.37) faithfully reproduce the predicted crossover from MBE to PLD. To demonstrate this we show in Fig. 2.6

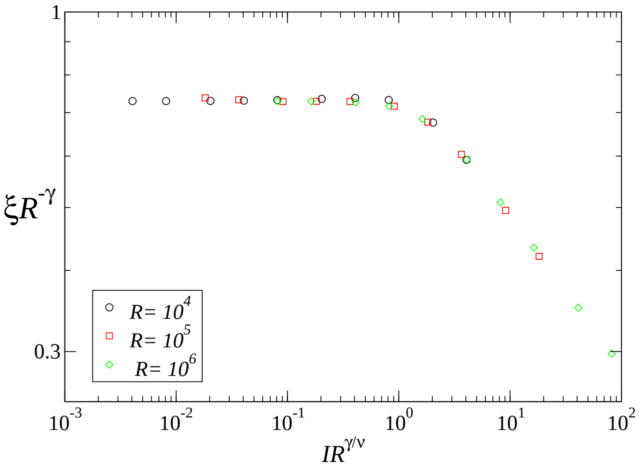

Figure 2.6: Data collapse to verify equation (2.6) obtained from numerical integration of (2.36) and (2.37) with $\alpha = 1$ at the coverage $\theta = 0.1$.

the corresponding data collapse according to the scaling form (2.6) with $\nu = 0.23$ and $\gamma = 0.15$, where we used $\alpha = 1$. We note that the value of the fit parameter α could be different for MBE and PLD. However, when considering the crossover from MBE to PLD one has to use a single value for which $\alpha = 1$ turned out to be a good choice. This approximation is justified since the value of this parameter does not change the type of scaling behavior. Nevertheless, this ambiguity regarding the value of α may lead to small numerical deviations in the estimates of the scaling exponents ν and γ.

In Figs. 2.7 and 2.8 we compare the numerical integration of the rate equations with numerical simulations of the full model. Fig. 2.7 shows the nucleation density and the mean island size as functions of the coverage for different values of the pulse intensity. As can be seen, simulations and numerical integration of the rate equations agree almost perfectly. As is shown in Fig. 2.8, the agreement is less good for the probability distribution (2.8). Such discrepancies are not surprising because the rate equations approach is a mean field theory, neglecting correlations in the system. Similar discrep-

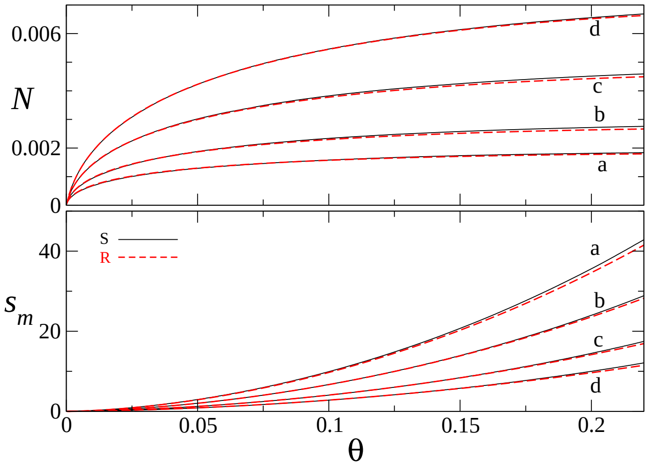

Figure 2.7: Comparison between simulations (S) and numerical integration of the rate equations (2.36) and (2.37) (R) of the nucleation density (upper panel) and mean island size (lower panel) in the PLD limit for the pulse intensities $I = 0.0001$ (a), $I = 0.0002$ (b), $I = 0.0005$ (c), and $I = 0.001$ (d).

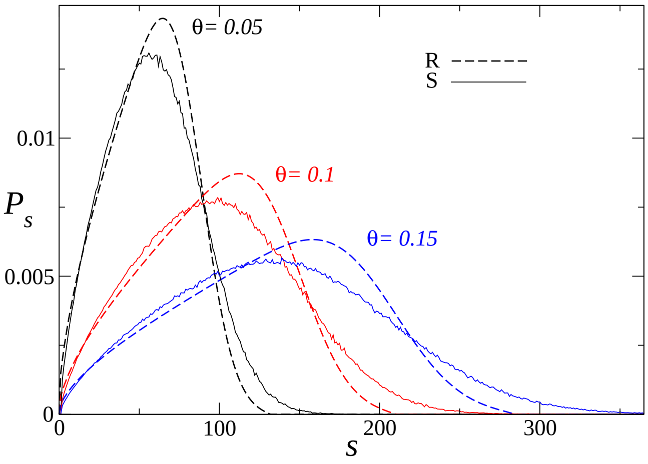

Figure 2.8: The probability distribution function (2.7) for $I = 0.0001$ in the PLD limit obtained from simulations (S) and from a numerical integration of the rate equations (R) (2.36) and (2.37).

ancies were already observed in the MBE limit [30]. The values of the fit parameter that we used are $\alpha \approx 1.7$ in the PLD limit and $\alpha \approx 0.3$ in the MBE limit.

This improved theory has considerable advantages when compared to the previous one. As shown in Fig. 2.6, it fully accounts for the crossover from MBE to PLD, and the observables, except for coverages where coalescence starts to play an important role, are in excellent agreement with simulations. This excellent agreement indicates that the improved mean field equations capture the most important features of the model while other possible sources of deviations such as correlations and fluctuations are probably less important.

2.6 Scaling properties of pulsed laser deposition

As mentioned in the introduction, it was proposed that PLD could be described by an unconventional logarithmic scaling form [21]. In this section we study this conjecture from a critical perspective.

Let us first recall the scaling properties of MBE. After an initial transient time and before the onset of coalescence, the probability distribution (2.7) is known to obey the scaling relation [30]

$$p_s(\theta) = \langle s \rangle^{-1} f\left(\frac{s}{\langle s \rangle}\right), \tag{2.38}$$

where $f(x)$ is a universal function independent of the control parameters R and θ. This means that, in the MBE regime, the model has only one characteristic size and therefore the morphology of the islands remains the same if the control parameters are varied.

Turning to the PLD limit, in Fig. 2.9 we observe that a convincing data collapse is obtained for different coverages if the pulse intensity is kept fixed, while the collapse is not satisfactory for different values of the pulse intensity

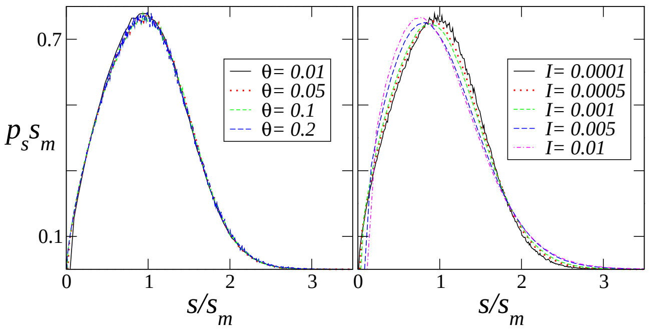

Figure 2.9: The probability distribution p_s, obtained from simulations, multiplied by mean island size $\langle s\rangle$ as a function of $s/\langle s\rangle$ for $I = 0.0001$ and different values of θ (left) as well as for $\theta = 0.1$ and different values of I (right).

and a fixed coverage. Therefore, in the PLD limit, the function $f(x)$ is not universal, instead it explicitly depends on one of the control parameters, namely, the pulse intensity I. However, for reasons that are explained below, the island morphology seems to be the same for different values of the pulse intensity.

To explain the failure of conventional scaling, the logarithmic scaling form (2.13) was suggested on a purely heuristical basis [21]. This scaling form had been applied previously to various other problems: experiments in turbulence [39], self-organized critical sandpile models [40, 41], and, as in the present case, DLA-related growth processes [42]. Fig. 2.10 shows a data collapse of the normalized nucleation density according to this scaling form, which at first glance seems to be convincing. Initially it was speculated that the unusual type of scaling behavior, which can be explained in terms of continuously varying critical exponents [31], may be related to the fractal structure of the islands, which become more and more compact as the first monolayer is filled up. However, later it was shown [25] that the same logarithmic scaling form can be used in a 1+1-dimensional model for pulsed deposition, where the (one-dimensional) islands are always compact.

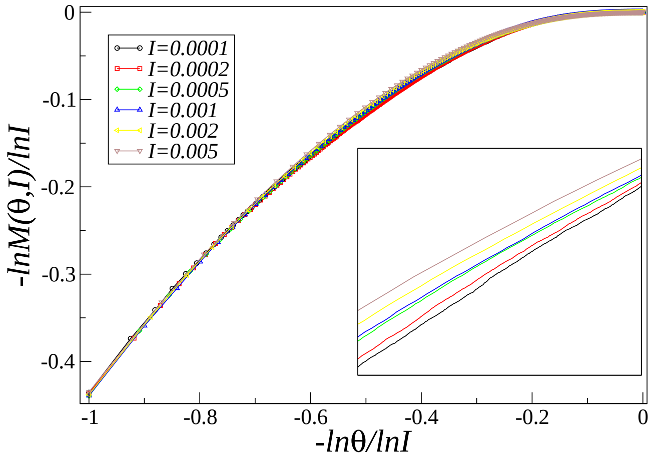

Figure 2.10: Data collapse of the normalized nucleation density, coming from simulations, with the logarithmic scaling form. The inset magnifies the interval $0.2 < \ln\theta/\ln I < 0.25$ where the scaling function increases with the pulse intensity I.

A closer look at Fig. 2.10 reveals that the collapse is not perfect, rather there are deviations with a clear systematic tendency. It seems that the curves become more straight as the intensity is reduced, questioning the concept of logarithmic scaling.

Although we are still unable to disprove or confirm the concept of logarithmic scaling applied to PLD, it is in our opinion useful to demonstrate that an alternative scaling concept yields at least as good if not even better results. Starting point is the observation that average quantities like the mean island size and the nucleation density exhibit a clean power-law dependence on I if the coverage θ is kept fixed. However, the value of the exponent varies with the coverage, i.e.

$$n(I,\theta) \sim I^{\alpha(\theta)}. \tag{2.39}$$

The plots of the nucleation density as a function of I for different values of θ (cf. Fig. 2.11) suggest that the exponent α increases monotonically with

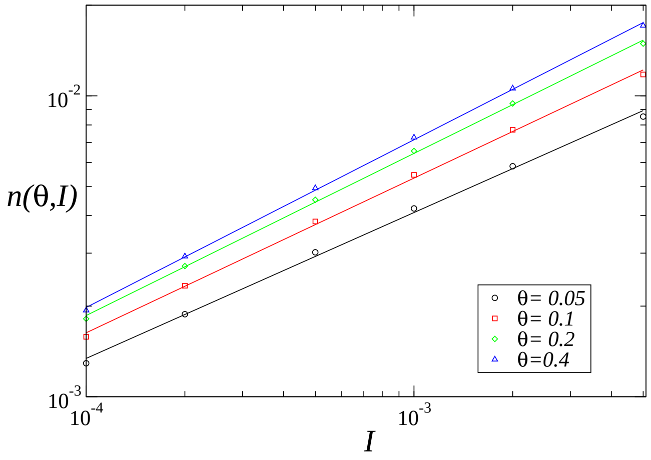

Figure 2.11: Nucleation density, obtained from simulations, as a function of I for different values of θ. The graph suggests that the exponent α increases with θ.

θ. Actually, $\alpha = 2\nu$ and therefore Eq. (2.3) should be corrected by introducing an exponent ν which depends continuously on the coverage. Since the exponent ν is related to the fractal dimensionality of the islands, this indicates that the fractal dimension of them effectively varies with θ. However, the data collapse of the probability distribution for different values of the coverage (Fig. 2.9) shows that this is clearly not the case.

We have also observed that in the one dimensional model, where the islands have no fractal properties, the nucleation density follows a power law for a fixed value of the coverage. Moreover, we observed that the function $f(x)$, defined in Eq. (2.38), does depend on the pulse intensity. This indicates that these two features of the model in the PLD limit are not related to the fractal dimension of the islands and hence we do not expect it to vary with the control parameters.

In Fig. 2.10 we present a data collapse using relation (2.13) for different values of the pulse intensity. Since $M(I,1) = 1$ and $M(I,I)$ follows a power-law, the first ($\theta = I$) and last ($\theta = 1$) points of the curves collapse. However, the situation in the middle of the curve ($I \ll \theta \ll 1$) is unclear. More specifically, as is shown in the inset of Fig. 2.10, for $0.2 < \ln\theta/\ln I < 0.25$ the value of $\ln M(I,\theta)$ increases *monotonically* with I, thus exhibiting a systematic deviation rather than a statistical error. Also, this scaling is in disagreement with relation (2.39), since from it the value of $M(I,\theta)$ should be constant for a fixed coverage. For these reasons we consider the numerical evidence supporting equation (2.39) as more reliable than the data collapse obtained using the logarithmic scaling form.

2.7 Conclusion

In this Chapter we have studied several variants of rate equations for pulsed deposition. First a simple set of rate equations, where the islands are treated as point-like objects, was considered. The equations were solved exactly in the limit of strong and temporally separate pulses (the so-called PLD limit as opposed to the MBE limit of continuous deposition), reproducing some features of the model for very small values of the coverage. Since this approximation does not take the dimension of the islands into account it was not possible to faithfully reproduce the crossover from MBE to PLD. This problem was overcome with a second improved set of rate equations that takes the dimension of the islands into account. As in the case of MBE [30], we showed that these improved equations lead to results which are in excellent agreement with simulations for pulsed deposition.

Another point of the present work was to revisit a recently proposed logarithmic scaling for pulsed deposition from a critical perspective. In the corresponding data collapses we have observed small violations for intermediate coverages with a systematic drift, indicating that logarithmic scaling may be a good approximation for pulse intensities in computer simulations and experiments but probably it is not asymptotically valid in the limit $I \to 0$.

As an alternative suggestion, we have proposed that the nucleation density, for a fixed value of the coverage, as a function of I follows a power law and that the exponent varies with the coverage. This suggestion is supported by numerical simulations and leads to numerical results which are more accurate than the data collapses obtained by using logarithmic scaling. This may be another hint that logarithmic scaling, as proposed in Ref. [21], has to be replaced by a different type of scaling theory.

We have pointed out another new feature of the two-dimensional model in the PLD limit, namely, the probability distribution p_s that a site belongs to a cluster of size s does not scale according to relation (2.38) for different values of the pulse intensity. At first glance this non-universal behavior may lead to the conclusion that for different pulse intensities the fractal dimension of the islands is different. However, studying the one-dimensional model, where islands have no fractal properties, the same effect is observed, indicating that this is not the case.

Let us finally comment on the one-dimensional model in more detail. This case was previously studied in Ref. [25], where a reasonable data collapse for the nucleation density based on logarithmic scaling was presented. Contrarily, we observe a clean power law behavior of the nucleation density as a function of I for a fixed θ and also a non-universal probability distribution for different values of I. Hence, the one dimensional model seems to exhibit a behavior which is as rich as in the two-dimensional case and a systematic study of the 1d case may be very useful for clarifying some aspects of PLD.

Chapter 3

Simplest phase transition into an absorbing state

3.1 Introduction

Phase transitions occurring in the bulk, but driven by specific conditions at its boundaries, are called *boundary-induced phase transitions* [43]. Examples include diffusive transport [44, 45] and traffic flow [46] models. A simple example is the one-dimensional totally asymmetric simple exclusion process [47], where particles enter the system at the left boundary, jump to the right in the bulk, and exit at the right boundary. Depending on the entering and exiting rates, the system exhibits qualitatively different phases, namely: a maximal current phase, a large current and low density phase and small current and high density phase.

In the present chapter, we are interested in boundary-induced phase transitions in systems with absorbing states. An absorbing state is a dynamical trap which can be reached but cannot be left [48, 50, 49]. Systems with absorbing phase transitions are controlled by a parameter, depending on which the system either enters the absorbing state with certainty or survives in a stationary fluctuating/active state. The most prominent family of phase transitions into an absorbing state is the very robust direct percolation (DP) universality class. A recent breakthrough has been the experimental observation of DP critical behavior for the first time [51].

A paradigmatic model in the DP universality class is the contact process (CP) [52]. It can be viewed as a simple model for the propagation of a disease where sick individuals can either infect healthy neighbors or become healthy spontaneously. More precisely, in the CP in d spatial dimensions, a particle (infected individual) can be created at an "empty" (healthy individual) site with a rate $\lambda n/2d$, where n is the number of nearest neighbors occupied by a particle, and an occupied site can become empty at rate 1. The empty configuration is an absorbing state. For λ larger than a certain critical threshold, λ_c, the process is able to sustain (in an infinite lattice) a non-vanishing density of particles, while for $\lambda < \lambda_c$ the dynamics ends up, ineluctably, in the absorbing state.

As continuous phase transitions involve long-range correlations, boundary effects may play an important role. In the context of absorbing phase transitions, previous studies focused primarily on DP confined to parabolas [53, 54], active walls [55], as well as absorbing walls and edges [56, 57]. Although such boundaries influence the dynamics deep into the bulk, the universality class of the bulk transition is not inherently changed, rather it is extended by an additional independent exponent describing the order parameter near the boundary. Therefore, the question arises whether it is possible to find boundary-induced absorbing phase transitions, absent in the corresponding systems without boundaries, constituting independent universality classes.

As a contribution of this thesis a new universality class of phase transitions into an absorbing state was introduced in Ref. [9] and further analyzed in [10, 11]. One model in this universality class has a CP like dynamic in one special boundary site and diffusion in the bulk, as we shall see it displays a boundary-induced phase transition into an absorbing state. We will also show that this model can be mapped onto a $0+1$-dimensional non-Morkavian model that is in the same universality class. In the study of this universality class we use numerical and analytical methods including Monte Carlo simulations, mean field approximations, exact solutions and field theory. A similar model, for a boundary induced phase transition into an absorbing state, to ours was first considered by Deloubrière and van Wijland in [58], who developed the field theoretical approach for this new universality class.

The Chapter is organized as follows: In the next section we introduce some basic concepts that are necessary to understand what we develop here, namely, DP, the CP and the field theoretical approach for DP. Sec. 3.3 and 3.4 are dedicated to boundary induced phase transitions into an absorbing state and the $0 + 1$-dimensional non-Markovian model, respectively. In Sec. 3.5 we conclude.

3.2 Basic concepts

3.2.1 Percolation and directed percolation

Percolation [59, 60] can be viewed as the passage of some fluid through a porous medium. The difference between percolation and diffusion is that, in percolation, the randomness is not in the fluid but in the lattice. A model for site percolation (there is also bond percolation where one considers the bonds between two neighbors, see below) is the following: consider a discrete square lattice where the sites can be either occupied with probability p or empty with probability $1 - p$. Such lattice will have clusters of occupied sites, parts of the porous medium where the fluid goes trough. The theory of percolation deals with the size, number and form of these clusters.

The probability p is the control parameter, and by varying it there is a phase transition. The order parameter of this transition is the probability of site to pertain to an infinity cluster P_∞. If p is bigger than a certain threshold

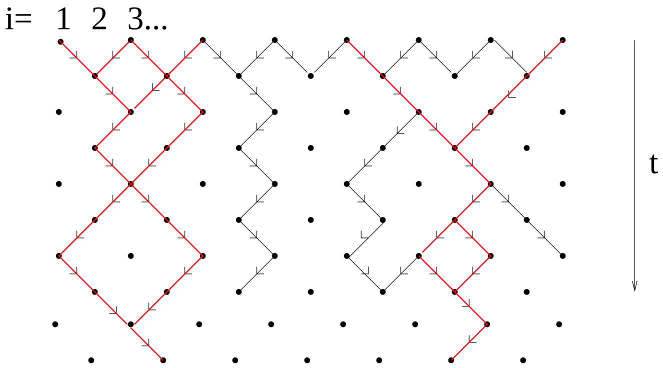

Figure 3.1: Lattice for directed percolation

p_c we have $P_\infty > 0$, otherwise $P_\infty = 0$. To illustrate this we consider site percolation on a one-dimensional lattice. In this case the probability of a cluster of size s is simply given by $\rho_s = p^s(1-p)^2$. The probability that a site pertains to a finite cluster P summed with the probability that it pertains to an infinite cluster P_∞ is equal to the probability that a site is occupied which is just p. In this one-dimensional case we have

$$P = \sum_{s=1}^{\infty} s\rho_s = p, \tag{3.1}$$

giving $P_\infty = 0$ for $p < 1$. For $p = 1$ there is only one infinity cluster in the lattice and $P_\infty = 1$. Therefore in the one-dimensional model there is no phase transition and the critical value is $p_c = 1$. A very instructive exercise is to solve site percolation on the Bethe lattice [60, 61, 62], the critical behavior is much richer than the trivial one-dimensional case.

In contrast to isotropic percolation considered so far, directed percolation [48] assumes that one direction is favored, as is the case of a fluid in a porous medium going down because of gravity. We consider the following model for directed percolation. On a diagonal square lattice like the one displayed in Fig. 3.1, where the favored direction is indicated by t, each site is active with probability p and each bond is open with probability q. In the dynamical interpretation of DP, that we consider form now on, t is identified as time. In bond and site DP, two sites are connected if they are active and the bond between them is open . A site can only be connected to a site in a neighbor layer, it cannot be connected to a site in the same layer. To each site i of the lattice we associate a random variable η_i such that $\eta_i = 1$ if the site is connected to a site at the layer $t = 0$ and $\eta_i = 0$ otherwise. Note that we have a discrete time Markov process, such that the value of η_i at time t depends only on η_{i-1} and η_{i+1} at time $t-1$. Since time is continuous in a Monte Carlo simulation we have parallel updates.

Following [62], the evolution of the one-site probability distribution is given by

$$P_{t+1}(\eta_i) = \sum_{\eta'_{i-1}} \sum_{\eta'_{i+1}} w(\eta_i | \eta'_{i-1}, \eta'_{i+1}) P_t(\eta'_i, \eta'_{i+1}), \tag{3.2}$$

where $w(\eta_i | \eta'_{i-1}, \eta'_{i+1})$ is the transition probability that the site i at the layer $t+1$ is in the state η_i, given that the sites $i-1$ and $i+1$ at the layer t are in the state η'_{i-1} and η'_{i+1}. Therefore, it is given by

$$\begin{aligned} w(1|1,1) &= pq(1-q) + p(1-q)q + pq^2, \\ w(1|1,0) = w(1|0,1) &= pq. \end{aligned} \tag{3.3}$$

Considering a homogenous system, which is the case for periodic boundary conditions, from equations (3.2) and (3.3) we obtain

$$P_{t+1}(1) = pq(2-q)P_t(1,1) + pqP_t(1,0) + pqP_t(0,1). \tag{3.4}$$

In the limit $t \to \infty$ we have $P_t(1) = P_{t+1}(1) = P_\infty$, which is the stationary state probability distribution in the dynamical interpretation. In the above equation the one-site probability distribution at time $t+1$ depends on the two-site probability distribution at time t. If we write the equation for the time evolution of the two-site probability distribution it will depend on the three-site probability distribution [62]. A straightforward way of making equation (3.4) solvable is to make a simple mean field approximation, where the two-site probability distribution is approximated by a simple factorized form. This approximation is very rough and it does not give the right critical point or exponents, nevertheless, within it there is a phase transition and the problem can be easily solved. We proceed calculating the order parameter P_∞ within the simple mean field approximation, i.e.,

$$\begin{aligned} P_l(1,1) &= P_l(1)P_l(1) \\ P_l(1,0) = P_l(0,1) &= P_l(1)P_l(0). \end{aligned} \tag{3.5}$$

Since $P_l(0) + P_l(1) = 1$, from (3.4) we obtain

$$-(pq^2)P_\infty^2 + (2pq-1)P_\infty = 0, \tag{3.6}$$

which has the solutions $P_\infty = 0$ and $P_\infty = \frac{2pq-1}{pq^2}$. In the case of site (bond) directed percolation, $q = 1$ ($p = 1$), $P_\infty = (2p-1)/p$ ($P_\infty = (2q-1)/q$) and $p_c = 1/2$ ($q_c = 1/2$). A central concept in DP is that of an absorbing state, which can be explained as follows. If at a time t we have $\eta_i = 0$ for all i then all the sites in the subsequent times will be inactive. That means, if the model enters the absorbing state it cannot leave it. Within mean field, considering bond percolation, if $q < 1/2$ the stationary state is the absorbing one, while if $q > 1/2$ the model has an active stationary state with $P_\infty > 0$. This is a phase transition into an absorbing state.

The DP class is the most robust universality class of phase transitions into an absorbing state [49]. Several other models are in the DP universality class, in the sense that they share the same critical exponents. In the next section we define these critical exponents (using the CP). We finish this section quoting the DP conjecture [63, 64] which says that all models with a set of properties should be in DP universality class. The properties are: a continuous phase transition from a fluctuating active state into an absorbing state, a positive one-component order parameter, only short-ranged interactions and no unconventional features like additional symmetries.

3.2.2 The contact process

The contact process [52] is a paradigmatic model in the DP universality class. It was introduced in [65] as a model for epidemic spreading, where

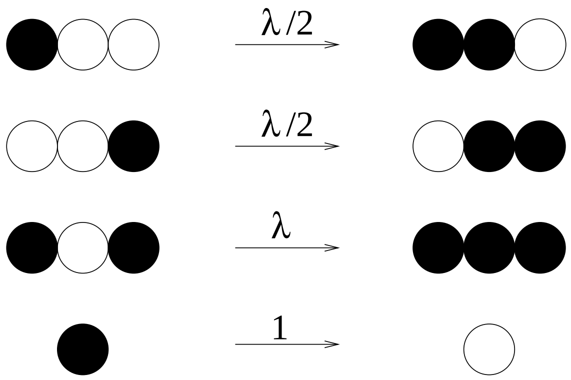

Figure 3.2: Transition rules of the contact process in one dimension.

infected sites can either infect nearest neighbors or spontaneously recover. The model evolves by random sequential updates, the control parameter is the rate of infection, the order parameter is the density of infected sites and the absorbing state corresponds to a lattice where all individuals are healthy. The transition rules for the CP on a d-dimensional cubic lattice of linear size L are:

- A lattice site i is randomly chosen.
- If it is healthy it can become infected with rate $\lambda n/2d$, where n is the number of infected nearest neighbors.
- If is infected it can become healthy spontaneously with rate 1.

To each site i of the lattice a random variable s_i is attached and infected (healthy) is represented by $s_i = 1$ ($s_i = 0$). In Fig. 3.2 we show the transition rules of the CP for $d = 1$.

The order parameter of the transition, the density of occupied sites, is defined by

$$\rho(t) = \langle \frac{1}{L^d} \sum_i s_i(t) \rangle, \tag{3.7}$$

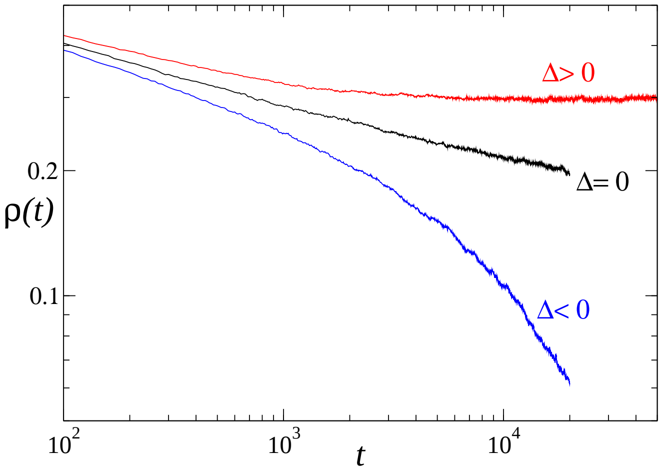

Figure 3.3: The density $\rho(t)$ below $(\Delta < 0)$, above $(\Delta > 0)$ and at $(\Delta = 0)$ criticality for the CP in one dimension with $L = 1024$.

where $\langle\rangle$ denotes an ensemble average and the initial condition is a fully occupied lattice (initially $s_i = 1$ for all i). If the rate λ is smaller than the critical value λ_c the stationary state is the absorbing one and the stationary value of the density of occupied sites $\rho^s = 0$. For $\lambda > \lambda_c$ the stationary state is a fluctuating active one and $\rho^s > 0$. In the following, the distance from criticality is denoted by $\Delta = \lambda - \lambda_c$. In Fig. 3.3 we show $\rho(t)$ for the CP in one dimension obtained from numerical simulations for different values of Δ. One can see that at criticality it decays algebraically and above (below) the critical point it saturates (goes to zero exponentially).

The critical exponent θ is associated to the algebraic decay of $\rho(t)$ at criticality. It is defined by

$$\rho(t) \sim t^{-\theta}, \tag{3.8}$$

valid for $\lambda = \lambda_c$ and in the limit $t \to \infty$. The critical exponent β is related to how the saturation value ρ^s tends to zero as criticality is approached, i.e.,

$$\rho^s \sim \Delta^{\beta}, \tag{3.9}$$

where the above relation is valid for $\Delta = \lambda - \lambda_c$ small and positive (near criticality). Other two critical exponents related to the spatial and temporal

Table 3.1: Critical exponents of the CP, data taken from [52].

	λ_c	β	$\nu_\parallel$	$\nu_\perp$
$d = 1$	3.29785(2)	0.27649(4)	1.73383(3)	1.09684(6)
$d = 2$	1.6488(1)	0.583(4)	1.295(6)	0.733(4)
$d = 3$	1.3169(1)	0.805(10)	1.105(5)	0.581(5)

correlation lengths are, respectively,

$$\zeta_\perp \sim \Delta^{-\nu_\perp}, \qquad \zeta_\parallel \sim \Delta^{-\nu_\parallel}, \tag{3.10}$$

where the above relation are valid for Δ positive and small. One can define more critical exponents for DP, related to the critical behavior of other quantities. Nevertheless, they will not be independent but rather determined by scaling relations. More precisely there are only three independent exponents in DP [48]. For example, by dimensional analysis of relations (3.8), (3.9) and (3.10) one can see that $\theta = \beta/\nu_\parallel$. In table 3.1 we show the values of λ_c for the CP and the critical exponents for the DP universality class for $d = 1, 2, 3$. The critical dimension is $d_c = 4$, above which mean field behavior sets in. We note that these exponents have been determined numerically. Models in the DP universality class are believed to be non-integrable and, meaning that methods for the exact calculation of the critical exponents are not known.

Besides starting with a fully occupied lattice, another commonly used initial configuration is starting with a seed (one occupied site). An important quantity to measure in seed simulations is the survival probability $P_s(t)$, which is the probability of not entering the absorbing state until time t. As density $\rho(t)$ starting with a fully occupied lattice, $P_s(t)$ decays algebraically at the critical point, goes to zero exponentially below it and saturates after some transient above it. Therefore like the exponent β is defined for $\rho(t)$ one can define an exponent β' for $P_s(t)$, i.e.,

$$P_s(\Delta) \sim \Delta^{\beta'}, \tag{3.11}$$

where this relation is again valid for Δ positive and small. It turns out that this is not a new critical exponent because of a special symmetry for DP that implies in $\beta = \beta'$ (see next Section).

Another important quantity which we denote by $c(t)$, is the density of occupied sites at time t starting with a single seed. Near enough the critical point, its stationary value c_s is proportional to the probability of a realization to survive multiplied by the density of occupied sites when the initial condition is a fully occupied lattice, therefore for small and positive Δ

$$c_s(\Delta) \sim \Delta^{\beta+\beta'}. \tag{3.12}$$

Suppose now that also spontaneous creation of particles is incorporated in the CP at rate h. The parameter h is like a magnetic field in the Ising model in the sense that it eliminates the phase transition (with spontaneous creation of particles there is no absorbing state anymore). Associated to this rate h we define the following critical relation, valid for $\lambda = \lambda_c$ and h small,

$$\rho^s \sim h^{\delta_h^{-1}} \tag{3.13}$$

where ρ^s is the saturation value of the density. The exponent δ_h is not independent. It can be related to other exponents by a scaling relation, which can by derived on a heuristic basis as follows. In the limit $t \longrightarrow \infty$ at $\lambda = \lambda_c$ and for small h the occupied sites, are mainly generated from seeds generated by the field h that produce a surviving cluster. Since a seed can be generated at any site of the L^d lattice and at any time, we have that

$$\rho^s \sim L^d h \int c(t) dt, \tag{3.14}$$

remembering that $c(t)$ gives the density of particles starting with a single seed. From dimensional analysis and relations (3.10), (3.12), and (3.13) follows the desired scaling relation:

$$\delta_h = (\nu_{\parallel} + d\nu_{\perp} - \beta')/\beta. \tag{3.15}$$

3.2.3 Field theoretical approach for DP

The DP action

We now consider a model that is in the DP universality class and from it we obtain the action and the Langevin equation for DP. The model is also a continuos time Markov process where, differently from the CP, the occupation number in each site can be zero or any natural number. Models of this type are called bosonic while models with hard-core interaction (only one particle per site is allowed), like the CP, are called fermionic. The reason to choose a bosonic model for the following demonstration is that there is no well established filed-theoretic formalism for the fermionic case (although some ideas have been proposed [66]). The transitions taking place in this model are: diffusion with rate D, where a particle jumps to one of it's nearest neighbors; pair-annihilation with rate σ, where two particles at the same site annihilate one another; particle creation with rate λ, where a particle creates another particle at the same site. The master equation for it reads

$$\begin{aligned}
&\frac{d}{dt}P(\{n\}) = D\sum_{<ij>}[(n_i+1)P(...,n_i+1,n_j-1,...) \\
&+(n_j+1)P(...,n_i-1,n_j+1,...)-(n_i+n_j)P(\{n\})] \\
&+\lambda\sum_i[(n_i-1)P(...,n_i-1,...)-n_iP(\{n\})] \\
&+\sigma\sum_i[(n_i+2)(n_i+1)P(...,n_i+2,...)-n_i(n_i-1)P(\{n\})], \qquad (3.16)
\end{aligned}$$

where n_i is the occupation number at site i, $\{n\}=(n_1,...,n_i,...)$, the sum $\sum_i$ runs over all sites of the lattice, the sum $\sum_{<ij>}$ runs over all $2d$ nearest neighbors and $P(\{n\})$ is the probability of the configuration $\{n\}$.

The master equation can be written in a different form using the quantum Hamiltonian formalism [45, 48, 67, 69]. In this formalism one uses the state vector

$$|\psi(t)\rangle = \sum_{\{n\}} P(\{n\},t)|\{n\}\rangle, \qquad (3.17)$$

where $|\{n\}\rangle = \otimes_i |n_i\rangle$ denotes the usual configuration basis (see [48, 45]), to write the master equation as an imaginary-time Schrödinger equation, i. e.,

$$\frac{d}{dt}|\psi(t)\rangle = -\hat{H}|\psi(t)\rangle\,, \tag{3.18}$$

where $\hat{H}$ is the time evolution operator. The time evolution operator is written in terms of bosonic creation and annihilation operators, which allows for the use of second-quantization methods (see [70] for an introduction). These ladder operators follow

$$\hat{a}_i|n_i\rangle = n_i|n_i - 1\rangle \qquad , \qquad \hat{a}_i^\dagger|n_i\rangle = |n_i + 1\rangle. \tag{3.19}$$

The time evolution operator for the master equation (3.16) is

$$\hat{H} = D\sum_{<ij>}(\hat{a}_i^\dagger - \hat{a}_j^\dagger)(\hat{a}_i - \hat{a}_j) + \sigma\sum_i(1-(\hat{a}_i^\dagger)^2)\hat{a}_i^2 + \lambda\sum_i[\hat{a}_i^\dagger(1-\hat{a}_i^\dagger)\hat{a}_i]. \tag{3.20}$$

Now we use the path integral formalism to obtain the field theoretical action of DP [68], the presentation here follows [69]. First we introduce coherent states, which are eigenstates of the creation and annihilation operators, i.e.,

$$\hat{a}|\phi\rangle = \phi|\phi\rangle \qquad \langle\phi|\hat{a}^\dagger = \langle\phi|\phi^* \tag{3.21}$$

where ϕ is some complex number. They do not form a orthogonal basis, because

$$\langle\phi_i|\phi_j\rangle = \exp(-|\phi_i|^2/2 - |\phi_j|^2/2 + \phi_i^*\phi_j), \tag{3.22}$$

however they have the property

$$\hat{1} = \frac{1}{\pi}\int d^2\phi|\phi\rangle\langle\phi|, \tag{3.23}$$

where $\hat{1}$ is the identity operator and $d^2\phi = d(Re\phi)d(Im\phi)$. The definition of a coherent state is

$$|\phi\rangle = \exp(-|\phi|^2/2 + \phi\hat{a}^\dagger)|0\rangle, \tag{3.24}$$

where $|0\rangle$ represents the absorbing state, and from it the above properties can be derived (see [70]). The above relations are for coherent states acting in one-particle space, in the case of a lattice the coherent states are denoted by $|\{\phi\}\rangle$ and relation (3.23), for example, is easily generalized by changing its right-hand-side to $\int \prod_i (d^2\phi_i \pi^{-1}) |\{\phi\}\rangle\langle\{\phi\}|$.

The solution of equation (3.18) can be formally written in the form

$$|\psi(t)\rangle = \exp(-\hat{H}t)|\psi(0)\rangle, \tag{3.25}$$

and the average of some observable $B(t)$ is given by

$$\langle B(t)\rangle = \sum_{\{n\}} B(\{n\})P(\{n\}, t) = \langle 1|B|\psi(t)\rangle, \tag{3.26}$$

where $\langle 1| = \sum_{\{n\}} \langle\{n\}|$. Discretizing time, so that

$$\exp(\hat{H}t) \rightarrow \prod_{\tau=\Delta_t}^{t} \exp(-\hat{H}\Delta_t), \tag{3.27}$$

and placing the identity operator expressed in the form (3.23) between every pair of terms, we obtain

$$B(t) \propto \int \prod_{i,\tau} (d^2\phi_{i,\tau}) \langle 1|\hat{B}|\{\phi\}_t\rangle \left(\prod_{\tau=\Delta t}^{t} \langle\{\phi\}_\tau| \exp(-\hat{H}\Delta t)|\{\phi\}_{\tau-\Delta t}\rangle \right) \langle\{\phi\}_0|\rho_0\rangle, \tag{3.28}$$

where the initial state is $|\psi(0)\rangle = |\rho_0\rangle$, a coherent state with $\phi_i = \rho_0$ for all i (note that this corresponds to Poisson initial conditions [69]). Since the operator $\hat{H}$ is a function of the creation and annihilation operators we have

$$\langle\{\phi\}_\tau| \exp(-\hat{H}\Delta t)|\{\phi\}_{\tau-\Delta t}\rangle = \langle\{\phi\}_\tau|\{\phi\}_{\tau-\Delta t}\rangle \exp(H[\{\phi\}^*_\tau, \{\phi\}_{\tau-\Delta t}]\Delta_t), \tag{3.29}$$

where $H[\{\phi\}^*_\tau, \{\phi\}_{\tau-\Delta t}]$ is given by the operator $\hat{H}$, from (3.20), with $\phi^*_{i,\tau}$ and $\phi_{i,\tau-\Delta t}$ replacing $\hat{a}^\dagger_i$ and $\hat{a}_i$, respectively. From (3.22) follows

$$\langle\{\phi\}_\tau|\{\phi\}_{\tau-\Delta t}\rangle = \prod_i \exp[-\phi^*_{i,\tau}(\phi_{i,\tau} - \phi_{i,\tau-\Delta t})] \exp[(|\phi_{i,\tau}|^2 + |\phi_{i,\tau-\Delta t}|^2)/2)]. \tag{3.30}$$

The first term, in the continuos time limit, becomes $\exp[-\phi^*_i(t)\partial_t\phi_i(t)dt]$. After multiplying $\exp[(|\phi_{i,\tau}|^2 + |\phi_{i,\tau-\Delta t}|^2)/2)]$ over the whole time interval only boundary terms do not cancel each other. We are still left with the boundary terms in expression (3.28), they are: $\langle 1|\hat{B}|\{\phi\}\rangle \prod_i \exp(|\phi_{i,t}|^2/2)$ and $\langle \{\phi\}_0|\rho\rangle \prod_i \exp(|\phi_{i,0}|^2/2)$. Considering that the operator B can be written as a function of the annihilation and creation operators we have

$$\langle 1|\hat{B}|\{\phi\}\rangle = \langle 1|\{\phi\}\rangle B(\{\phi\}). \tag{3.31}$$

We now take the continuum time limit where $\int \prod_{i,\tau} d^2\phi_{i,\tau} \to \int \prod_i D\phi_i D\phi_i^*$, with $\int \prod_i D\phi_i D\phi_i^*$ representing a functional integration. In this limit, equation (3.28) becomes

$$\langle B(t)\rangle \propto \int \prod_i (D\phi_i D\phi_i^*) B[\{\phi\}(t)] \exp(-S[\{\phi^*\},\{\phi\}]) \tag{3.32}$$

where the action is given by

$$\begin{aligned} S[\{\phi^*\},\{\phi\}] = & \sum_i [\phi_i(t) - \rho_0 \phi_i^*(0) + |\phi_i(0)|^2] \\ & + \int_0^t dt' \bigg(\sum_i \phi_i^* \partial_{t'} \phi_i + H[\{\phi^*\},\{\phi\}] \bigg) \end{aligned} \tag{3.33}$$

Taking the continuum limit for the lattice position variable (see [69] for details), where $\phi_i(t) \to \phi(x,t)$ and $\phi_i^*(t) \to \tilde{\phi}(x,t)$, we obtain the following action

$$S[\tilde{\phi},\phi] = \int d^dx \bigg(\rho_0 \phi(x,0) - \phi(x,t) \int dt' \tilde{\phi}(\partial_{t'} - D\nabla^2)\phi + H_{int}[\tilde{\phi},\phi] \bigg) \tag{3.34}$$

where H_{int} is given by (3.20) without the diffusion part, i. e., $H_{int} = \sigma(1 - \tilde{\phi}^2)\phi^2 + \lambda(\tilde{\phi}(1-\tilde{\phi})\phi$. By using the shifted field $\bar{\phi} = \tilde{\phi} - 1$ the final boundary term $\phi(x,t)$ is eliminated and a new initial boundary term appears. It turns out that initial boundary terms can be discarded (see [69] for a discussion), leading to

$$S[\bar{\phi},\phi] = \int d^dx dt \bigg(\bar{\phi}(\partial_t - \lambda - D\nabla^2)\phi - \lambda\phi\bar{\phi}^2 + 2\sigma\phi^2\bar{\phi} + \sigma\phi^2\bar{\phi}^2 \bigg) \tag{3.35}$$

Finally trowing out the fourth order term, which is irrelevant under a renormalization group transformation, and doing the transformation

$$\phi \to \phi\sqrt{\lambda/2\sigma}, \qquad \tilde{\phi} \to \tilde{\phi}\sqrt{2\sigma/\lambda}, \tag{3.36}$$

we obtain the DP action, which reads

$$S_{DP}[\bar{\phi},\phi] = \int d^d x dt \bar{\phi}[\partial_t - D\nabla^2 - a + \frac{g}{2}(\phi - \bar{\phi})]\phi, \tag{3.37}$$

where $g = 2\sqrt{2\lambda\sigma}$ and $a = \lambda$. This is the effective action of Reggeon field theory [71], which was introduced in particle physics. Only later it was discovered that it represents a stochastic process [72].

A very important point concerns the interpretation of the fields ϕ and $\bar{\phi}$, the first corresponds to measure the density and the second to place a seed. In the following we provide an explanation for this interpretation. The fields ϕ and $\bar{\phi}$ have the following relation with the ladder operators: $\phi \to \hat{a}$ and $\bar{\phi} \to \hat{a}^\dagger - 1$. The pair connectedness function $c(i,t;j,t')$, which is the density at site i and time t starting at t' with a seed at j, can be written in terms of the creation and annihilation operator in the form

$$\begin{aligned} c(i,t;j,t') &= \langle 1|\hat{a}_i \exp[-\hat{H}(t-t')]\hat{a}_j^\dagger|0\rangle \\ &= \langle 1|\hat{a}_i \exp[-\hat{H}(t-t')](\hat{a}_j^\dagger - 1)|0\rangle \end{aligned} \tag{3.38}$$

where the second equality comes from the fact that if one starts with the absorbing state there is no subsequent dynamics. In the above expression the creation operator places a seed at position j and the annihilation operator measures the density at position i. Therefore, in the same way, the field $\bar{\phi}(x',t')$ places a seed at position x' and time t' and the field $\phi(x,t)$ measures the density at position x and time t. This demonstrates that

$$c(x,t;x',t') = \langle \phi(x,t)\bar{\phi}(x',t')\rangle, \tag{3.39}$$

where $\langle \phi(x,t)\bar{\phi}(x',t')\rangle \propto \int D[\bar{\phi}]D[\phi]\phi(x,t)\phi(x',t')\exp(-S_{DP})$.

The DP Langevin equation can be derived as follows. First we consider the dynamical partition function $Z \propto \int D[\phi]D[\bar{\phi}]\exp(-S_{DP})$. Introducing the gaussian noise $\eta(x,t)$ that follows

$$\exp\left(\frac{\Gamma}{2}\bar{\phi}^2\phi\right) \propto \int D[\eta]\exp(-\eta^2/2)\exp(\tilde{\phi}\eta\sqrt{\Gamma\phi}), \tag{3.40}$$

it can be written in the form

$$Z \propto \int D[\bar{\phi}]D[\eta]D[\phi]\exp(-\eta^2/2)\exp[-\tilde{\phi}(\partial_t\phi - a\phi + \frac{g}{2}\phi^2) + \sqrt{g\phi}\eta]. \quad (3.41)$$

This shows that the DP Langevin equation is given by

$$\partial_t\phi(x,t) = D\nabla^2\phi(x,t) - \lambda\phi(x,t) - \frac{g}{2}\phi(x,t)^2 + \sqrt{g\phi(x,t)}\eta(x,t), \quad (3.42)$$

where η is a gaussian white noise with unitary variance. Alternatively one can derive the DP Langevin equation from the CP and from it, introducing the response field $\tilde{\phi}$ with the integral representation of the delta function, integrate out the noise to obtain the DP action [63].

Time reversal symmetry

Considering the problem of bond DP in one dimension, the backbone [73] is the path that connects active sites at the initial row with the active sites at the final row (they are the red paths in Fig. 3.1). It is invariant under time reversal, which means that the probability of having a specific backbone is independent of the direction one chooses for time. In Fig. 3.1, the probability of having the red path is the same, independent of starting at the lowest row and going up or starting at the highest row and going down. The backbone is the only subset that contributes to the density of particles and the survival probability, while the dangling branches (the black lines in Fig. 3.1) do not contribute. If we consider Fig 3.1, we see that by going down we obtain the particle density starting with a fully occupied lattice and going up we have the survival probability starting with two seeds. Since only the backbones contribute and they have the same probability under time reversal, we have the following exact relation for bond DP, $P_s(t) = \rho(t)$. For other DP models time reversal symmetry may not hold exactly, however, it holds in the limit $t \rightarrow \infty$ and, therefore, for the DP universality class, one has $\beta = \beta'$.

We now show the time reversal symmetry for the CP with an exact calculation [72]. The master equation for the CP can also be written in the from (3.18). It differs from bosonic models in so far that for the CP we have to consider fermionic creation and annihilation operators. Instead of (3.19), they satisfy

$$\hat{a}_i|s_i\rangle = s_i|s_i - 1\rangle \qquad , \qquad \hat{a}_i^\dagger|s_i\rangle = (1-s_i)|s_i+1\rangle, \tag{3.43}$$

where $s_i = 0, 1$. The operator $\hat{H}$ for the CP is given by

$$\hat{H} = \sum_i [\hat{a}_i^\dagger - 1)\hat{a}_i] + \lambda \sum_{<ij>} [(\hat{a}_i - 1)\hat{a}_i^\dagger \hat{a}_j^\dagger \hat{a}_j]. \tag{3.44}$$

The density of particles at some site i is given by

$$\rho_i(t) = \langle 0|\hat{a}_i \hat{V}|\psi(t)\rangle \tag{3.45}$$

where $\hat{V} = \prod_j (1 + \hat{a}_j)$. If the initial condition is a fully occupied lattice we have

$$\rho_i(t) = \langle 0|\hat{a}_i \hat{V} \exp(-\hat{H}t) \prod_j \hat{a}_j^\dagger |0\rangle. \tag{3.46}$$

The pseudo-Hermitian operator $\bar{H} = \hat{V}\hat{H}\hat{V}^{-1}$ obeys the relation [72]

$$\bar{H}^\dagger = \hat{\sigma}\bar{H}\hat{\sigma}, \tag{3.47}$$

where $\hat{\sigma} = \hat{\sigma}^\dagger = \hat{\sigma}^{-1} = \prod_j [\hat{a}_j, \hat{a}_j^\dagger]$. Therefore, from equation (3.46), follows

$$\rho_i(t) = \langle 0|\hat{a}_i \exp(-\bar{H}t)\hat{V}^\dagger|0\rangle = \langle 0|V\hat{\sigma}\exp(-\bar{H}t)\hat{\sigma}\hat{a}_i^\dagger|0\rangle. \tag{3.48}$$

Since $\hat{V}^\dagger\hat{\sigma}\hat{V}^\dagger|0\rangle = |0\rangle$ and $\hat{\sigma}\hat{a}_i^\dagger|0\rangle = -\hat{a}_i^\dagger|0\rangle$, we obtain

$$\rho_i(t) = \langle 0|\exp(\bar{H}t)\hat{V}^{-1}\hat{a}_i^\dagger|0\rangle = 1 - \langle 0|\exp(\bar{H}t)\bar{V}^{-1}\hat{a}_i^\dagger|0\rangle = P_s(t). \tag{3.49}$$

This shows that for the CP $P_s(t) = \rho(t)$ is also exact. As pointed out in [72], this equality is valid for continuous time and in a simulation where time is discretized by using random sequential updates it is valid only asymptotically, which is nevertheless enough to prove $\beta = \beta'$.

In the field theoretical approach, time reversal symmetry means that S_{DP} is invariant under the transformation

$$\phi(t) \to -\bar{\phi}(-t)\,, \quad \bar{\phi}(t) \to -\phi(-t)\,. \tag{3.50}$$

This shows that the fields ϕ and $\bar{\phi}$ have the same dimension. As shown in [74], with numerical integration of the DP Langevin equation, the probability that the space integral of the field $\phi(x,t)$ is larger than a certain arbitrary constant A, starting at time t_0 with a seed at x_0, follows the same critical behavior as the survival probability. This quantity can be written in the form [74]

$$P_A(t) \propto \int D\phi D\tilde{\phi}\Theta\Big(\int d^dx\phi - A\Big)\exp(-S_{DP})\bar{\phi}(x_0,t_0), \tag{3.51}$$

where Θ is the Heaviside step function. From this follows that the field $\tilde{\phi}$ has the dimension of survival probability. Since ϕ has the dimension of density, time reversal symmetry implies in $\beta = \beta'$.

The renormalization group approach for DP

We now outline the renormalization group approach for DP. First we consider that the fields ϕ and $\bar{\phi}$ are slow-varying, i.e., there is a cut-off k_0^{-1} so that they can be written in the following form

$$\phi(x,t) = \frac{\int d^dk d\omega}{(2\pi)^{d+1}}\Phi(k,\omega) \tag{3.52}$$

where the integral goes form $0 < |k| < k_0$. The cut-off k_0^{-1} is proportional to the lattice spacing (distance between two nearest neighbors) and the supposition that the fields are slow varying comes from the fact that in a physically meaningful continuos description the fields cannot vary considerably in distances smaller than the lattice spacing.

In terms of the Fourrier transforms $\Phi(k,\omega)$ the action $S_{DP} = S_0 + S_{int}$ becomes

$$\begin{aligned} S_0[\bar{\Phi},\Phi] &= \int d_{k\omega}\bar{\Phi}(-k,-\omega)G_0^{-1}(k.\omega)\Phi(k,\omega) \\ S_{int} &= \int d_{k\omega}d_{k'\omega'}\Phi(-k,-\omega)\bar{\Phi}(-k',-\omega')[\Phi(k+k',\omega+\omega') - \bar{\Phi}(k+k',\omega+\omega')] \end{aligned} \tag{3.53}$$

where $d_{kw} = d^d k d\omega (2\pi)^{-d-1}$ and $G_0(k,\omega) = (-i\omega + Dk^2 - a)^{-1}$ is the bare propagator. In the first step of the Wilson's renormalization group method one integrates over the Fourier transformed fields with k in the momentum shell $k_0/b < |k| < k_0$, with $b > 1$, denoted by $\Phi_>$. It is assumed that the new action $\tilde{S}_{DP}[\bar{\Phi}_<, \Phi_<]$, where $\Phi_<$ is the Fourrier trasnformed field with $0 < |k| < k_0/b$ field, given by

$$\exp\left(-\tilde{S}_{DP}[\bar{\Phi_<}, \Phi_<]\right) = \int D[\bar{\Phi}_>] D[\Phi_>] \exp(-S_{DP}[\bar{\Phi}, \Phi]) \tag{3.54}$$

has the same form as the action S_{DP}. With renormalized propagator $\tilde{G}(k,\omega)$ and coupling constant $\tilde{g}$. The right hand side of (3.54) is calculated with a perturbative expansion and the terms in this expansion can be represented by the Feynman diagrams displayed in Fig. 3.4. The basic elements of the Feynmann diagrams are the arrows, which represent the bare propagator and the three-leg vertex, which represent the interaction term (see Fig. 3.4). The diagrams for the one-loop correction of the propagator and the coupling constant are displayed in Fig. 3.4. From them we obtain that, to one-loop order,

$$\tilde{G}^{-1}(k,\omega) = G_0^{-1}(k,\omega) - \frac{g^2}{2} \int_> d_{k'\omega'} G_0(\frac{k}{2} + k', \frac{\omega}{2} + \omega') G_0(\frac{k}{2} - k', \frac{\omega}{2} - \omega') \tag{3.55}$$

and

$$\tilde{g} = g - 2g^3 \int_> d_{k\omega} G_0^2(k,\omega) G_0(-k,-\omega) \tag{3.56}$$

where the subscript $>$ indicates and integration in the moment shell $k_0/b < |k| < k_0$. In the second step of Wilson's method we make the scaling $k \to bk$ so that we recover the original cut-off. These two steps constitute a renormalization group transformation. By analyzing how the parameters in the action changes under infinitesimal renormalization group transformation one obtains valuable information about the critical behavior. We do not go further here for the case of DP, since we will do this in Sec. 3.4 for an action similar to S_{DP}, where the one-loop corrections of the propagator and

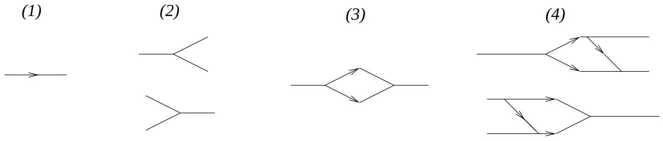

Figure 3.4: The Feynman diagrams for the DP action: (1) bare propagator; (2) merging three-leg vertex, related to the interaction term $\tilde{\Phi}\tilde{\Phi}\Phi$, and branching tree-leg vertex, related to $\tilde{\Phi}\Phi\Phi$; (3) one-loop correction term for the propagator; (4) one loop correction terms for the coupling constant.

the coupling constant have the forms (3.55) and (3.56), respectively. For an introduction to the renormalization group approach see [75, 76] and for a review on the renormalization group approach for DP see [77].

3.2.4 Algebraically distributed waiting times

The CP has only short range interactions, because an infected site can only infect it's nearest neighbors. If one wants a more realistic model for the propagation of a disease it is reasonable to consider long range interactions, and a possible form for the long range interactions is provided by spatial Lévy flights. In this case an infected site, at the origin, can infect a site at some randomly chosen distance with the following asymptotic form

$$P(x) \sim |x|^{-d-\sigma}. \tag{3.57}$$

Such long-range interactions alter the Langevin equation describing the CP, which is the DP Langevin equation. The new Langevin equation, accounting for these Lévy flights has the following extra term

$$\begin{aligned} \nabla^{\sigma}\phi(x,t) &= \int d^d x' P(x')[\phi(x+x',t) - \phi(x,t)] \\ &\propto \int d^d x' |x'|^{-d-\sigma}[\phi(x+x',t) - \phi(x,t)]. \end{aligned} \tag{3.58}$$

It is also possible to consider temporal Lévy flights [78], where the time intervals, instead of having a Poisson distribution, are picked from a probability distribution with the following asymptotic form

$$P(\Delta t) \sim \Delta t^{-1-\kappa}. \tag{3.59}$$

If we consider a model in the DP universality class with these algebraically distributed waiting times, the DP Langevin equation describing it is

$$\partial_t^\kappa \phi(x,t) = D\nabla^2\phi(x,t) - \lambda\phi(x,t) - \frac{\Gamma}{2}\phi(x,t)^2 + \sqrt{\Gamma\phi(x,t)\eta(x,t)}. \tag{3.60}$$

where ∂_t^κ is a fractional derivative [79, 80] operator, defined by

$$\partial_t^\kappa \phi(x,t) = \frac{1}{\Gamma(1-\kappa)}\int_0^\infty dt' t'^{-1-\kappa}(\phi(x,t) - \phi(x,t-t')), \tag{3.61}$$

where $0 \le \kappa \le 1$. The property we are going to use about this fractional derivative is its action on the Fourier modes,

$$\partial_t^\kappa \exp(i\omega t) = (i\omega)^\kappa \exp(i\omega t). \tag{3.62}$$

Because of this property the Langevin equation (3.60), more precisely the action corresponding to it, is amenable to field theoretical calculations: the difference, in relation to the usual DP field theory, is that the term $i\omega$ in the propagator is substituted by a term $(i\omega)^\kappa$. We note that the fractional derivative (3.61) is the Marchaud fractional derivative different than the more usual Riemmann-Liouville fractional derivative (see [80]).

3.3 Boundary induced phase transition into an absorbing state

3.3.1 Basic model definition and simulations

Definition of the model

The model for a boundary induced phase transition into an absorbing state is defined on a one-dimensional semi-infinite discrete lattice where each site

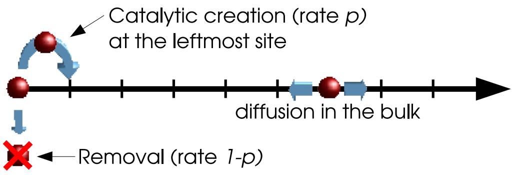

Figure 3.5: Model on a semi-infinite lattice with symmetric diffusion in the bulk and special dynamical rules at the left boundary (see main text).

is either occupied by a particle ($s_i = 1$) or empty ($s_i = 0$). All lattice sites have two neighbors, except for the boundary ($i = 0$) with a single one. The dynamics is a combination of an unbiased random walk in the bulk and a CP-like dynamics at the left boundary. It is implemented as follows:

(a) A particle is randomly selected.

(b) If it is located at the leftmost site, it generates another particle at site 1 with probability p, provided that it is empty ($s_1 = 0$), or it dies ($s_0 = 0$) with probability $1 - p$.

(c) Particles in the bulk perform a symmetric exclusion process, moving to any of their two neighbors with equal probability, provided that the destination site is empty (otherwise nothing happens).

Starting with a single particle at the leftmost site in an otherwise absorbing (i.e. empty) configuration, the process evolves as follows: the initial particle at site 0 either dies or generates another particle at the neighboring site 1. The newly created particle performs a random walk in the bulk until eventually it returns to the origin to create another offspring or to disappear. As we will show, this model has a phase transition into an absorbing state and the universality class it pertains is a new universality class different from DP. We shall argue that it is the simplest universality class of phase transitions into an absorbing state. The control parameter of the model is p and the critical point is located at $p_c = 0.74435(15)$.

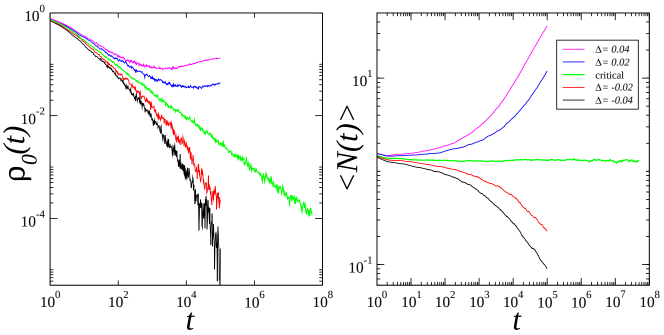

Figure 3.6: Density of particles at the leftmost site $\rho_0(t)$ (left) and the average total number of particles $N(t)$ (right) as functions of time for different values of $\Delta = p - p_c$, below, above, and at criticality. At the critical point, $\rho_0(t)$ decays as $t^{-1/2}$ while $\langle N(t) \rangle$ is essentially constant.

3.3.2 Order parameters

A possible order parameter for this model is the average density of particles at the leftmost site:

$$\rho_0 = \langle s_0 \rangle \,, \tag{3.63}$$

where $\langle \rangle$ stands for ensemble averages. This quantity is plotted in Fig. 3.6 as a function of time for different values of $\Delta := p - p_c$. At the critical point, $\rho_0(t)$ decays algebraically in time as:

$$\rho_0(t) \;\sim\; t^{-\alpha} \tag{3.64}$$

with an exponent $\alpha = 0.50(1)$, compatible with a rational value $\alpha = 1/2$.

Another possibility is to choose as an order parameter the average total number of particles, $\langle N(t) \rangle$, which, as shown in Fig. 3.6, goes to zero for $p < p_c$ and increases steadily for $p > p_c$ (actually, it is limited only by the system size). At criticality, $\langle N(t) \rangle$ is found to be constant and of the order of 1 in the large time limit.

As we saw, in the usual scaling picture of absorbing phase transitions, the critical exponent β is related to the probability that a given site belongs to an infinite cluster generated from a fully occupied lattice at $t = -\infty$.

This quantity tends to zero as the control parameter approaches the critical value from above. Similarly, the exponent β' is related to the probability that a localized seed generates an infinite cluster extending to $t = +\infty$. Therefore, in the supercritical phase ($\Delta > 0$), the averaged activity of the site at the origin for $t \to \infty$ *measured in seed simulations* averaging over all runs, scales as $\rho^s \sim \Delta^{\beta+\beta'}$, where the superscript 's' stands for 'stationary'. At criticality, this function is expected to decay as $\rho(t) \sim t^{-(\beta+\beta')/\nu_\|}$, where $\nu_\|$ is the correlation time exponent. Moreover, in the DP class, because of time-reversal symmetry, $\beta = \beta'$. As shown in [58] (see also below), time reversal symmetry also holds in the present type of models. This implies that in supercritical seed simulations, the density of active sites at the boundary is expected to saturate as:

$$\rho_0^s \sim \Delta^{2\beta}\,, \tag{3.65}$$

while, at criticality:

$$\rho_0(t) \sim t^{-2\beta/\nu_\|}, \tag{3.66}$$

implying that α in Eq. (3.64) is

$$\alpha = 2\beta/\nu_\|\,. \tag{3.67}$$

Assuming that $\alpha = 1/2$, then $\beta/\nu_\| = 1/4$.

Stationary properties

In numerical simulations in the active phase, it takes a very long time, especially for small values of Δ, to reach the steady state. Moreover, we observed the unusual fact that, for $\Delta > 0$, the density ρ_0 goes through a minimum before reaching the stationary state (see left panel of Fig. 3.6 and also [81], where similar non-monotonous curves were reported). However, it turns out that the value ρ_0^m at the minimum and the saturation value ρ_0^s differ by a constant factor, entailing that both quantities scale in the same way, i.e.:

$$\rho_0^m \sim \Delta^{2\beta}\,. \tag{3.68}$$

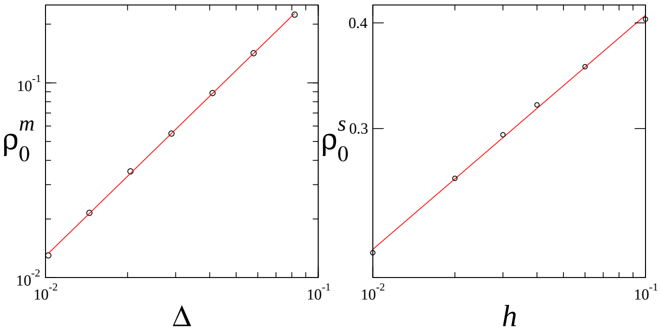

Figure 3.7: Left panel: Density of particles at the leftmost site, at the time when it reaches its minimal value as a function of the distance from criticality Δ. This gives the exponent $\beta = 0.68(5)$. Right panel: The same quantity, at criticality and in the stationary state, as a function of the external field h, giving $\delta_h^{-1} = 0.29(5)$, compatible with the conjectured value 1/3.

Note that this can be true only if the density $\rho_0(t)$ in seed simulations obeys the scaling relation:

$$\rho_0(t) = \Delta^{2\beta}\, R(t\Delta^{\nu_\parallel}) \tag{3.69}$$

i.e. if it is possible to collapse the data by plotting $\rho_0\Delta^{-2\beta}$ versus $t\Delta^{4\beta}$. Indeed, this will be shown to be the case at the end of this section for a 0-dimensional non-Markovian process argued to be in the same universality class.

Relying on this observation, one can determine the value of the exponent β by measuring the density ρ_0^m at the minimum, which is reached much earlier than the stationary state. In Fig. 3.7 we plot ρ_m as a function of Δ, inferring $\beta = 0.68(5)$.

External field

As discussed above in the CP, the external field, conjugate to the order parameter, can be implemented by creating active sites at some constant rate h, thereby destroying the absorbing nature of the empty configuration. At criticality, the external field drives a d+1-dimensional DP process towards

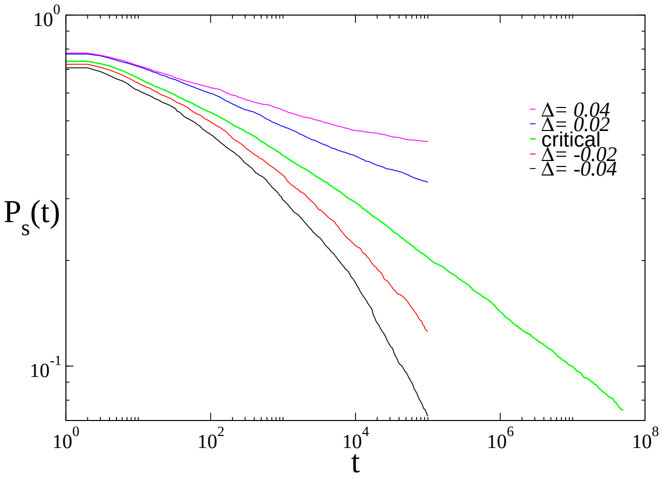

Figure 3.8: Survival probability $P_s(t)$ as function of time below, above, and at criticality. At the critical point, it decays with the exponent $\delta = 0.15(2)$, different from $\beta/\nu_\parallel$, and in agreement with the conjectured value 1/6.

a stationary state with $\rho^s \sim h^{1/\delta_h}$ where $\delta_h^{-1} = \beta/(\nu_\parallel + d\nu_\perp - \beta')$, and $\nu_\perp$ is the correlation length critical exponent.

In the present model, the external field, conjugate to the order parameter ρ_0, corresponds to spontaneous creation of activity at the leftmost site at rate h. The hyperscaling relation (3.15) for δ_h is thus expected to be fulfilled by taking $d = 0$:

$$\rho_0^s \sim h^{1/\delta_h}. \tag{3.70}$$

with

$$\delta_h^{-1} = \beta/(\nu_\parallel - \beta'). \tag{3.71}$$

From this expression, exploiting the fact that $\beta = \beta'$ and using Eq.(3.67) as well as the conjectured rational value $\alpha = 1/2$, a prediction $\delta_h^{-1} = 1/3$ is obtained. Our numerical estimate, $\delta_h^{-1} = 0.29(5)$ (see Fig. 3.7) is compatible with this result.

Survival probability

As is the case in the CP, the survival probability $P_s(t)$ is defined as the fraction of runs that, starting with a single seed at the boundary, survive *at least* until time t. At criticality, this quantity is expected to decay algebraically:

$$P_s(t) \sim t^{-\delta} \tag{3.72}$$

with the so-called survival exponent δ, while in the super-critical regime it saturates in the long time limit. Since $P_s(\infty)$ coincides with the probability for a seed to generate an infinite cluster, the saturation value of the survival probability as a function of the distance from criticality gives the exponent β'. As in DP, one expects $P_s(t)$ to decay in time with an exponent $\delta = \beta'/\nu_\| = 1/4$. However, as shown in Fig. 3.8, one finds a much smaller exponent $\delta = 0.15(2)$. Therefore, the usual relation $\delta = \beta'/\nu_\|$ does not hold. The power-law behavior in Fig. 3.8 is not clean and it may look imprudent to conclude that $\delta \neq \beta'/\nu_\|$ from this numerical evidence. Nevertheless, in the next section with numerical simulations of a different model in the same universality class we obtain convincing results showing that $\delta \neq \beta'/\nu_\|$. We also observed that it is not possible to collapse different curves of $P_s(t)$ for different values of Δ, i.e. the survival probability seems to exhibit an anomalous type of scaling behavior. We expect that off-critical simulations of the survival probability give the exponent β' but the simulation times needed to reach steady state are prohibitively long.

An explanation for the value $\delta = 0.15(2)$, differing from $\beta/\nu_\|$ is given in the following.

Time reversal symmetry

In bond DP, the density $\rho(t)$ in simulations with fully occupied initial state and the survival probability $P_s(t)$ in seed simulations coincide because of time reversal symmetry. Since it also holds for the present model, the survival probability $P_s(t)$ in seed simulations should scale in the same way as the density of active sites at the boundary $\rho_0(t)$ in a process starting with a *fully occupied lattice* in the bulk. A numerical test, which approximates such a situation, confirms this conjecture, i.e. one has $\rho_0(t) \sim t^{-\delta}$ with $\delta \approx 0.15$ for a fully occupied initial state.

This observation can be used to provide an heuristic explanation for the fact that $\delta \neq \beta/\nu_{\|}$. It is known that, if the boundary acts as a sink or perfect trap (e.g. if $p = 0$), then, in a process starting with a fully occupied lattice, one observes a growing depletion zone around the boundary whose linear size $l'(t)$ increases as $l' \sim t^{\alpha_l}$, with $\alpha_l = 1/2$ (see [82] and the next subsection). Thus, the density of active sites decays as $t^{-1/2}$. Hence, the influx of particles from the bulk to the leftmost site may be considered as an effective time-dependent external field $h(t) \sim t^{-1/2}$. Making the assumption that this field varies so slowly that the response of the process (i.e. the actual average activity at the boundary) behaves adiabatically as if the field was constant, then in a critical process starting from an initially fully occupied state:

$$\rho_0(t) \sim t^{-\frac{1}{2\delta_h}} \sim t^{-1/6}. \tag{3.73}$$

Owing to the time reversal property, this quantity should decay as the survival probability. This chain of heuristic arguments leads to the conjecture that the survival exponent is given by $\delta = 1/6$, in agreement with the numerical estimate $\delta = 0.15(2)$. This unusual value of the exponent δ is clearly related to the fact that the present problem is inhomogeneous. The argumentation presented above does not work for the CP, for example, since there is no special site and, therefore, a fully occupied lattice cannot be interpreted as a time dependent field acting on a special site.

Density profile

Now, we consider the density profile $\rho(x,t)$ in the bulk, where $x \in \mathbb{N}$ is the spatial coordinate (distance to the boundary), computed at the critical point. In the left panel of Fig. 3.9, we compare the data collapse of the

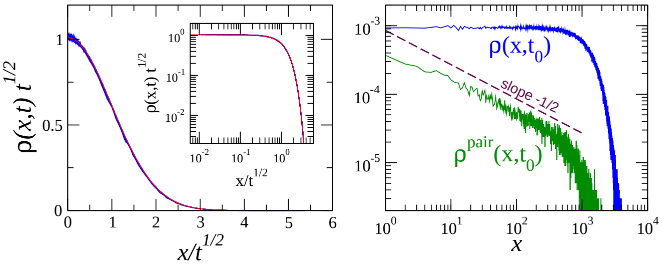

Figure 3.9: Left: Data collapse of the rescaled profiles of the particle density at criticality for $t_0 = 64, 128, \ldots, 8192$ (blue) compared to a Gaussian distribution (red). Inset: The same data collapse in a double-logarithmic representation. Right: Density of particles (blue) and pairs (green) at $t_0 = 10^6$, showing the presence of correlations which decay in space as $x^{-1/2}$, indicating that $\beta/\nu_\perp = 1/2$.

curves $\rho(x,t)t^{1/2}$ as a function of $x/t^{1/2}$ with a Gaussian and observe an excellent agreement, indicating random-walk like behavior with a dynamical exponent $z = 2$. However, in contrast to a simple random walk, particles are mutually correlated. This is illustrated in the right panel of Fig. 3.9, where the connected correlation function between two nearest neighbors

$$\rho^{\text{pair}}(x,t) = \langle \rho(x+1,t)\rho(x,t)\rangle - \langle \rho(x+1,t)\rangle\langle \rho(x,t)\rangle \qquad (3.74)$$

in a system at the critical point is plotted against time. One observes an algebraic decay with distance x as $x^{-1/2}$. According to the standard scaling theory this implies that $\beta/\nu_\perp = 1/2$, confirming that $z = \nu_\parallel/\nu_\perp = 2$. Moreover, these results are in full agreement with field theoretical calculations presented in Ref. [58] (see section 3.3.4), which predict $z = 2$ and $\alpha = 1/2$.

3.3.3 Mean field approximation

Here, we study mean field approximations at different levels. Let us denote by η_i the probability to find a particle at site i. The temporal evolution within a simple (one-site) mean field approximation is given by:

$$\begin{aligned}
\frac{d\eta_0}{dt} &= -(1-p)\eta_0 + \frac{1}{2}\eta_1(1-\eta_0), && (3.75)\\
\frac{d\eta_1}{dt} &= p\eta_0(1-\eta_1) + \frac{1}{2}\left(\eta_2 + \eta_0\eta_1 - 2\eta_1\right), && (3.76)\\
\frac{d\eta_i}{dt} &= \frac{1}{2}\left(\eta_{i+1} + \eta_{i-1} - 2\eta_i\right), \quad \text{for } i = 2, 3, \ldots && (3.77)
\end{aligned}$$

Note that the equations for the boundary site and its neighbor, Eq. (3.75) and Eq. (3.76), include quadratic terms due to the exclusion constraint, while the equation for sites in the bulk, Eq. (3.77), describes in this approximation a symmetric random walk, *i.e.* it is a diffusion equation. The critical point within simple mean field theory (where the equation for η_1 also becomes a diffusion equation) is $p_c = 1/2$.

Considering a localized initial condition at the boundary, $\eta_i = \delta_{i,0}$, after a transient time the densities at sites 0 and 1 should, approximately, coincide. Therefore, from Eq. (3.75) with $\eta_0 \approx \eta_1$, it follows that, at criticality, $\eta_0 \sim t^{-1/2}$.

In the stationary regime, Eq. (3.75) leads to $\eta_0 \sim (p - 1/2)$ for $p \geq 1/2$. From these results we obtain the mean field exponents

$$\alpha^{MF} = 1/2\,, \qquad \beta^{MF} = 1\,. \tag{3.78}$$

To obtain the survival exponent, δ, we follow the arguments of the preceding section and study the decay of activity from a fully occupied lattice, $\eta_i = 1$ for all i. Integrating Eqs. (3.75), Eq. (3.76) and Eq. (3.77) numerically with this initial condition, we obtain an exponent in agreement with

$$\delta^{MF} = 1/4\,. \tag{3.79}$$

A more accurate approximation can be obtained by keeping the correlation between the first two sites, which is expected to be more relevant than the correlation between other neighboring sites. Such a pair-approximation was used recently in a model where a boundary site also plays a special role [83]. In this approximation, the master equation reads:

$$\begin{aligned}
\frac{d\sigma_{00}}{dt} &= (1-p)\sigma_{10} + \frac{1}{2}[\sigma_{01}(1-\eta_2) - \sigma_{00}\eta_2], \qquad (3.80)\\
\frac{d\sigma_{01}}{dt} &= (1-p)\sigma_{11} + \frac{1}{2}[\sigma_{00}\eta_2 - \sigma_{01}(2-\eta_2)],\\
\frac{d\sigma_{10}}{dt} &= -\sigma_{10} + \frac{1}{2}[\sigma_{01} - \sigma_{10}\eta_2 + \sigma_{11}(1-\eta_2)],\\
\frac{d\sigma_{11}}{dt} &= p\sigma_{10} - (1-p)\sigma_{11} + \frac{1}{2}[\sigma_{10}\eta_2 - \sigma_{11}(1-\eta_2)],\\
\frac{d\eta_2}{dt} &= \frac{1}{2}\left(\eta_3 + \sigma_{11} + \sigma_{01} - 2\eta_2\right),\\
\frac{d\eta_i}{dt} &= \frac{1}{2}\left(\eta_{i+1} + \eta_{i-1} - 2\eta_i\right) \text{ for } i = 3, 4, \ldots
\end{aligned}$$

where $\sigma_{s_0 s_1}$ is the probability that the occupation numbers of the first two sites are s_0 and s_1. Numerical integration of these equations leads to an improved critical point estimation, $p_c \approx 0.634$, but to the same mean-field exponents as above.

3.3.4 Related models and field theoretical approaches

Bosonic variant

The model for a boundary induced phase transition into an absorbing state defined above is fermionic. We now consider the following bosonic variant:

(a) A particle is chosen randomly.

(b) If the particle is located at the leftmost site it can: create another particle at the leftmost site ($n_0 = n_0 + 1$) at rate λ, die ($n_0 = n_0 - 1$) at rate σ, or diffuse to the next neighbor at rate D.

(c) If the particle is located in the bulk, it diffuses to the right or to the left at equal rates D.

The corresponding master equation is

$$\begin{aligned}
\frac{dP(\{n\},t)}{dt} &= \lambda\big[(n_0-1)P(n_0-1,...,t)-n_0P(\{n\},t)\big] \\
&+ \sigma\big[(n_0+1)P(n_0+1,...,t)-n_0P(\{n\},t)\big] \\
&+ D\Big[\sum_{\langle ij\rangle}P(...,n_i-1,n_j+1,...,t) \qquad (3.81)\\
&+ P(...,n_i+1,n_j-1,...,t)-2P(\{n\},t)\Big],
\end{aligned}$$

giving the following Hamiltonian,

$$\begin{aligned}
\hat{H} &= D\sum_{\langle ij\rangle}(\hat{a}_i^\dagger-\hat{a}_j^\dagger)(\hat{a}_i-\hat{a}_j) \qquad (3.82)\\
&\quad +\sigma(\hat{a}_0^\dagger-1)\hat{a}_0+\lambda\hat{a}_0^\dagger(1-\hat{a}_0^\dagger)\hat{a}_0.
\end{aligned}$$

As is the case for the bosonic contact process [84], the equations for the time evolution of the density of particles close allowing an exact solution. From the Heisenberg equation of motion, $\frac{d\hat{B}}{dt}=[\hat{H},\hat{B}]$ and Eq. (3.82), one obtains:

$$\begin{aligned}
\frac{d\rho_0}{dt} &= D(\rho_1-\rho_0)+\Delta\rho_0 \qquad (3.83)\\
\frac{d\rho_i}{dt} &= D(\rho_{i+1}+\rho_{i-1}-2\rho_i) \qquad i=1,2,3\dots
\end{aligned}$$

where $\rho_i(t)=\langle a_i^\dagger(t)a_i(t)\rangle=\langle a_i(t)\rangle$ and $\Delta=\lambda-\sigma$.

From these equations, we can see that the critical point is $\Delta=0$, where Eq.(3.83) is a diffusion equation. In the continuum limit, Eq. (3.83) reads:

$$\frac{\partial\rho(x,t)}{\partial t}=\frac{\partial^2\rho(x,t)}{\partial x^2}+\Delta\delta(x)\rho(x,t) \qquad (3.84)$$

where x is the spatial coordinate and, without loss of generality, we have set $D=1$. We note that in order to take the continuum limit in equation (3.83), a site -1, with $\rho_{-1}=\rho_0$, has to be introduced, so that appropriate boundary conditions are satisfied. The solution of this inhomogeneous diffusion equation is:

$$\rho(x,t)=\int_0^\infty\delta(\zeta)G(x,\zeta,t)d\zeta$$

$$+\int_0^t \int_0^\infty \Delta\delta(\zeta)\rho(\zeta,\tau)G(x,\zeta,t-\tau), d\zeta d\tau \tag{3.85}$$

where $G(x,\zeta,t) = (e^{-(x+\zeta)^2/(4t)} + e^{-(x-\zeta)^2/(4t)})/(\sqrt{\pi t})$ is the Green's function and the first term on the right hand side comes from the initial condition $\rho(x,0) = \delta(x)$. From Eq. (3.85) we have

$$\rho_0(t) = \frac{2}{\sqrt{\pi t}} + 2\Delta \frac{d^{-1/2}}{dt^{-1/2}}\rho_0(t) \tag{3.86}$$

where $\rho_0(t) = \rho(0,t)$, and the operator $\frac{d^{-1/2}}{dt^{-1/2}}$, defined by

$$\frac{d^{-1/2}}{dt^{-1/2}}f(t) = \int_0^t \frac{f(\tau)}{\sqrt{\pi(t-\tau)}}d\tau, \tag{3.87}$$

is a half integral (Riemann-Liouville) operator [79]. Equation (3.86) involves (owing to the delta function in the interaction term in Eq. (3.84)) only the density at the leftmost site. This justifies the mapping of this model onto an effective one-site non-Markovian process (see below). Using some rules for half integration [79] to solve Eq. (3.86), we find:

$$\rho_0(t) = \frac{2}{\sqrt{\pi t}} + 4\Delta \exp(4\Delta^2 t)\mathrm{erf}(-2\Delta\sqrt{t}), \tag{3.88}$$

where erf(x) is the error function. This implies that, above the critical point, ρ_0 grows exponentially in the long time limit, and does not reach a stationary value, *i.e.* there is a first order transition and, hence, $\beta = 0$ in this bosonic model. From equation Eq. (3.88), we deduce $\beta' = 1$ and $\nu_\parallel = 2$. We have not been able to calculate the survival-probability exponent exactly, but numerical simulations suggest $\delta = 1/4$, in agreement with the mean field exponent.

Partially bosonic variant

Let us now introduce a *partially bosonic* variant of the previous model by retaining the exclusion constraint only at the boundary, but not in the bulk. The rules, in this case, are:

(a) A particle is randomly chosen.

(b) If it is located at the leftmost site, it can generate a particle at site 1 (provided that $s_1 = 0$) with probability p or die ($s_0 := 0$) with probability $1 - p$.

(c) Particles in the bulk diffuse to the right or to the left with the same probability, 1/2.

Numerical simulations show that this variant exhibits the same critical behavior as the original model, even though the critical point is shifted to $p_c = 0.6973(1)$. This shows that the fermionic constraint is relevant only at the boundary, where it induces a saturation of the particle density and leads the transition to become continuous.

Models with pair annihilation at the boundary

In the models discussed so far, particles at the boundary either create an offspring or die spontaneously at some rate. Instead, a very similar model was perviously introduced in Ref. [58], for which particles at the boundary annihilate only in *pairs*. In its fermionic variant, particles at sites 0 and 1 annihilate with each other (provided that both sites are occupied) at some rate, while isolated particles at the boundary cannot disappear:

$$\begin{aligned} \text{present models:} \quad & A \to 2A\,, \quad A \to \emptyset\,, \\ \text{models of Ref. [58]:} \quad & A \to 2A\,, \quad 2A \to \emptyset\,. \end{aligned}$$

Analogously, one can define a bosonic version, in which two particles at the boundary can annihilate. In the following discussion we consider these two variants in d spatial dimensions where, as is the case $d = 1$, only a single site has “special” dynamics.

In the bosonic case, proceeding as above (see Eq.(3.82)) one obtains the following time evolution operator,

$$\begin{aligned}\hat{H} &= D\sum_{\langle ij\rangle}(\hat{a}_i^\dagger - \hat{a}_j^\dagger)(\hat{a}_i - \hat{a}_j) \\ &\quad +\sigma[(\hat{a}_0^\dagger)^2 - 1]\hat{a}_0^2 + \lambda\hat{a}_0^\dagger(1-\hat{a}_0^\dagger)\hat{a}_0. \end{aligned}\tag{3.89}$$

which gives, using the same procedure we used to derive the DP action, leads to the following action [58]

$$S[\bar{\phi},\phi] = \int d^dx dt\Big(\bar{\phi}(\partial_t - a\delta^d(x) - \nabla^2)\phi + \delta^d(x)\frac{g}{2}\bar{\phi}\phi(\phi-\bar{\phi})\Big), \tag{3.90}$$

where, all terms, except for the Laplacian, are multiplied by a δ function at the boundary; *i.e.* the non-diffusive part of the dynamics operates only at the boundary. An ϵ-expansion analysis of Eq.(3.89) was done by Deloubrière and van Wijland [58], it gives $\alpha = 1/2$ and $z = 2$ as exact results to all orders of perturbation theory, and $\beta = 1-3(4-3d)/8$, up to first order in $\epsilon = 4/3-d$ around the critical dimension $d_c = 4/3$. We perform this ϵ-expansion in the next section and compare it with simulations using a (0+1)-dimensional non-Markovian model that is in the same universality class, where performing a simulation in a situation that corresponds to a fractional dimension in the present problem is a trivial task.

Performing simulations with this bosonic model we obtain the following results. From the time decay of $\rho_0(t)$, as shown in Fig. 3.10, we determine $\delta = 0.21(3)$, while from a finite size scaling analysis of the saturation values of the order parameter at criticality we measure $\beta/\nu_\perp = 0.51(2)$ (see Fig. 3.10), in reasonable agreement with the expected results, $\delta = 1/6$ and $\beta/\nu_\perp = 1/2$, respectively. Moreover, from spreading simulations (not shown) we estimate $\alpha \approx 1/2$ and $z \approx 2$. All the exponents are in agreement with the ones presented in the previous section for single particle annihilation models.

Actually, a simple argument explains why the model of section 3.3.1 and the pair-annihilation model share the same critical behavior. This is plausible because the chain reaction $A \to 2A \to \emptyset$ in the model with pair annihilation

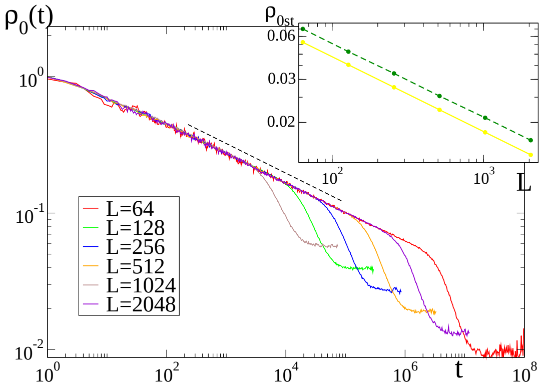

Figure 3.10: Temporal behavior of ρ_0 for the bosonic pair-annihilating model, starting from a homogeneous initial condition for different system sizes (from $L = 64$ to $L = 2048$). The exponent $\beta/\nu_\perp$ can be measured from the scaling of the different saturation values as a function of system size (see inset; yellow line). The inset also shows (dashed green line) the scaling of saturation values for the fermionic version of the same model, showing the same type of scaling.

generates effectively the reaction $A \longrightarrow \emptyset$ of the model considered with CP-like dynamics. Hence, the field theoretical predictions discussed above apply also to the CP-like model. In $d = 1$, the one-loop prediction $\beta = 5/8 = 0.625$ [58], is not far from the exponent measured in section 3.3.1, $\beta = 0.68(5)$.

On the other hand, the fermionic version of the pair-annihilating model has been conjectured to yield in a different universality class, and a prediction for its critical exponents is made in [58] (for instance, $\beta = 1$). Our numerical simulations disprove such a claim; all the measured critical exponents for the fermionic variant of the pair-annihilation model are numerically indistinguishable from their bosonic counterparts (see Fig. 3.10).

In summary, all the defined models, either with single particle annihilation or with pair-annihilation, fermionic or bosonic, exhibit a boundary induced phase transitions and, except for one of them, they all are continuous and share the same critical behavior. The exception to this rule is the CP-like model without a fermionic constraint at the boundary, which lacks of a saturation mechanism in the active phase, leading to unbounded growth of particle density at the leftmost site above the critical point and to a discontinuous transition.

3.3.5 Relation to a $(0 + 1)$-dimensional non-Markovian process

On an heuristic basis, we explain the relation between boundary induced phase transitions into an absorbing state and a (0 + 1)-dimensional non-Markovian process. Consider the fermionic version of the model. A particle at the origin may die or create a new particle that will go for a random walk coming back to the origin after a time τ. What happens during this random walk is irrelevant from the perspective of the leftmost site; the only relevant aspect is the time needed for a created particle to come back to the boundary. Once it returns it may die or create new offsprings which, on their turn, will undergo random walks in the bulk.

Our simulations above show that the fermionic constraint is irrelevant in the bulk. Therefore, we can consider without lost of generality the bulk-bosonic version in which there is no effective interaction among diffusing particles. In this case, the probability distribution of the returning time to the origin has the well-known asymptotic form [85]:

$$P(\tau) \sim \tau^{-3/2} \, . \tag{3.91}$$

Taking all these elements into account we define the following non-Markovian model on a single site:

(a) Set initially $s(t) := \delta_{t,0}$ for all times, t.

(b) Select the lowest t for which $s(t) = 1$.

(c) With probability p, generate a waiting time τ according to the distribution Eq. (3.91), truncate it to an integer, and set $s(t + \tau) := 1$; otherwise (with probability $1 - p$) set $s(t) := 0$.

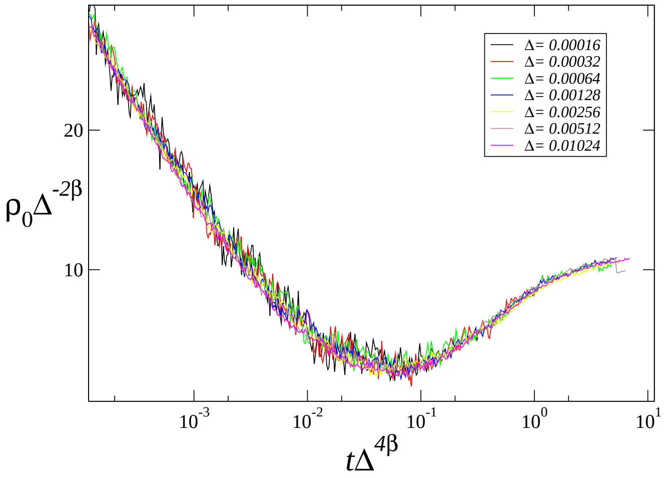

Figure 3.11: Off-critical data collapse with the one-site model: $\langle s(t)\rangle\Delta^{-2\beta}$ as a function of $t\Delta^{4\beta}$ for different values of Δ, with $\beta = 0.71(2)$.

(d) Go back to (b).

The process runs until the system enters the absorbing state ($s(t') = 0$ for all $t' > t$) or a predetermined maximum time is exceeded. The density of particles at the leftmost site of the original model is related to $\langle s(t)\rangle$ in the single-site model, the survival probability at time t is given by the fraction of runs surviving at least up to t, and the initial condition $s(t) := \delta_{t,0}$ corresponds to start with a single particle at the boundary in the full model. Critical exponents can be defined as in the original model. However, the simulation results for the single-site non-Markovian model are more reliable because it is possible to perform much longer runs and, in the case of off-critical simulations, one can work with smaller values of Δ. With time-dependent simulations at the critical point $p_c = 0.574262(2)$, we obtained $\alpha = 0.500(5)$ and $\delta = 0.165(3)$, in good agreement with the conjectured values $\alpha = 1/2$ and $\delta = 1/6$. As an example, we show the results of supercritical simulations in Fig. 3.11, where we obtained a convincing data collapse by plotting $\langle s(t)\rangle\Delta^{-2\beta}$ as a function of $t\Delta^{4\beta}$ for different values of Δ with $\beta = 0.71(2)$. The latter estimate is in agreement with $\beta = 0.68(5)$, coming from the original model.

This mapping explains why the fermionic interaction in the bulk does not alter the critical behavior. As we observed with simulations the probability distribution of returning time to the origin has the asymptotic behavior (3.91), also when we keep the exclusion principle in the bulk. Therefore, follows that bosonic models with a saturation mechanism and the fermionic model should have the same critical behavior.The present model is a specific case of a more general non-Markovian one-site model that we study in the next section.

3.4 The timeline spreading process

3.4.1 Model definition

In the present section we consider a class of probabilistic spreading processes on a timeline. As sketched in Fig. 3.12, the timeline consists of discrete sites $t \in \mathbb{Z}$ which can be either active or inactive. After specifying a certain initial configuration of active and inactive sites along this timeline, the process evolves dynamically by subsequent updates of the lattice site according to the following probabilistic rules:

- If the updated site at time t_u is active, it attempts to active $n(t_u)$ lattice sites in the future, where $n(t_u) = 0, 1, 2, \ldots$ is randomly selected from a given distribution with a finite average $\bar{n}$.
- For each of these attempts a random time interval $\Delta t = 1, 2, \ldots$ is drawn from another probability distribution $P(\Delta t)$. If the target site at time $t_u + \Delta t$ is still inactive it will be activated, otherwise nothing happens.

In the following we are interested in the special case where the time intervals are asymptotically distributed by a power law

$$P(\Delta t) \sim (\Delta t)^{-1-\kappa}, \tag{3.92}$$

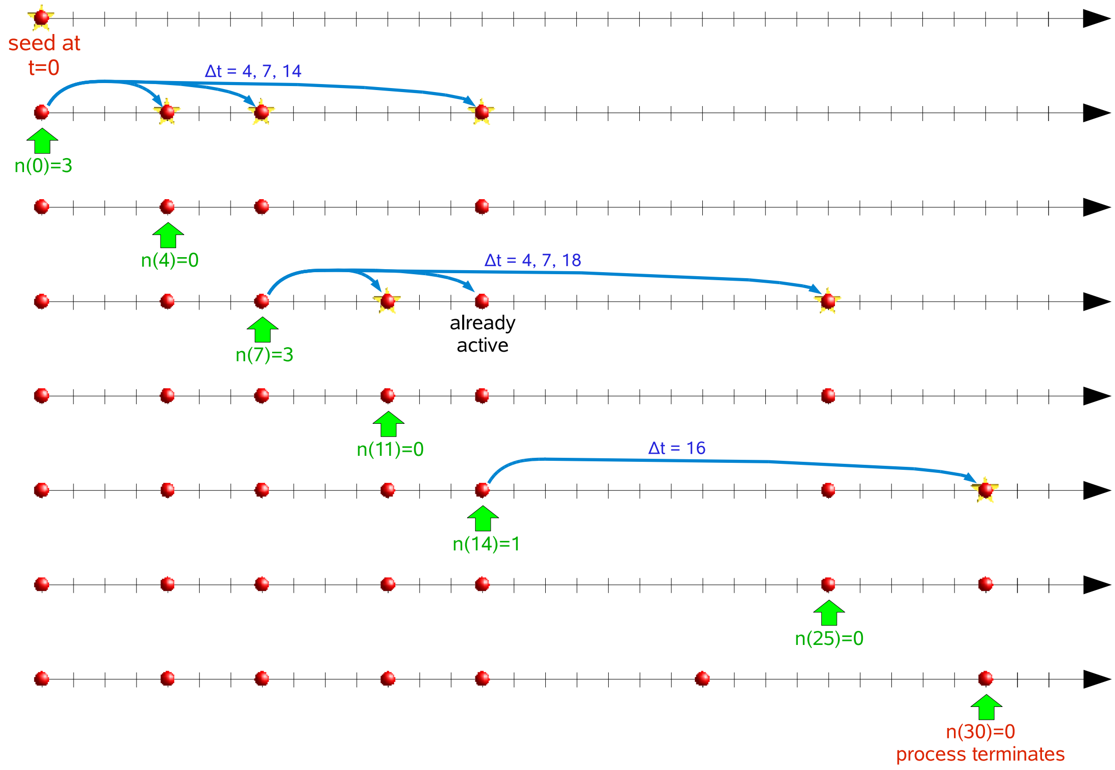

Figure 3.12: Timeline spreading process (TSP): Example of a temporal evolution starting with a single active site at $t = 0$. Active sites are updated from left to right, as marked by the green arrows. The blue arrows indicate how activity spreads by Lévy flights over randomly chosen displacements Δt.

where $0 < \kappa < 1$. We also choose $n(t_u)$ from the probability distribution $p^{n(t_u)}(1-p)$, which gives $\bar{n} = p/(1-p)$. The case $\kappa = 1/2$ corresponds to the model presented in the final of the last section and varying κ corresponds to vary the dimension of the models for boundary induced phase transitions into an absorbing state. In the following we use the TSP to study the present universality class for different values of κ, using numerical simulations and the field theoretical approach.

We note that the TSP is also of conceptual interest. According to a well-known theorem by Landau, phase transitions in *equilibrium* models with short-range interactions require at least two space dimensions. In the nonequilibrium case, however, phase transitions in models with short-range couplings such as DP are possible in one spatial dimension. Here we demonstrate, with the TSP, that by introducing a non-Markovian (i.e. temporally nonlocal) dynamics phase transitions are possible even in zero space dimensions.

3.4.2 Field theoretical approach for the TSP

In this section we describe a field-theoretic approach for the TSP which allows one to compute the critical exponents perturbatively by a loop expansion. This field theory was first introduced by Deloubrière and van Wijland, somewhat hidden in an appendix of Ref. [58]. Here we rederive their results independently, calculating the critical exponents to one-loop order and confirming their results.

The field-theoretic action

The ingredients of the TSP are: CP-like dynamics, 0 dimensions and temporal Lévy flights. From the first fact follows that the action for the TSP should have the same structure as the action for DP. Since it is a one-site process we take out the Laplacian form the DP action. Because of the algebraically distributed waiting times the regular time derivative has to be replaced by the fractional derivative (3.61). From this reasoning arises the action

$$S[\phi,\bar\phi] = \int_{-\infty}^{+\infty} dt\ \bar\phi(t)\Big[\tau\tilde\partial_t^\kappa - a\Big]\phi(t) + \frac{g}{2}\int_{-\infty}^{+\infty} dt\ \bar\phi(t)\Big[\phi(t)-\bar\phi(t)\Big]\phi(t)\,. \tag{3.93}$$

Deloubrière and van Wijland showed that this action can be formally obtained from the action (3.90) by integrating out the fields related to diffusion.

Rapidity reversal symmetry

As pointed out in [58] the well-known rapidity reversal symmetry of directed percolation still holds in the present case, i.e. the field-theoretic action derived above is invariant under the replacement

$$\phi(t) \to -\bar{\phi}(-t)\,, \quad \bar{\phi}(t) \to -\phi(-t)\,. \tag{3.94}$$

To see this it is convenient to represent the action in frequency space by introducing the Fourier transforms $\Phi(\omega) := \int_{-\infty}^{+\infty} dt\, e^{-i\omega t}\phi(t)$ and likewise $\bar{\Phi}(\omega)$, turning the action (3.93) into

$$\begin{aligned} S_0 &= \int_{-\infty}^{+\infty} \frac{d\omega}{2\pi}\, \bar{\Phi}(-\omega)\Big[\tau(-i\omega)^{\kappa} - a\Big]\Phi(\omega) \qquad (3.95)\\ S_{\rm int} &= \frac{g}{2}\int_{-\infty}^{+\infty} \frac{d\omega_1}{2\pi} \int_{-\infty}^{+\infty} \frac{d\omega_2}{2\pi}\, \bar{\phi}(-\omega_1)\Big[\phi(\omega_1+\omega_2) - \bar{\phi}(\omega_1+\omega_2)\Big]\phi(-\omega_2)\,, \end{aligned}$$

As can be seen both parts of the action are invariant under the replacement $\Phi(\omega) \to -\bar{\Phi}(-\omega)$ and $\bar{\Phi}(\omega) \to -\Phi(-\omega)$, hence the rapidity reversal symmetry still holds. This symmetry implies that the scaling dimensions of the fields ϕ and $\bar{\phi}$ have to be identical, i.e., $\beta = \beta'$.

Dimensional analysis

Using the rapidity reversal symmetry the theory at tree level is expected to be invariant under the scale transformation

$$t \to \lambda t\,, \qquad \phi \to \lambda^{-\chi}\phi\,, \qquad \bar{\phi} \to \lambda^{-\chi}\bar{\phi} \tag{3.96}$$

with a time dilatation factor $\lambda > 0$ and a field exponent $\chi = \beta/\nu_{\|}$. In the Fourier-transformed action this corresponds to the replacement

$$\omega \to \lambda^{-1}\omega\,, \qquad \Phi \to \lambda^{1-\chi}\Phi\,, \qquad \bar{\Phi} \to \lambda^{1-\chi}\bar{\Phi}\,. \tag{3.97}$$

It is easy to check that this scale transformation can be compensated by changing the coefficients as

$$\tau \to \lambda^{2\chi-1+\kappa}\tau\,, \quad a \to \lambda^{2\chi-1}a\,, \quad g \to \lambda^{3\chi-1}g\,. \tag{3.98}$$

In order to establish scale invariance at tree level all coefficients have to be invariant. Firstly, the invariance of τ implies that $\chi = (1-\kappa)/2$. Secondly, we have $2\chi - 1 = \kappa > 0$ so that coefficient a is relevant, hence it has to be set to zero which is just the mean-field critical point. Finally, scale invariance at tree level requires the coefficient g to be irrelevant, i.e. $3\chi - 1 < 0$ or equivalently $\kappa < 1/3$. Therefore the value

$$\kappa_c = \frac{1}{3} \tag{3.99}$$

plays the role of a lower critical threshold where mean-field behavior sets in, comparable to the upper critical dimension d_c in ordinary directed percolation. For $\kappa < \kappa_c$ the model is expected to exhibit mean-field behavior with the critical exponents

$$\beta^{\mathrm{MF}} = 1 \,, \qquad \nu_{\|}^{\mathrm{MF}} = \kappa^{-1} \,. \tag{3.100}$$

The case $\kappa > \kappa_c$, where fluctuation effects have to be taken into account, will be addressed in the following section.

Wilsons renormalization group scheme

For $\kappa > 1/3$, where the critical behavior of the TSP is influenced by fluctuations, the integrals in the loop expansion diverge in the limit $\omega \to \infty$. In this case the bare continuum description is no longer meaningful, instead the discrete nature of the process has to be restored through the back door by regularizing the integrals.

In the following we apply the Wilson's renormalization group method, explained in Sec. 3.2, to the TSP. In this case momenta is absent, we introduce a cutoff Ω in the frequencies instead, i.e., the integration range of the loop integrals is restricted to $\omega \in [-\Omega, +\Omega]$. Here we invert the order of the two steps, explained in Sec. 3.2, of a renormalization group transformation, that is: first we perform a infinitesimal scaling transformation with $\lambda = 1 - \epsilon$ and after that we perform the shell integration with $|\omega| \in [\Omega, \, (1+\epsilon)\Omega]$ to recover the original cut-off. From Eq. (3.98) we have that

$$\begin{aligned}\partial_\epsilon \ln \tau &= 1-\kappa-2\chi-L_\tau \\ \partial_\epsilon \ln a &= 1-2\chi-L_a \\ \partial_\epsilon \ln g &= 1-3\chi-L_g,\end{aligned} \tag{3.101}$$

where the loop corrections L_τ, L_a, and L_g depend on the parameters τ, a, g as well a the cutoff Ω and will be computed below.

Renormalization hypothesis of the Lévy operator

In preceding studies of models with long-range interactions by Lévy flights it turned out that field-theoretic loop corrections do not renormalize the fractional derivative itself, instead they always renormalize the corresponding short-range operator. Technically this can be traced back to the fact that loop expansions always yield power series in $\vec{k}$ and ω with *integral* powers which correspond to ordinary derivatives in real space. This observation implies that fractional derivatives are modified under scale transformations exclusively by their scaling part, giving rise to an *exact* scaling relation among critical exponents. Assuming the same to be true in the present case, this means that $L_\tau = 0$ even in the fluctuation-dominated regime $\kappa > \kappa_c$, implying the scaling relation

$$\chi = \frac{\beta}{\nu_\parallel} = \frac{1-\kappa}{2}\,. \tag{3.102}$$

This scaling relation is expected to hold exactly over the full range $0 < \kappa < 1$ to all orders of perturbation theory. As a direct consequence, the density in seed simulations $\varrho(t)$, which is proportional to $G(t) = \langle\phi(t)\bar{\phi}(0)\rangle$, is predicted to decay as

$$\varrho(t) \sim t^{-2\beta/\nu_\parallel} \sim t^{-(1-\kappa)} \tag{3.103}$$

for any $0 < \kappa < 1$, i.e. the time-decay exponent of the density is given by

$$\alpha = 1-\kappa. \tag{3.104}$$

In numerical simulations (see below) this prediction is confirmed with high precision.

Analysis of the renormalization group flow

Since the action for the TSP has the same structure as the action for DP the corrections in the propagator and the coupling constant, to one-loop order, have the forms (3.55) and (3.56), respectevelly. Therefore we have

$$\tilde{G}^{-1}(\omega) = G_0^{-1}(\omega) + \frac{g^2}{2}\int_> \frac{d\omega'}{2\pi} G_0(\frac{\omega}{2}+\omega')G_0(\frac{\omega}{2}-\omega') \tag{3.105}$$

and

$$\tilde{g} = g - 2g^3 \int_> \frac{d\omega}{2\pi} G_0^2(\omega)G_0(-\omega)\,. \tag{3.106}$$

Here $G_0(\omega) = (\tau(-i\omega)^\kappa - a)^{-1}$ is the free propagator and $' >'$ denotes integration over the frequency shell $|\omega| \in [\Omega,\, (1+\epsilon)\Omega]$. Integrating and expanding to lowest order one obtains

$$\begin{aligned} \int_> \frac{d\omega'}{2\pi} G_0(\frac{\omega}{2}+\omega')G_0(\frac{\omega}{2}-\omega') &= \frac{\epsilon\Omega}{\pi(a^2+\tau^2\Omega^{2\kappa}-2a\tau\Omega^\kappa\cos\left(\frac{\pi\kappa}{2}\right))} + \mathcal{O}(\omega^2) \\ \int_> \frac{d\omega'}{2\pi} G_0^2(\omega')G_0(-\omega') &= \frac{-\epsilon\Omega(a-\tau\Omega^\kappa\cos\left(\frac{\pi\kappa}{2}\right))}{\pi(a^2+\tau^2\Omega^{2\kappa}-2a\tau\Omega^\kappa\cos\left(\frac{\pi\kappa}{2}\right))}\,. \end{aligned} \tag{3.107}$$

Therefore, the loop corrections are given by

$$L_a = \frac{g^2\Omega}{2\pi a\left(a^2+\tau^2\Omega^{2\kappa}-2a\tau\Omega^\kappa\cos\left(\frac{\pi\kappa}{2}\right)\right)} \tag{3.108}$$

$$L_g = -\frac{2g^2\Omega\left(a-\tau\Omega^\kappa\cos\left(\frac{\pi\kappa}{2}\right)\right)}{\pi\left(a^2+\tau^2\Omega^{2\kappa}-2a\tau\Omega^\kappa\cos\left(\frac{\pi\kappa}{2}\right)\right)^2} \tag{3.109}$$

Together with the scaling relation (3.102) the RG equations read

$$\begin{aligned} \partial_\epsilon \ln\tau &= 0 \\ \partial_\epsilon \ln a &= \kappa - L_a \\ \partial_\epsilon \ln g &= \frac{3\kappa-1}{2} - L_g\,. \end{aligned} \tag{3.110}$$

Their non-trivial fixed point is given by

$$L_a^* = \kappa\,, \qquad L_g^* = \frac{3\kappa - 1}{2} \tag{3.111}$$

or, in terms of the original parameters, by

$$\begin{aligned} a^* &= \frac{\kappa\Omega^\kappa \left(2(7\kappa-1)\cos\left(\frac{\pi\kappa}{2}\right) + \sqrt{2}\sqrt{\cos(\pi\kappa)(1-7\kappa)^2 + (14-17\kappa)\kappa - 1}\right)}{22\kappa - 2} \\ (g^*)^2 &= \frac{8\pi\kappa^2\tau^3\Omega^{3\kappa-1}}{(11\kappa-1)^3}\Bigg[-\cos\left(\frac{3\pi\kappa}{2}\right)(1-7\kappa)^2 \\ &\qquad +\sqrt{2}\cos(\pi\kappa)\sqrt{\cos(\pi\kappa)(1-7\kappa)^2 + (14-17\kappa)\kappa - 1}(1-7\kappa) \\ &\qquad +(\kappa(73\kappa-22)+1)\cos\left(\frac{\pi\kappa}{2}\right) \\ &\qquad +4\sqrt{2}\kappa\sqrt{\cos(\pi\kappa)(1-7\kappa)^2 + (14-17\kappa)\kappa - 1}\Bigg]\,. \end{aligned} \tag{3.112}$$

In order to determine the exponent $\nu_\parallel$ let us consider the RG flow in the vicinity of this fixed point. The linearized flow field is given by the matrix

$$M = \left.\begin{pmatrix} \partial_a a(\kappa - L_a) & \partial_a a(\frac{3\kappa-1}{2} - L_g) \\ \partial_g g(\kappa - L_a) & \partial_g g(\frac{3\kappa-1}{2} - L_g) \end{pmatrix}\right|_{a=a^*,g=g^*} \tag{3.113}$$

and can be computed explicitly

$$M = \begin{pmatrix} (1-\kappa)/4 & f(\kappa) \\ -2\kappa & 1-3\kappa \end{pmatrix}\,, \tag{3.114}$$

where

$$\begin{aligned} f(\kappa) &= 2\kappa\csc^2\left(\frac{\pi\kappa}{2}\right) - \frac{23\kappa}{4} - \frac{1}{4\kappa} + 2 \\ &\quad -\frac{1}{2\sqrt{2}}\sqrt{\cos(\pi\kappa)(1-7\kappa)^2 + (14-17\kappa)\kappa - 1}\cot\left(\frac{\pi\kappa}{2}\right)\csc\left(\frac{\pi\kappa}{2}\right)\,. \end{aligned} \tag{3.115}$$

The eigenvalues of this 2 × 2 matrix can be computed explicitly. Defining the distance

$$\varepsilon = \kappa - \kappa_c = \kappa - \frac{1}{3} \tag{3.116}$$

which plays a similar role as the dimensional difference $\varepsilon = d_c - d$ in field theories with spatial degrees of freedom, and expanding the eigenvalues to lowest order in ε one obtains

$$\lambda_1 = -3\varepsilon + \mathcal{O}(\varepsilon^2)\,, \qquad \lambda_2 = \frac{1}{3} + \frac{\varepsilon}{4} + \mathcal{O}(\varepsilon^2)\,. \tag{3.117}$$

The first eigenvalues is always negative while the positive one describes how the critical parameter vanishes under rescaling. Therefore, one can identify the second eigenvalue with $\nu_\| = \lambda_2^{-1}$, leading to the main result

$$\nu_\| = 3 - \frac{9}{4}\varepsilon + \mathcal{O}(\varepsilon^2)\,. \tag{3.118}$$

Together with the exact scaling relation (3.102) this implies

$$\beta = 1 - \frac{9}{4}\varepsilon + \mathcal{O}(\varepsilon^2)\,. \tag{3.119}$$

These findings are in full agreement with the results by Deloubrière and van Wijland in the Appendix of Ref. [58]. Their calculation involves a dimension-like parameter d which is related to the control parameter κ by $d = 2 - 2\kappa$.

3.4.3 Numerical results

First we determined the critical parameter p_c and estimated the exponent α for various values of κ. It turned out that the scaling relation $\alpha = 1 - \kappa$ (see Eq. (3.104)) is obeyed with at least three digits accuracy in the range $0.3 < \kappa < 0.8$ so that we have no doubt that this scaling relation is correct. That is why we decided to consider this scaling relation as given and to use it for a precise determination of the critical point. The results are listed in Table 3.2. As can be seen, the estimates are less accurate for very small values of κ, where the Lévy flights become extremly long-ranged, as well as in the limit $\kappa \to 1$, where the particle densities are so high so that the algorithm is no longer efficient.

The same type of simulations was used to measure the survival probability $P_s(t)$ at the critical point. As shown in the right panel of Fig. 3.13, the power laws are less clean in this case. A conservative analysis leads to the estimates reported in Table 3.2. Apart from a slight systematic deviation inside the

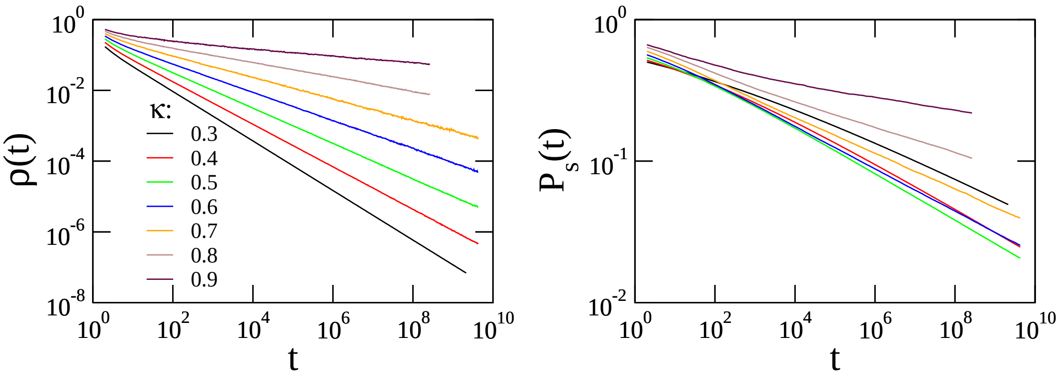

Figure 3.13: Decay of the density of active sites $\varrho(t)$ (left) and the survival probability $P_s(t)$ (right) in seed simulations of the TSP at criticality for various values of κ averaged over 4×10^5 up to 1.4×10^8 runs. The density of active sites shows a very clean power law $\varrho(t) \sim t^{-(1-\kappa)}$. The survival exponent δ is estimated by averaging over the last four decades in the right panel.

error bars, these estimates are in good agreement with the predicted value δ_c which will be derived below in Eq. (3.123).

In order to determine the exponent $\nu_\|$ we performed extensive off-critical simulations. A typical data set is shown in the left panel of Fig. 3.14. Assuming the usual scaling form $\varrho(t, p-p_c) \simeq t^{-\alpha} R\big(t(p-p_c)^{\nu_\|}\big)$ and using the scaling relation $\alpha = 1-\kappa$ the curves should collapse if $t^\alpha \varrho$ is plotted against $t(p-p_c)^{\nu_\|}$. As demonstrated in the right panel of Fig. 3.14, one obtains a very clean collapse below and above criticality. This allowed us to estimate the exponent $\nu_\|$, as listed in Table 3.2.

As a visual summary the estimates for the critical exponents are plotted as functions of κ in Fig. 3.15 and compared with the analytical predictions. As expected, the field-theoretic one-loop expansion is tangent to the data in $\kappa = \kappa_c = 1/3$, as indicated by the red lines. As can be seen, our numerical simulations fully support the field-theoretic results. They would even allow us to verify the results of a future two-loop calculation by fitting a parabola.

κ	p_c	$\nu_\parallel$	δ	δ_c	β
0	1/2	2	0	0	1
0.1	0.501(1)	2.2(1)	0.04(2)	0.050	1
0.2	0.51080(2)	2.50(8)	0.09(1)	0.100	1
0.3	0.525720(5)	2.86(5)	0.14(1)	0.150	1
1/3 (MF)	0.532231(2)	3.00(2)	0.155(10)	0.167	1.00(2)
0.35	0.535762(2)	2.98(2)	0.160(10)	0.169	0.97(2)
0.375	0.541379(2)	2.95(2)	0.164(10)	0.169	0.93(2)
0.4	0.547357(2)	2.92(2)	0.165(10)	0.171	0.88(2)
0.45	0.560264(5)	2.86(2)	0.169(3)	0.171	0.79(2)
0.5	0.574262(2)	2.83(2)	0.165(3)	0.167	0.71(2)
0.6	0.604870(5)	2.87(3)	0.148(5)	0.150	0.57(2)
0.7	0.63823(1)	2.98(5)	0.120(5)	0.126	0.45(3)
0.8	0.67401(3)	3.17(8)	0.085(5)	0.089	0.32(2)
0.9	0.7127(1)	3.9(2)	0.045(10)	0.047	0.20(2)
1	≈ 0.76	∞	0	0	0

Table 3.2: Numerical estimates of the percolation threshold p_c and the critical exponents $\nu_\parallel, \delta$ for various values of κ. Entries without error bars are based on analytical arguments. The estimates for δ have to be compared with the predicted values δ_c according to the conjecture in Eq. (3.123) truncated to three digits. The values for β in the last column were computed from the previous exponents using the scaling relation $\beta = \delta\nu_\parallel$.

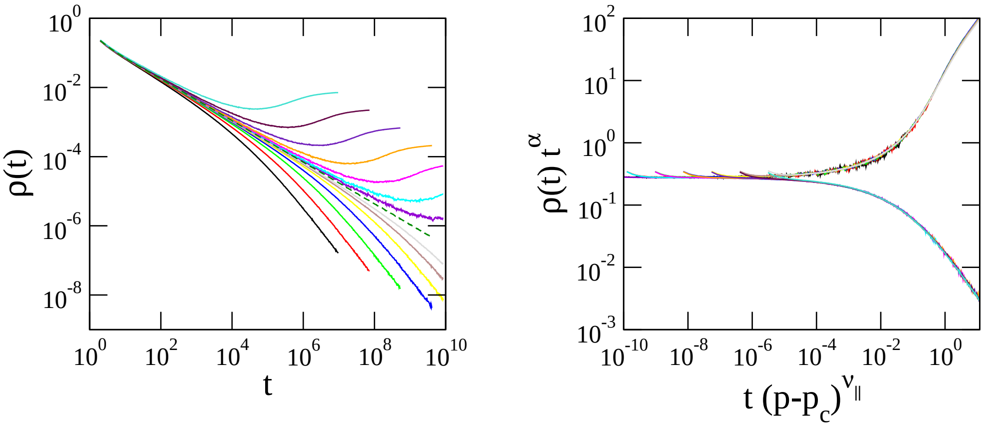

Figure 3.14: Off-critical simulations, here for $\kappa = 0.4$ with $p - p_c$ ranging from ± 0.00016 to ± 0.01024. The measured curves (left) can be collapsed convincingly (right), allowing one to estimate the exponents α and $\nu_\parallel$.

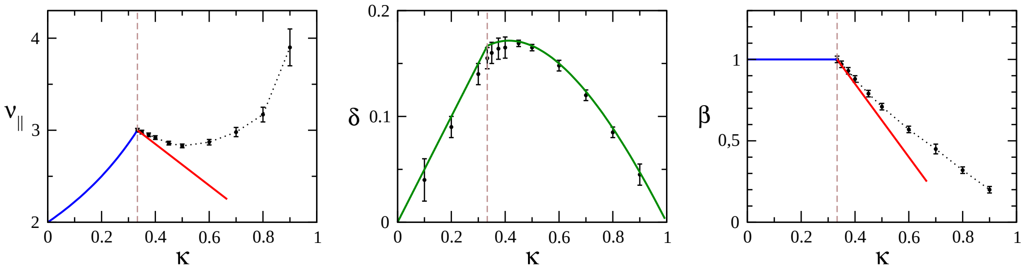

Figure 3.15: Numerically measured critical exponents (black) for various values of κ according to Table 3.2 compared with the mean-field prediction (blue), the field-theoretic one-loop approximation (red) and the conjectured formula for δ (green), see Eq. (3.123).

Obviously the two-loop corrections should have the opposite sign.

Conjugate field

As we did for the models for a boundary induced phase transition into an absorbing state we can also consider spontaneous creation of particles a a rate h, that acts like a field that eliminates the transition.From (3.15) together with the scaling relation (3.102) one arrives at

$$\rho_{\text{stat}} \sim \begin{cases} h^{1/2} & \text{for } \kappa \leq \frac{1}{3} \\ h^{\frac{1-\kappa}{1+\kappa}} & \text{for } \kappa > \frac{1}{3}\,. \end{cases} \tag{3.120}$$

This power law is in good agreement with numerical results (not shown here) as is also the case of the boundary induced phase transitions into an absorbing state (see Fig. 3.7).

Fully occupied initial state for $t < 0$

So far we considered simulations starting with a single active seed at $t = 0$. However, the initial condition is not determined by the state of the site at $t = 0$ alone, instead the non-Markovian dynamics requires us to specify the configuration of *all* sites along the entire time line, in principle even including all sites at negative times $t < 0$. As an example let us consider the initial configuration

$$s(t) = \begin{cases} 1 & \text{if } t \leq 0 \\ 0 & \text{if } t > 0 \end{cases} \tag{3.121}$$

where all sites at negative times are initially occupied. This initial density is shown as a black step function in the left panel of Fig. 3.16. For this initial configuration the process has to start at $t_u = -\infty$. Upon reaching $t_u = 0$ the update rule will have activated many sites at $t > 0$. These active sites are randomly distributed and uncorrelated with an expectation value decaying asymptotically as

$$\varrho(t) = \langle s(t) \rangle \sim t^{-\kappa} \qquad (t_u = 0) \tag{3.122}$$

as indicated by the blue curve in Fig. 3.16.

Subsequently, as the update rule advances from $t = 0$ to $t \to \infty$, even more sites will be activated along the timeline. The resulting density of active sites is shown as red curve in the figure. As can be seen, the density seems

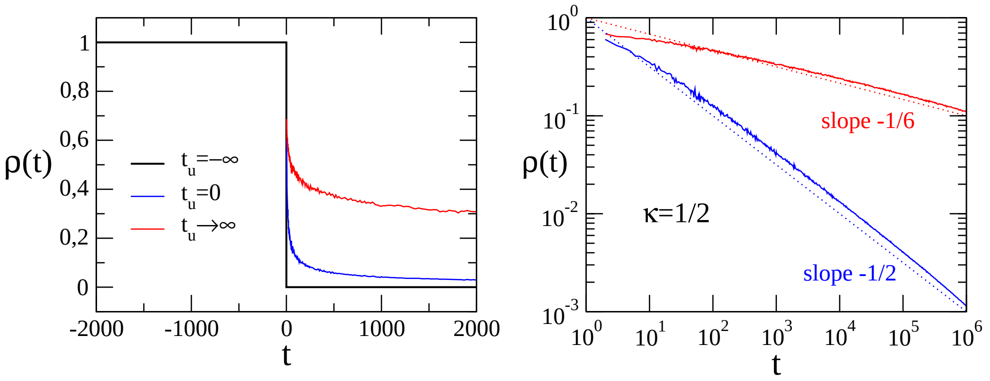

Figure 3.16: Initial configuration where all sites at negative times are active. The left panel shows the initial configuration (black), the density profile in the moment when the update rule reaches $t_u = 0$ (blue) and the final density profile in the limit $t_u \to \infty$ (red). The right panel shows the same data in a double logarithmic representation.

to decay asymptotically as $\varrho(t) \sim t^{-1/6}$ for $\kappa = 0.5$. Obviously, this density is much larger than the density produced by a single seed (where one would obtain $\varrho(t) \sim t^{-1/2}$).

Moreover, the observed exponent 1/6 coincides with the survival exponent in seed simulations. This relationship is valid for all κ and is a direct consequence of the time reversal symmetry. On a qualitative level it can be explained as follows. As sketched in Fig. 3.17 a particular run in seed simulations is said to survive (at least) up to time t if there is a connected path of subsequent Lévy flights from the seed to some site at $t' \geq t$. The lower part of the figure shows the same but horizontally reflected realization of Lévy flights. In such a time-reversed situation survival translates into the condition that a site at time t is connected *backwards* in time to some site at $t' \leq 0$, or equivalently, that a site at time t is activated by an initial configuration where all sites at negative times are active.

We therefore conclude that the survival probability in seed simulations decays asymptotically in the same way as the particle density in simulations

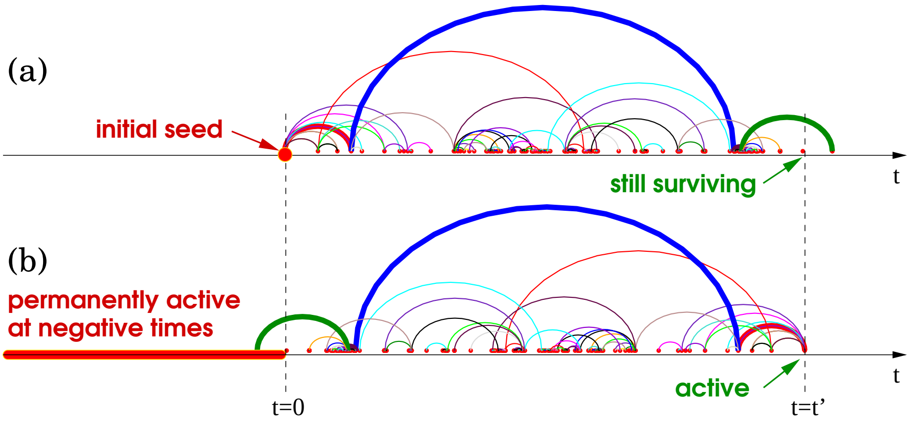
(a)
initial seed
still surviving
t
(b)
permanently active
at negative times
active
t
t=0
t=t'

Figure 3.17: Illustration of the time reversal symmetry. The upper part (a) shows a particular realization of Lévy flights in a simulation starting with a single seed. At time t' the process is still surviving because there is at least one connected path (bold lines) that activates a site at $t \geq t'$. The lower part (b) shows the time-reversed configuration of Lévy flights which has the same statistical weight. Here the site at time t' becomes active if there is at least one connected path to a site at $t \leq 0$. Therefore, a fully activated initial state at $t < 0$ (indicated as a red bar) will lead to a density profile that decays in the same way as the survival probability.

starting with fully occupied lattice at negative times. This unusual relationship will be used in the following to determine the value of δ.

The survival exponent δ

We now propose a conjecture for an exact scaling relation that determines the value of the survival exponent, similar to the one presented in the last section to find $\delta = 1/6$, which corresponds to the case $\kappa = 1/2$. Let us consider again the TSP starting with the initial configuration (3.121) where all sites at negative times are active. As discussed before and demonstrated in Fig. 3.16 the process evolves in two steps:

1. During the updates from $t_u = -\infty$ to $t_u = 0$, the process produces an uncorrelated random distribution of active sites at $t > 0$ which on average decays as $t^{-\kappa}$.

2. This random distribution can be interpreted as a time-dependent external field $h(t) \sim t^{-\kappa}$, which causes the process to create additional active sites as a response during the updates from $t_u = 1$ to $t_u = \infty$.

We now assume that this external field $h(t)$ decays so slowly that the response of the process changes *adiabatically* as if h was stationary. Numerical simulations support the validity of this assumption over the full range of κ. This would lead to the conjecture that the final density of active sites (the blue curve in Fig. 3.16) decays as $\rho(t) \sim h^{\beta/\sigma} \sim t^{-\kappa\beta/\sigma}$, hence the survival exponent should be given by $\delta = \kappa\beta/\sigma$. Inserting Eq. (3.120) this would mean that

$$\delta(\kappa) = \begin{cases} \frac{\kappa}{2} & \text{for } \kappa \leq \frac{1}{3} \\ \frac{\kappa-\kappa^2}{1+\kappa} & \text{for } \kappa > \frac{1}{3} \end{cases} \tag{3.123}$$

As can be seen in Table 3.2 and in the central panel of Fig. 3.15, this prediction is in excellent agreement with the numerical estimates for the survival exponent δ. This observation raises the hope that the formula (3.123) may qualify as an exact scaling relation.

3.5 Conclusion

We have introduced boundary-induced phase transitions into an absorbing state in one-dimensional systems with creation/annihilation dynamics at the boundary and simple diffusive dynamics in the bulk. The non-trivial dynamics at the boundary induces a phase transition in the bulk. We have analyzed such a transition for different though similar models, including different ingredients: either single-particle annihilation or pairwise annihilation, fermionic constraint or lack of it, etc. A particular bosonic version can be exactly solved; due to the lack of any saturation mechanism, the density of particles grows unboundedly in the active phase, leading to a discontinuous transition with trivial critical exponents. The rest of the analyzed models exhibit a continuous transition and define a unique universality class. In the bulk, the dynamics is governed by random-walks, entailing the exponent values $z = 2$ and $\alpha = 1/2$. On the other hand, some critical exponents take non-trivial values: *i)* the survival probability from a localized seed at the boundary exponent, which from an heuristic argument supported by simulations results, turns out to be $\delta = 1/6$, as well as *ii)* the order parameter exponent, $\beta = 0.71(2)$. The remaining exponents can be obtained from these ones using scaling relations.

It has been shown that the class of boundary induced phase transitions studied here can be related to a single-site non-Markovian model, the TSP. As we showed, it is a convenient model for the comparison of the results obtained form the ϵ-expansion and simulations. The field theory for theTSP is particularly simple due to the absence of spatial degrees of freedom, and the model can be seen as $0-$dimensional limit of DP with temporal Lévy flights. The TSP is also of conceptual interest in the sense that it shows that nonequilibrium phase transitions can occur even in $0+1$ dimensions by choosing an adequate non-Markovian dynamics.

The models analysed here possibly constitute the simplest universality class of nonequilibrium phase transition into an absorbing state, in the sense that the transition occurs because of the special dynamics of just one site and, in contrast to DP, some critical exponents can be obtained exactly from the field theory.

Chapter 4

Nonequilibrium wetting

4.1 Introduction

Wetting [1] is well exemplified by considering a liquid droplet on a substrate. Depending on the physical properties of the system, determining the shape of the droplet, the substrate will be more or less wet. More specifically, the contact angle Θ (see Fig. 4.1) is related to the surface tensions through Young's equation,

$$\cos\Theta = (\sigma_{S,V} - \sigma_{S,L})/\sigma_{L,V}, \tag{4.1}$$

where $\sigma_{S,V}$, $\sigma_{S,L}$ and $\sigma_{L,V}$ are the surface tensions of the substrate-vapor, substrate-liquid and liquid-vapor interfaces, respectively. Total wetting happens if $\Theta = 0$, and $0 < \Theta < \pi$ corresponds to partial wetting.

Cahn [87] observed that by approaching the critical temperature T_c, for $T < T_c$, the liquid-vapor surface tension $\sigma_{L,V}$ goes to zero faster than the difference $(\sigma_{S,V} - \sigma_{S,L})$, therefore, at a temperature $T_W < T_c$ a wetting transition should take place. In this wetting transition, $\Theta > 0$ for $T < T_W$ and $\Theta = 0$ for $T \geq T_W$. This observation introduced the notion that wetting could be viewed as a type of critical phenomenon.

More generally, a wetting transition occurs in a thermodynamic system constituted of a bulk phase A and a substrate that attracts a second coex-

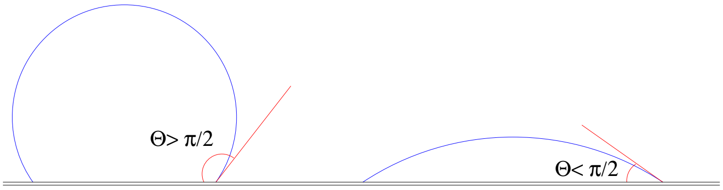

Figure 4.1: Two drops on a substrate. The left one has a contact angle $\Theta > \pi/2$ and wets less the substrate, in comparison to the right one with $\Theta < \pi/2$.

isting phase B. Depending on the control parameters, like e.g. temperature and chemical potential, the system will be in the moving phase or in the bound phase. At the wetting transition a macroscopic layer of the absorbed phase B is formed and phases A and B coexist. In the bound phase only the phase A is stable and the AB interface stays pinned to the substrate, whereas in the moving phase the AB interface grows and only phase B is stable.

Abraham [88] introduced a two-dimensional Ising model that could be solved exactly and displayed the same kind of transition predicted by Cahn [87]; it was also shown that in the solid on solid (SOS) limit the model still exhibited a wetting transition. The advantage of taking this limit is that it simplifies the calculations and with it several exact results can be obtained using the transfer matrix method [89, 90, 91].

The SOS model, defined on an one-dimensional lattice with periodic boundary conditions and size L, has the following Hamiltonian,

$$H = J \sum_{i=1}^{L} |h_{i+1} - h_i| + \sum_{i=1}^{L} V(h_i), \tag{4.2}$$

where $h_i \geq 0$ is a discrete random variable representing height, J is a positive coupling, $V(h_i)$ is a potential accounting for the interaction between the wall ($h_i = 0$) and the absorbed phase and no overhangs are allowed. The region $h > h_i$ corresponds to the phase A and the region $h < h_i$ to the coexisting phase B, therefore, the height gives the position of the AB interface. By varying the temperature this model presents a wetting transition at a temperature T_W, at which the average height of the interface diverges.

On a coarse-grained level equilibrium wetting transitions can be studied using the Hamiltonian [92]

$$H = \int d^d\mathbf{x}\{\frac{\sigma}{2}|\nabla h(\mathbf{x})|^2 + V[h(\mathbf{x})]\}, \tag{4.3}$$

where $\mathbf{x}$ is a continuous variable giving the position on the d-dimensional substrate. The height $h(\mathbf{x})$ gives the position of the interface and the potential $V[h(\mathbf{x})]$ accounts for the presence of the substrate and a possible interaction between the substrate and the interface. In order to consider the dynamics of wetting, Lipowsky [93] introduced the following Langevin equation,

$$\frac{\partial h(\mathbf{x},t)}{\partial t} = a + \sigma\nabla^2 h(\mathbf{x},t) - \frac{\delta V[h(\mathbf{x},t)]}{\delta h(\mathbf{x},t)} + \zeta(\mathbf{x},t), \tag{4.4}$$

where the deterministic part of it originates from $-\delta H[h(x)]/\delta h(x)$, with H given by (4.3), and $\zeta(\mathbf{x},t)$ is a Gaussian noise with zero mean and variance given by

$$\langle\zeta(\mathbf{x},t)\zeta(\mathbf{x}',t')\rangle = D\delta^d(\mathbf{x}-\mathbf{x}')\delta(t-t'). \tag{4.5}$$

Equation (4.4) is the Edwards-Wilkinson (EW) equation [94], which is known to describe the motion of an equilibrium interface with velocity a (see [20, 95]), with an extra term: the potential $V[h(\mathbf{x})]$.

The Kardar-Parisi-Zahng (KPZ) [96] equation differs from the EW equation by the presence of the nonlinear term $\lambda(\nabla h)^2$. The basic difference of an interface described by the KPZ equation (when compared to one described by the EW equation) is that the velocity of the interface depends on the local interface slope $\nabla h(\mathbf{x})$. The non-linear term comes from an expansion of the velocity with respect to the local interface slope, and it can be shown that higher order terms in the expansion are irrelevant under a renormalization group transformation [20, 95]. That is why the KPZ equation defines a robust universality class for nonequilibrium moving interfaces.

Since the paper of Cahn [87], equilibrium wetting has been intensively studied, theoretically and experimentally (see [92, 97, 98] for reviews). Contrarily, nonequilibrium wetting is at its very beginning and experimental studies are still lacking. One way to study nonequilibrium wetting is to add the nonlinear term of the KPZ equation $\lambda(\nabla h)^2$ to equation (4.4). Such an equation was considered for the first time by Tu et al. [99]. Hinrichsen et al. [100] and Muñoz and Hwa [101] introduced microscopic models in the KPZ universality class in the presence of a hard wall, showing that nonequilibrium wetting could also be studied with them. A considerable amount of work on nonequilibrium wetting has already emerged and our aim is to review it here.

In this chapter we present a detailed description of nonequilibrium wetting, reviewing the very rich phenomenology that is obtained from numerical and analytical methods used to study the Langevin equation and the microscopic models. Two reviews on the subject, more focused on the Langevin equation approach, are [102, 103], and there is some overlap between them and the present chapter. Nevertheless, in the account we make here many aspects of nonequilibrium wetting are presented in more detail, mainly when it comes to microscopic models.

Our contributions to nonequilibrium wetting constitute the development of mean field approximations for the restricted solid-on-solid model with a wall (introduced in 4.2.2) [13], which is explained in 4.5.2, and a detailed numerical study of the same model [14], which is resumed in Sec. 4.4. Also we wrote a topical review about nonequilibrium wetting [12] and the present chapter is this review with some small changes.

The chapter is organized in the following way. In the next section we define the Langevin equations and the microscopic models to be analyzed. Moreover, the quantities of interest and the exponents associated with them are defined. Sec. 4.3 contains exact calculations, that are possible for microscopic models when detailed balance is fulfilled. In Sec. 4.4 Monte Carlo simulations of microscopic models and numerical integration of the Langevin equations are presented. The content of Sec. 4.5 is mean field approximations for microscopic models. The case of a substrate with more than one dimension is treated in Sec. 4.6, where mean field approximations for the continuum model, naive power-counting and some renormalization group arguments are used. We end with final remarks in Sec. 4.7.

4.2 Definition of the problem

4.2.1 Continuum model

The Langevin equation we are going to consider, describing the motion of an interface in the presence of a wall, is the bounded KPZ (bKPZ) equation, given by [99]

$$\frac{\partial h(\mathbf{x},t)}{\partial t} = a - \frac{d}{dh}V(h) + \sigma\nabla^2 h(\mathbf{x},t) + \lambda(\nabla h(\mathbf{x},t))^2 + \zeta(\mathbf{x},t). \tag{4.6}$$

This is equation (4.4) added with the nonlinear term $\lambda(\nabla h(\mathbf{x},t))^2$. In contrast to the unbound KPZ interface, the sign of λ is of great importance, because, as we will see, it leads to different universality classes. We call them bKPZ+ and bKPZ– universality classes.

The potential $V(h)$ has to account for the presence of a substrate and the interaction between the absorbed phase and the substrate. A natural way to consider the presence of a substrate is to forbid negative heights with a hard-wall potential, that is given by

$$V(h) = \begin{cases} 0 & \text{if } h >= 0 \\ \infty & \text{if } h < 0. \end{cases} \tag{4.7}$$

The problem with this potential is that it is not suitable for calculations (analytical and numerical). A potential that overcomes this problem and is used in the study of equilibrium and nonequilibrium wetting with short range interactions is [92]

$$V(h) = \frac{b}{s}\exp(-sh) + \frac{c}{2s}\exp(-2sh), \tag{4.8}$$

where $s \geq 1$ controls the hardness of the wall, b is a control parameter that in equilibrium and near the transition is proportional to $|T - T_W|$ and $c \geq 0$. If $b > 0$ the wall is repulsive and the term $\exp(-2sh)$ is irrelevant while for $b < 0$ and $c > 0$ we have an attractive wall. The order parameter of the wetting transition is $n = e^{-h}$. In the bound phase the mean height is finite and the interface stays pinned to the substrate, therefore $n > 0$. In the moving phase the mean height grows linearly with time and $n = 0$. As we will see, in the microscopic models a hard-wall is introduced, and the critical behavior of them is the same as the critical behavior of the bKPZ equation with the soft-wall potential (4.8).

It turns out that the bKPZ equation (4.6), with $V(h)$ given by (4.8), can be transformed into a Langevin equation with multiplicative noise. This is done with the Cole-Hopf transformation $n = e^{-h}$, which, in the case that the sign of the nonlinear term is negative, gives the following equation for the order parameter [104],

$$\frac{\partial n(\mathbf{x}, t)}{\partial t} = -\frac{d}{dn} V(n) + \sigma \nabla^2 n(\mathbf{x}, t) + n(\mathbf{x}, t) \zeta(\mathbf{x}, t), \tag{4.9}$$

where without loss of generality we set $\lambda = -\sigma$ and chose to interpret the Langevin equation in the Stratonovich sense (interpreting it in the Ito sense would just produce a shift in the factor multiplying the linear term [7]). The potential, as a function of n, is now given by

$$V(n) = \frac{a}{2} n^2 + \frac{b}{2+s} n^{2+s} + \frac{c}{2+2s} n^{2+2s}, \tag{4.10}$$

where the linear term $-an$ appearing in equation (4.9) is now incorporated in the potential. This equation was introduced by Grinstein et al. [104], later it was pointed out that it was equivalent to the bKPZ equation [99]. The universality class it defines is called multiplicative noise 1 (MN1), obviously MN1 and bKPZ– are the same universality classes. The MN1 equation is also related to the synchronization transition in coupled map lattices [105], therefore, there is a relation between this transition and the wetting transition. We do not discuss this point here, references about it are [106, 107, 102].

By applying the same transformation to the bKPZ+ case (now with $\lambda = \sigma$), the resulting equation is

$$\frac{\partial n(\mathbf{x},t)}{\partial t} = -\frac{d}{dn}V(n) + \sigma\nabla^2 n(\mathbf{x},t) - 2\sigma\frac{(\nabla n(\mathbf{x},t))^2}{n(\mathbf{x},t)} + n(\mathbf{x},t)\zeta(\mathbf{x},t). \quad (4.11)$$

This equation is known as the multiplicative noise 2 (MN2) equation. The MN1 (4.9) and MN2 (4.11) equations will be very important in the course of this chapter, because they are more convenient in several situations. For example, integrating them numerically is simpler than integrating the bKPZ equation directly, which suffers by numerical instability problems [108].

With this map between the bKPZ equations and the MN equations it is easy to see what are the effects of considering an upper wall instead of a lower wall. An upper wall is implemented with the potential $V(h) = \frac{b}{s}\exp(sh) + \frac{c}{2s}\exp(2sh)$ in equation (4.6), in this case a negative (positive) λ corresponds to the case of a lower wall with positive (negative) λ. This can be verified by performing the Cole-Hopf transformation, but now with $n = e^h$, in the bKPZ equation with an upper wall. The result is: with a positive (negative) λ the obtained equation is MN1 (MN2). Here we always consider a lower wall, also in the microscopic models.

Before going to the definition of the microscopic models we point out that, although the bKPZ equation is defined for d spatial dimensions, in most of this chapter we will restrict to the case $d = 1$, the exception being Sec. 6. For this reason, the microscopic models are defined, in the following, on an one-dimensional substrate.

4.2.2 Microscopic models

Restricted solid on solid model

The model for nonequilibrium wetting described in what follows was introduced by Hinrichsen et al. [100]. It is a growth process taking place on a one-dimensional discrete lattice with periodic boundary conditions and size

L. To each site i a random variable h_i is attached, it can take the values $h_i = 0, 1, 2, 3...$ and is interpreted as the interface height. Nearest neighbors respect the restricted solid on solid (RSOS) constraint, i. e.,

$$|h_i - h_{i\pm1}| \leq 1, \tag{4.12}$$

which introduces an effective surface tension. The interface evolves in time by random-sequential updates in the following way. A site i of the lattice is randomly chosen and the processes that may occur are (see Fig. 4.2):

(a) deposition of a particle ($h_i \to h_i + 1$) with rate q,

(b) evaporation of a particle ($h_i \to h_i - 1$) at the edges of plateaus with rate r,

(c) evaporation of a particle ($h_i \to h_i - 1$) from the middle of a plateau with rate p.

If the final configuration would violate the RSOS condition or would lead to a negative height, then it is not carried out. After L attempts a Monte Carlo step is completed, and time is increased by one. The initial condition is a flat interface at height zero and we, without loosing generality, set $r = 1$. A hard wall is present because evaporation events at the bottom layer ($h_i = 0$) are forbidden. Since this model respects the RSOS condition and there is a hard-wall, we refer to it as RSOSW model.

The wetting transition can be explained as follows. Consider a free interface (negative heights are allowed). It may propagate, depending on the deposition and evaporation rates, in the directions of increasing or decreasing height. In the phase where the velocity of the interface v is positive (increasing height direction), the presence of the wall makes no difference: After some transient the interface will propagate with the same velocity as if the wall was not present. In contrast, when the rates are such that $v < 0$, the wall changes the scenario completely because the interface stays bounded

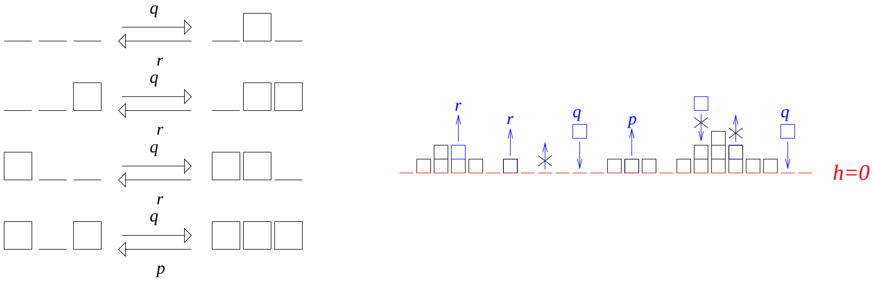

Figure 4.2: Transition rates for RSOSW model (left) and an example of an interface configuration with transitions that may take place (right).

to the wall. Therefore, by forbidding negative heights, a wetting transition from a bound to a moving phase takes place, and the phase transition line $q_c(p)$ corresponds to a free interface with $v = 0$. The phase diagram of the RSOSW model is displayed in Fig. 4.3.

This model was generalized by Hinrichsen et al. [109] in order to include an attractive interaction between the substrate and the interface. This is done by considering a different deposition rate $q_0 < q$ at zero height. Because q_0 is smaller than q the detachment of the interface from the substrate becomes harder and, therefore, this change in the dynamical rules simulates an attractive force between the substrate and the interface. As we will show, using microscopic models and the bKPZ equation, the presence of an attractive potential leads to new physics.

The sign of the factor multiplying the nonlinear term of the the KPZ equation can be determined in a microscopic model. An initially tilted interface is related to how the interface velocity varies with the tilt [20]. In Fig. 4.3 the dotted line where $\lambda = 0$ is displayed, above (below) it $\lambda < 0$ $(\lambda > 0)$. This shows that for $0 < p < 1$ the phase transition is in the bKPZ–, for $p = 1$ in the bEW and for $p > 1$ in the bKPZ+ universality class. $p = 0$ is a particular case that will be addressed in Sec. 4.

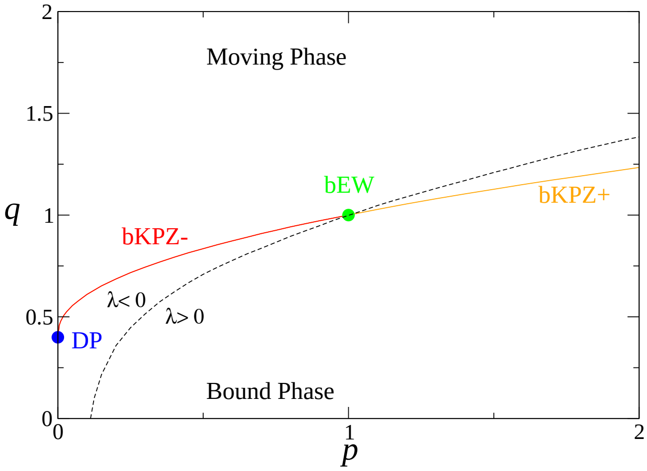

Figure 4.3: Phase diagram of the RSOSW model. At $p = 0$ the transition is in the direct percolation (DP) universality class; for $0 < p < 1$ it is in the bKPZ– universality class; for $p = 1$, where detailed balance is satisfied, it belongs to the bEW universality class; for $p > 1$ in the bKPZ+ universality class. The dashed line marks the region where $\lambda = 0$.

Single-step model

Another microscopic realization of nonequilibrium wetting is the so-called single-step model with a wall (SSW), introduced by Ginelli et al. [110]. Here we use a more specific version of it, studied in [111, 112].

In the SSW model, the difference of height between two neighbors is restricted through the condition

$$|h_i - h_{i+1}| = 1. \tag{4.13}$$

As in the previous model, it is defined on an one-dimensional lattice of size L and with periodic boundary conditions. It evolves random-sequentially by the following rules:

(a) deposition of a particle ($h_i \to h_i + 2$) with probability p,

(b) evaporation of a particle ($h_i \to h_i - 2$) with probability $1 - p$,

at a chosen site i occurs if the configuration after the move is carried out does not violate the single-step constraint. The initial condition is $h_i = 1$ ($h_i = 0$) if i is odd (even). In the case of the SSW model λ is proportional to $1/2 - p$, therefore for $p = 1/2$ we have the bEW case and for $p > 1/2$ ($p < 1/2$) the bKPZ– (bKPZ+) case. The incorporation of a wall, in comparison to the previous case, is a bit more complicated, it is done in the following way. For the SSW model, it is not possible to vary the velocity of the interface keeping λ fixed. This happens because, in contrast to the RSOSW model, there is just one control parameter, namely p. Fortunately, for the single-step model (free interface case) the velocity of the interface in the long time limit is known exactly, it is given by

$$v_L = (p - 1/2)(1 + 1/L). \tag{4.14}$$

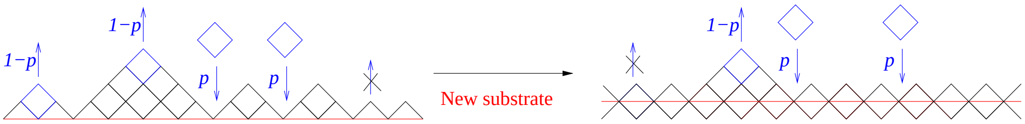

Figure 4.4: Example of an interface configuration of the SSW model with some transitions that can occur. The horizontal line indicates the height of the moving wall $\bar{h}$. The right panel shows the interface after the substrate moves, $\bar{h} \rightarrow \bar{h}+1$.

Therefore, in order to study nonequilibrium wetting the system is tuned to criticality by considering a wall that moves with velocity v_L given by (4.14). This is done by forbidding evaporation events below the substrate height $\bar{h}(t) = v_L t$.

In this thesis we focus on the cases $p = 1/2$, $p = 1$ and $p = 0$ which are in the bEW, bKPZ– and bKPZ+ universality classes, respectively. For $p = 1/2$, since $v_L = 0$, the height of the wall is $\bar{h}(t) = 0$. At $p = 1$, during a simulation, after every $\Delta t = 2(1 - 1/L)$ we increment the substrate height by one unity, $\bar{h} \rightarrow \bar{h} + 1$. This means that all sites below the new $\bar{h}$ are increased and evaporation events at the new $\bar{h}$ are forbidden. For the bKPZ+ case ($p = 0$) after every time interval $\Delta t = 2(1 - 1/L)$ we have $\bar{h} \rightarrow \bar{h} - 1$.

The SSW model is particularly useful to obtain critical exponents numerically, since in this case one knows the critical point exactly. On the other hand the advantage of the RSOSW model is that it exhibits a richer behavior. The SSW model is also important for the study of mean field approximations (see Sec. 4.5).

4.2.3 Observables and related exponents

Finally, we define the physical quantities that we are going to consider in this chapter, and the exponents associated with them. They are defined in the context of the RSOSW model and will be generalized to the continuum model at the end of this section. The generalization to any other microscopic model is straightforward.

Scaling exponents

A key quantity in what follows is the mean height of the interface, defined by

$$\langle h \rangle = \langle L^{-1} \sum_{i=1}^{L} h_i \rangle, \tag{4.15}$$

where $\langle\rangle$ denotes the ensemble average. Another observable of great importance is the interface width w, given by

$$w^2 = \langle L^{-1} \sum_{i=1}^{L} h_i^2 \rangle - \langle h \rangle^2. \tag{4.16}$$

If the interface width of an infinite system grows with time and does not reach a stationary value in the long time limit, the interface is called rough. Otherwise, if w saturates after some transient it is smooth. In the one-dimensional case, the wetting transition is a roughening transition, the interface is smooth for $q < q_c$ and rough for $q \geq q_c$. Obviously, if the system is finite w saturates, even if the interface is rough. If one wants to verify wether an interface is rough or smooth by doing simulations in finite systems, one has to consider different sizes and see how the saturation value $w_s(L)$ varies with L. If $w_s(L)$ grows with L, than the interface is rough; if it tends to a saturation value independent of L, then the interface is smooth. This is shown in Fig. 4.5.

The KPZ universality class describes the self-affine properties of the roughening interface under scale transformations. The scaling exponents are defined by the relations [20, 95]

$$w(t) \sim t^{\gamma}, \qquad w_s \sim L^{\alpha}, \qquad t_s \sim L^{z}, \tag{4.17}$$

where t_s is the time at which the interface width saturates at the value w_s. γ is known as the growth exponent, α is the roughness exponent and z

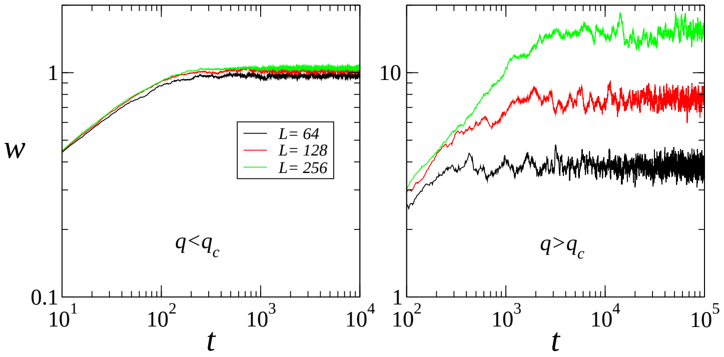

Figure 4.5: Interface width w for the RSOSW model as a function of time in the bound phase (left) and in the moving phase (right) for $L = 64, 128, 256$. In the bound phase $q = 0.9$ and in the moving phase $q = 3.0$, where $p = 1.0$. One can see that the saturation value of w tends to a constant in the bound phase (smooth interface) and grows with L in the moving phase (rough interface).

the dynamical exponent. They are not all independent, but related by the Family-Vicsek scaling relation [113]

$$w(t, L) = L^{\alpha} f(tL^{-z}), \tag{4.18}$$

where $f(x)$ is a scaling function. From this last relation it follows that $z = \alpha/\beta$. In one dimension the scaling exponents of the EW universality class are $\alpha = 1/2$, $\beta = 1/4$ and $z = 2$; while for the KPZ universality class they are $\alpha = 1/2$, $\beta = 1/3$ and $z = 3/2$ [20, 95].

We stress that the definition of the scaling exponents does not depend on the presence of the wall, they are related to the scale invariance of w. However, the definition of critical exponents just make sense with a wall. As we will show, by introducing a wall, only one new independent critical exponent arises, the others can be determined by scaling relations and the values of the scaling exponents.

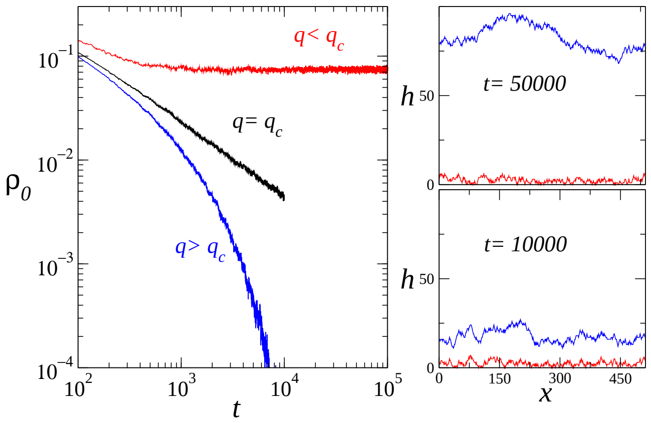

Figure 4.6: The left panel shows $\rho_0(t)$ below ($q = 0.97$), at ($q = 1.0$) and above ($q = 1.01$) criticality, with $L = 512$ and $p = 1.0$. Note that at the critical point $\rho_0(t)$ decays algebraically, above it goes to zero exponentially and below it saturates. On the right, typical bounded and moving interfaces are showed for different times. For $q = 0.97$ it stays bounded to the wall and for $q = 1.01$ it advances.

Critical exponents

The order parameter of the wetting transition is the density of sites at zero height, i. e.,

$$\rho_0 = \langle L^{-1} \sum_{i=1}^{L} \delta_{h_i,0} \rangle . \tag{4.19}$$

In the bound phase $\rho_0 > 0$, while in the moving phase, where the interface detaches from the wall, $\rho_0 = 0$. Another order parameter for the transition is the velocity of the interface, which is zero in the bound phase and non-zero in the moving phase.

Fig. 4.6 shows the typical time evolution of ρ_0 above, below and at criticality. For $q < q_c$ the order parameter reaches a constant positive value in the stationary state. At the critical point, it goes to zero with a power-law behavior and for $q > q_c$ it vanishes exponentially. The exponent θ is defined at the critical line by the relation

$$\rho_0(t) \sim t^{-\theta}. \tag{4.20}$$

Near and below criticality we have

$$\rho_0^s \sim (q_c - q)^{\beta}, \tag{4.21}$$

where ρ_0^s is the saturation value of the order parameter. As discussed above the mean height is finite in the bound phase and diverges at criticality. The exponent associated with this divergence is defined by

$$\langle h \rangle \sim (q_c - q)^{-\zeta}, \tag{4.22}$$

where the above relation is valid near and below criticality. In one dimension the interface width is also finite for $q < q_c$ and diverges at the critical point. Since it has the same dimension as $\langle h \rangle$, we expect it to diverge with the same exponent ζ. In this sense, when dealing with an one-dimensional substrate, we consider the above definition also valid for w. When analytical calculations are possible, we calculate both quantities and show that, indeed, they have the same critical behavior.

At the wetting transition, like the interface width, the mean height follows the relation $\langle h \rangle \sim t^{\gamma}$. In the moving phase $\langle h \rangle$ grows linearly with time. Therefore, the interface velocity goes to zero as the critical point is approached from above. The critical exponent β_v is defined by

$$v \sim (q - q_c)^{\beta_v}, \tag{4.23}$$

where the above relation is valid above and near criticality.

The spatial correlation length $\xi_\perp$ diverges near the critical point as,

$$\xi_\perp \sim (q_c - q)^{-\nu_\perp}. \tag{4.24}$$

The same happens with the temporal correlation length $\xi_\parallel$,

$$\xi_\parallel \sim (q_c - q)^{-\nu_\parallel}. \tag{4.25}$$

The saturation of the interface width w in a finite system, for a rough interface, happens when $\xi_\perp$ becomes of the same order of the system size L, at the time t_s proportional to $\xi_\parallel$. All this lead to

$$\xi_\parallel \sim \xi_\perp^z, \tag{4.26}$$

which gives the following scaling relation,

$$z = \nu_\parallel / \nu_\perp. \tag{4.27}$$

Another scaling relation is

$$\theta = \beta / \nu_\parallel, \tag{4.28}$$

which comes from (4.20), (4.21) and (4.25). Since the spatial correlation length is of the order of the system size when w saturates, $w_s \sim L^\alpha$ can be written as $w_s \sim \xi_\perp^\alpha$. Hence, with (4.22) and (4.24), we have

$$\zeta = \nu_\perp \alpha. \tag{4.29}$$

We are considering the case $q_0 = q$ where there is no attraction between the wall and the absorbed particles. For the bKPZ equation, where the order parameter is $n = e^{-h}$, we have a non-attractive wall if b assumes some positive fixed value (in this case the term $\exp(-2sh)$ is irrelevant and one can set $c = 0$). The control parameter a is analogous to q in the RSOSW model and, therefore, relations (4.20) and (4.21) become: $n(t) \sim t^{-\theta}$ (valid at $a = a_c$) and $n_s \sim (a_c - a)^\beta$, where n_s is the saturation value.

Attractive substrate

If there is an attractive force between the substrate and the particles, different physical properties are observed. Within the RSOSW model the situation is as follows. For the bEW and the bKPZ+ universality classes ($p \geq 1$), as q_0 decreases (more attraction), there is a threshold q_0^*, which depends on p, such that the transition becomes first order for $q_0 < q_0^*$. In both cases the critical point q_c remains unaltered, see Fig. 4.7.

In the bKPZ– class ($0 < p < 1$) below q_0^*, a new critical value $q_c^{(2)}$ arises, this is shown in Fig. 4.7. For $q_0 < q_0^*$ there is a phase coexistence region in the sense that, depending on the initial conditions, the interface will be a moving or a bound one. For example, if a flat interface at a height far enough from the substrate is taken as initial condition, the interface will grow and not stay pinned to the substrate. Inside the phase coexistence region, the bound phase is the stable one in the thermodynamic limit, i. e., the average time for the interface to detach from the wall grows exponentially with the system size [109, 114, 115]. The critical behavior of this new transition, taking place at value $q_c^{(2)}$, will be addressed in Sec. 4.4.

Considering the bKPZ equation (4.6) instead of the RSOSW model, the situation is the same as the one depicted in Fig. 4.7, with the parameter a playing the role of q, the parameter b the role of q_0 and c having a fixed positive value. Note however that a and q or b and q_0 do not have precisely the same meaning and their exact relationship is not known.

In equilibrium wetting, at $a = a_c$, the transition that occurs when approaching b_W from below (analogous to q_0^*), is known as critical wetting. On the other hand, the transition taking place at $b > b_W$, by approaching a_c from below is known as complete wetting [92]. Therefore, critical (complete) wetting corresponds to $q = q_c$ ($q_0 > q_0^*$) and q_0 (q) approaching q_0^* (q_c) with $q_0 < q_0^*$ ($q < q_c$) in the RSOSW model. As pointed out in [115], the transition taking place for $q_0 < q_0^*$ by varying q at the new critical point $q_c^{(2)} > q_c$ (for the bKPZ– class) is not a wetting transition but rather a depinning transition because there is no phase coexistence at criticality (phase coexistence corresponds to $q = q_c$, where the interface velocity is zero).

At the tricritical point $q_0 = q_0^*$, a new type of critical behavior is observed. We define the exponents associated to it using the superscript t. For example, at $q_0 = q_0^*$, we have

$$\rho_0^s \sim (q - q_c)^{\beta^t}. \tag{4.30}$$

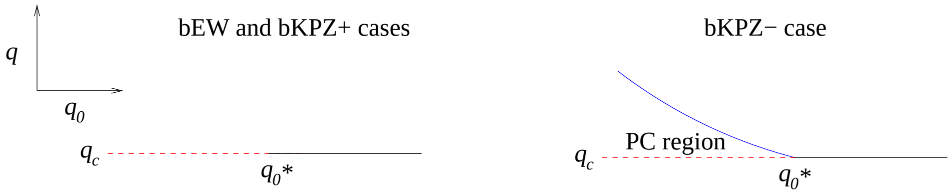

Figure 4.7: Representation of the situations generated by the attractive force between substrate and particles, for a fixed value of s. For the bKPZ+ and the bEW cases the transition goes from second order (full line) to first order (dotted line) depending on the value of q_0. The critical point q_c is not changed. For the bKPZ– case there is a phase coexistence (PC) region. Considering the bKPZ equation, the situation is the same with a playing the role of q and b the role of q_0.

We also define the following exponents associated to critical wetting,

$$\rho_0^s \sim (q_0^* - q_0)^{\beta^{(2)}}, \tag{4.31}$$

$$w \sim (q_0^* - q_0)^{\zeta^{(2)}}, \tag{4.32}$$

where the above relations are valid at $q = q_c$.

4.3 Exact results

The solution of the RSOSW model in the regime described by the bEW universality class, is presented below. For $p = 1$ detailed balance holds and the model can be solved exactly for $(q \leq 1)$ [100]. First we solve the model for $q_0 = q$, then we consider the more general case $q_0 \leq q$ [109]. Concerning exact solutions obtained with the height probability distribution in the stationary state in the bound phase, our presentation follows [116]. Also, by using a method introduced in [117], we calculate the velocity of a free interface for the RSOS model, leading to an exact calculation of the exponent β_v, which, to our knowledge, is not calculated elsewhere.

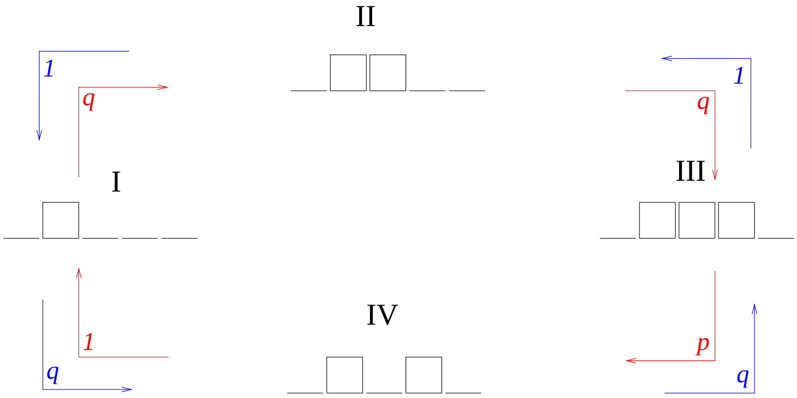

Figure 4.8: Four different interface configurations forming a closed cycle and the respective transition rates.

4.3.1 Transfer matrix formalism

In a general dynamical system, detailed balance is fulfilled if, for every pair of microscopic σ and σ', the probability currents cancel each other, i. e.

$$P_\sigma w_{\sigma\to\sigma'} = P_{\sigma'} w_{\sigma'\to\sigma}, \tag{4.33}$$

where P_σ is the probability of being in the state σ in the stationary state and $w_{\sigma\to\sigma'}$ is the transition rate from σ to σ'. From Fig. 4.8 we see that, for the RSOSW model, it is satisfied only if

$$P_I = q^{-1}P_{II} = q^{-2}P_{III} = q^{-1}p^{-1}P_{IV} = p^{-1}P_I, \tag{4.34}$$

which implies in $p = 1$.

The detailed balance condition (4.33), with $p = 1$, implies in the relation

$$P(\{h_i\}) = qP(\{h_i - 1\}), \tag{4.35}$$

where the configurations $\{h_i\} = h_1, ..., h_i, .., h_L$ and $\{h_i - 1\} = h_1, ..., h_i - 1, .., h_L$ are such that the RSOS constraint is obeyed. A simple ansatz arising from this condition is

$$P(\{h_i\}) = Z_L^{-1}\prod_{i=1}^{L} q^{h_i}, \tag{4.36}$$

where Z_L is the partition function. It is given by

$$Z_L = \sum_{\{h\}} \prod_{i=1}^{L} q^{h_i}, \tag{4.37}$$

where the sum is over all configurations satisfying the RSOS constraint. We can write the probability distribution (4.36) in the form

$$P(h_1, ..., h_L) = Z_L^{-1} \prod_{i=1}^{L} T_{h_i,h_{i+1}}, \tag{4.38}$$

where $T_{h_i,h_{i+1}}$ is the transfer matrix and we are using periodic boundary conditions ($h_{L+1} = h_1$). The elements of the transfer matrix are given by

$$T_{k,k'} = q^{(k+k')/2}(\delta_{k,k'} + \delta_{k,k'+1} + \delta_{k,k'-1}), \tag{4.39}$$

where $k \geq 0$ and $k' \geq 0$. Note that the transfer matrix is tridiagonal and this is a direct consequence of the RSOS constraint.

Within the transfer matrix formalism, the partition function reads

$$Z_L = \sum_{h_1} ... \sum_{h_L} T_{h_1,h_2} T_{h_2,h_3} ... T_{h_{L-1},h_L} T_{h_L,h_1} = \sum_{h_1} T^L_{h_1,h_1} = \mathrm{Tr}(T^L), \tag{4.40}$$

where the operator Tr gives the trace of the matrix. We are interested in calculating the density of sites at height k, which can be written as

$$\rho_k = Z_L^{-1} \sum_{\{h\}} \delta_{h_1,k} \prod_{i=1}^{L} T_{h_i,h_{i+1}} = Z_L^{-1} \sum_{h_2} ... \sum_{h_L} T_{k,h_2} ... T_{h_L,k} = Z_L^{-1} T^L_{k,k}, \tag{4.41}$$

where the term $\delta_{h_1,k}$ imposes the constraint of summing only over configurations with $h_1 = k$. In bra-ket notation the same quantity becomes

$$\rho_k = Z_L^{-1} \langle k | T^L | k \rangle, \tag{4.42}$$

where the vectors $|k\rangle$ form the canonical configuration basis in height space.

In most of the following calculations the limit $L \to \infty$ will be taken. In this limit we have

$$Z_L \approx \Lambda^L \tag{4.43}$$

and

$$\rho_k = \frac{|\langle k|\phi\rangle|^2}{|\langle\phi|\phi\rangle|}, \tag{4.44}$$

with Λ being the maximum eigenvalue of the transfer matrix and $|\phi\rangle$ the corresponding eigenvector, i.e.

$$T|\phi\rangle = \Lambda|\phi\rangle. \tag{4.45}$$

After setting up the transfer matrix formalism we proceed to calculate the critical exponents of the bEW universality class.

4.3.2 Calculation of the critical exponents

Based on dimensional analysis, (4.21) and (4.24) we observe that the conditional correlation function,

$$c(l) = \frac{\langle \delta_{h_i,0}\delta_{h_i+l,0}\rangle}{\langle \delta_{h_i,0}\rangle}, \tag{4.46}$$

is expected to follow the relation

$$c(l) \sim l^{-\beta/\nu_\perp}, \tag{4.47}$$

valid at the critical point. This quantity is equal to the sum of all possible paths, each of which multiplied by its respective weight, connecting two points at height zero with a distance l from each other. At the critical point all non-zero elements of the transfer matrix are equal to one, implying that all possible paths have the same weight. Therefore, for large enough l and at criticality, the number of all possible paths connecting two points at height zero at a distance l from each other is equivalent to the probability that a random walk starting at the origin will come back to the origin for the first time at time l. It is known that the probability distribution of the time that a random walker takes to return to the origin for the first time τ is given by $P(\tau) \sim \tau^{-3/2}$ [85]. From this it follows that, at criticality,

$$c(l) \sim l^{-3/2} \tag{4.48}$$

and, therefore, $\beta/\nu_\perp = 3/2$. We note that this kind of random-walk argument was successfully used in equilibrium wetting [118].

We now consider the problem in the thermodynamic limit, $L \to \infty$. From equations (4.39) and (4.45) it follows that

$$q^k(q^{-1/2}\phi_{k-1} + \phi_k + q^{+1/2}\phi_{k+1}) = \lambda\phi_k, \tag{4.49}$$

where ϕ_k is a component of the vector $|\phi\rangle$. In order to solve this equation we take the continuum limit, which should be valid when we are close enough to criticality. In this limit: $k \to h$, $\phi_k \to \phi(h)$ and equation (4.49) becomes

$$\frac{d^2}{dh^2}\phi(h) + (3-\Lambda)\phi(h) - 3\epsilon h\phi(h) = 0, \tag{4.50}$$

where $\epsilon = 1 - q$. The solution of it is

$$\phi(h) = Ai\left(\frac{3\epsilon h + \Lambda - 3}{(3\epsilon)^{2/3}}\right), \tag{4.51}$$

where $Ai(x)$ is the Airy function. From the condition that $\phi(h)$ has to vanish for $h < 0$ it follows that $\Lambda = 3$ and

$$\phi(h) = Ai(3^{1/3}\epsilon^{1/3}h). \tag{4.52}$$

With this explicit form of $\phi(h)$ the calculation of the mean height and the interface width is straightforward, they are given by

$$\langle h\rangle = A^{-1}\int_0^\infty \phi(h)^2 h dh \sim \epsilon^{1/3} \qquad w = \sqrt{A^{-1}\int_0^\infty \phi(h)^2[h-\langle h\rangle]^2 dh} \sim \epsilon^{1/3}, \tag{4.53}$$

where $A = \int_0^\infty \phi(h)^2 dh$. Since $\phi(0) = 0$, in order to calculate the density of sites at zero height in the continuum limit we have to calculate $\rho(h)$ at some small fixed height $h = \delta$. Considering that δ is much bigger than ϵ and small enough such that $\phi(\delta) \approx \delta\phi'(0)$ is a good approximation, we have

$$\rho(0) \sim A^{-1}(\phi'(0)^2), \tag{4.54}$$

which gives

$$\rho(0) \sim \epsilon. \tag{4.55}$$

These exact results are all for the stationary state, the present method does not allow us to calculate time-dependent quantities. In order to obtain them we resort to Monte Carlo simulations [116] or numerical integration of a set of equations obtained with the supposition that the time-dependent probability distribution is pair-factorized, which seems to be the case (see Sec. 4.5). Both methods give the results

$$\langle h \rangle \sim t^{1/4}, \qquad w \sim t^{1/4} \tag{4.56}$$

and

$$\rho_0 \sim t^{-3/4}. \tag{4.57}$$

We have obtained the critical exponents of the bEW universality class for $d = 1$, they are: $\beta = 1$, $\nu_\perp = 2/3$ and $\nu_\parallel = 4/3$. The above calculations are not possible for the bKPZ case ($p \neq 1$), where we have to use numerical simulations to obtain the critical exponents. Next we consider the new scenario generated by an attractive substrate for the bEW class.

4.3.3 Attractive wall: the case $q_0 \neq q$

With $q_0 < q$, below a certain value of the deposition rate at height zero q_0^* the phase transition becomes first-order. We now calculate the value q_0^*, show that the transition is first-order for $q_0 < q_0^*$ and calculate the exponents associated to the tricritical point.

The only elements of the transfer matrix that are changed for $q_0 \neq q$ are $T_{0,0} = q/q_0$, $T_{0,1} = (q/q_0)^{1/2}$, and $T_{1,0} = (q/q_0)^{1/2}$. The new transfer matrix can be written in the form

$$T_{k,k'} = q^{(k+k')/2}(q/q_0)^{(\delta_{k,0}+\delta_{k',0})/2}(\delta_{k,k'} + \delta_{k,k'+1} + \delta_{k,k'-1}), \tag{4.58}$$

where $k \geq 0$ and $k' \geq 0$. Using (4.38), one can verify that the probability distribution obtained with this transfer matrix satisfies detailed balance.

For $q > 1$, the probability distribution is clearly not normalizable, independently of the value of q_0. This shows that the critical point is unchanged with the attractive force between the substrate and the absorbed particles. For $q = 1$, we make the assumption that

$$\phi_k = x^k \qquad \text{with } k \geq 1, \tag{4.59}$$

where $x < 1$. Using the transfer matrix (4.58), the set of equations obtained by applying (4.59) to equation (4.45) is

$$\begin{aligned} q_0^{-1}\phi_0 + q_0^{-1/2}x &= \Lambda\phi_0, \\ q_0^{-1/2}\phi_0 + x + x^2 &= \Lambda x, \\ x^{-1} + 1 + x &= \Lambda. \end{aligned} \tag{4.60}$$

It has the solution

$$\phi_0 = q_0^{1/2}, \qquad x = \frac{\sqrt{1 + 2q_0 - 3q_0^2}}{2(1 - q_0)} - \frac{1}{2}, \qquad \Lambda = \frac{x + 1}{q_0}. \tag{4.61}$$

Combining these results with equation (4.44) gives

$$\rho_0 = \frac{1 + q_0 - 6q_0^2 + \sqrt{1 + 2q_0 - 3q_0}}{2 + 4q_0 - 6q_0} \tag{4.62}$$

From this result we see that $\rho_0 = 0$ at $q_0^* = 2/3$, $\rho_0 > 0$ for $q_0 < q_0^*$ while for $q_0 > q_0^*$ the assumption (4.59) is not valid. Since ρ_0 is finite at the critical point $q = 1$ for $q_0 < q_0^*$, the transition is first-order.

The exponents related to critical wetting can be obtained exactly as follows. From equation (4.62), with q_0 below and near enough $q_0^* = 2/3$, we have

$$\rho_0 \sim (q_0^* - q_0)^1, \tag{4.63}$$

giving $\beta^{(2)} = 1$ for the bEW class. The density of particles at any height h can also be calculated from (4.44) and (4.61), giving

$$\rho_k = \frac{x^{2k}}{q_0 + x^2/(1 - x^2)}. \tag{4.64}$$

The above equation with $\langle h\rangle = \sum k\rho_k$ and $w^2 = \sum(k-\langle h\rangle)^2\rho_k$, gives

$$\langle h\rangle \sim (q_0^* - q_0)^{-1}, \qquad w \sim (q_0^* - q_0)^{-1}, \tag{4.65}$$

therefore $\zeta^{(2)} = 1$.

The critical exponents defined at the tricritical point and its vicinity, with $q < q_c$ and $q_0 = q_0^*$, were obtained numerically in [116]. The results are in agreement with:

$$\rho_0 \sim (q_c - q)^{1/3}, \tag{4.66}$$

$$\langle h\rangle \sim (q_c - q)^{-1/3} \qquad w \sim (q_c - q)^{-1/3}, \tag{4.67}$$

$$\rho_0 \sim L^{-1/2}, \tag{4.68}$$

where the first two relations are valid near and below criticality and the third at the critical point. The off-critical results can be confirmed by numerical diagonalization of the transfer matrix, whereas the finite-size result can be reproduced by evaluating the product of L transfer matrices. Time-dependent results, as in the case of complete wetting, are obtained by MC simulations [116] or numerical integration of the set of equations, obtained by assuming that the time-dependent probability distribution factorizes (see Sec. 5), they are:

$$\langle h\rangle \sim t^{1/4}, \tag{4.69}$$

$$\rho_0 \sim t^{-1/4}. \tag{4.70}$$

These results give the exponents $\beta^t = 1/3$, $\nu_\perp^t = 2/3$ and $\nu_\parallel^t = 4/3$, different from the bEW critical exponents. Nevertheless, the exponents $z = 2$ and $\gamma = 1/4$ are still the same.

4.3.4 Exact calculation of the velocity of a free interface

A method to obtain exact results for the RSOS model without the wall in the long time limit was developed by Neergaard and den Nijs [117]. Here we use this method to calculate the velocity of a free interface and, consequently, obtain the exponent β_v. The calculations presented below are summarized in the appendix of [119] for a slightly different model.

The variables $\sigma_i = h_{i+1} - h_i$ can take only the values $-1, 0, 1$ because of the RSOS condition. With them the free interface problem can be mapped onto a problem of particles jumping on a lattice with the following rules:

$$\begin{aligned}
00 &\rightarrow +- &&\text{with rate } q\\
0+ &\rightarrow +0 &&\text{with rate } q\\
-0 &\rightarrow 0- &&\text{with rate } q\\
-+ &\rightarrow 00 &&\text{with rate } q\\
00 &\rightarrow -+ &&\text{with rate } p\\
0- &\rightarrow -0 &&\text{with rate } 1\\
+0 &\rightarrow 0+ &&\text{with rate } 1\\
+- &\rightarrow 00 &&\text{with rate } 1.
\end{aligned} \tag{4.71}$$

Since the initial condition is a flat interface and all possible transitions conserve the total charge, the number of positive charges ($\sigma_i = 1$) in the system is equal to the number of negative charges ($\sigma_i = -1$). In [117] it was shown (in a more general context) that in the region of the phase diagram where

$$p = q\frac{2-q}{2q-1} \qquad \text{and} \qquad q > 1 \tag{4.72}$$

the ansatz

$$P(N) = Z_L^{-1}\left(\frac{q}{2q-1}\right)^{-N}, \tag{4.73}$$

where $P(N)$ is the probability of having a configuration with N positive charges in the limit $t \rightarrow \infty$ and Z_L is a normalization constant, is in agreement with the dynamical rules (4.71). The normalization condition gives

$$Z_L = \sum_{N=0}^{L/2} \frac{L!}{N!N!(L-2N)!}\left(\frac{q}{2q-1}\right)^{-N}. \tag{4.74}$$

In the thermodynamic limit, $L \to \infty$, the sum in the partition function Z_L is dominated by the term $N = L/(2 + 1\sqrt{q/(2q-1)})$, giving the following density of positive (or negative) charges:

$$\rho = \frac{1}{2 + \sqrt{(2q-1)/q}} + o(1/L). \tag{4.75}$$

The interface velocity is given by

$$v = (q-p)\langle 00\rangle + q\langle 0+\rangle - \langle +0\rangle - \langle -0\rangle + q\langle -0\rangle + q\langle -+\rangle - \langle +-\rangle. \tag{4.76}$$

Because of (4.73), $\langle 00\rangle = (1-2\rho)^2 + o(1/L)$, $\langle +0\rangle = \langle 0+\rangle = \langle -0\rangle = \langle 0-\rangle = (1-2\rho)\rho + o(1/L)$ and $\langle -+\rangle = \langle +-\rangle = \rho^2 + o(1/L)$. Hence, we arrive at an exact expression for the asymptotic velocity, which is

$$v = (q-1)2\rho + o(1/L), \tag{4.77}$$

where ρ is given by (4.75).

We obtained the asymptotic velocity for the free interface case, which is equal to the asymptotic velocity of the RSOSW model in the moving phase. Even though the exponent β_v is defined in the horizontal direction in the $q \times p$ plane we expect it to be the same in other directions, because numerical calculations of the exponent β_v for different values of p are all compatible with $\beta_v = 1$ [100]. Therefore, we have computed the exponent β_v exactly.

4.4 Numerical simulations

Here we discuss some technical aspects of Monte Carlo simulations of the RSOSW model and summarize numerical results for the bKPZ– universality class obtained in [14]. We then establish a scaling relation between the exponents, based on heuristic arguments and in agreement with the numerical results, which shows that with the introduction of the wall just one new independent exponent arises. We explain how to integrate the bKPZ equation numerically in an efficient way and demonstrate numerical results based on this method. The attractive wall case and extensions of the problem are also discussed.

4.4.1 The exponents of bKPZ– universality class

In order to calculate the critical exponents numerically by simulating a lattice model one can use off-critical, finite-size and time-dependent simulations. With off-critical simulations it is possible to calculate the exponents β and ζ, while the exponents θ and $\nu_\perp$ can be obtained with time-dependent and finite-size simulations, respectively.

A technical problem with the off-critical simulations is the EW-KPZ crossover, which manifests itself as follows. For a moderate simulation effort, it gives the impression that the critical exponents β and ζ (measured for a fixed value of p) depended continuously on p, varying from the EW exponent $\beta = 1$ and $\zeta = 1/3$, when p is near 1, to larger values as p gets smaller, where we are considering the bKPZ– class ($0 < p < 1$). But this is not the case: When making measures near the equilibrium point one has to access regions closer to criticality in order to get appropriates value for β and ζ, they first look like bEW exponents and then they slowly cross over to the bKPZ– values. Because of this crossover, simulations with small values of p provide better results, that is why in [14] the simulations were done at $p = 0.001$. The off-critical simulations are presented in Fig. 4.9, from which we read off the exponents

$$\beta = 1.67(5)\,, \qquad \zeta = \nu_\perp \alpha = 0.41(5)\,. \tag{4.78}$$

The EW-KPZ crossover also takes place in the bKPZ+ case ($p > 1$), with the difference that in this case, in order to get better numerical results, one has to use large values of p.

As for finite-size simulations, what is appropriate for the RSOSW model is to measure how the critical point varies with the system size, because, as observed in [14], this variation is very pronounced. From relation (4.24) it is expected that

$$q_c(\infty) - q_c(L) \sim L^{-1/\nu_\|}, \tag{4.79}$$

where $q_c(L)$ is the critical point for a system of size L and $q_c(\infty)$ is the extrapolated value. Using this relation, Fig. 4.10 gives

$$\nu_\perp = 1.00(3). \tag{4.80}$$

From the scaling relation (4.29) and the above numerical result we get the exponent $\zeta = 0.5(1)$, in agreement with the value coming from off-critical simulations 0.41(5).

With time-dependent simulations the exponent θ is obtained by plotting n_0 as a function of time at criticality. From Fig. 4.10, we obtain the estimate

$$\theta = \beta/\nu_\| = 1.15(3). \tag{4.81}$$

From the scaling relations (4.27), (4.28), the finite-size result $\nu_\perp = 1.00(3)$ and $z = 3/2$ one can see that $\theta = 1.15(3)$ is in agreement with the off-critical result $\beta = 1.67(5)$.

Results coming from finite-size and time-dependent simulations are certainly more reliable than those extracted from off-critical simulations. Nevertheless, off-critical simulations are important to confirm scaling relations. Next we propose a scaling relation and show that it is in agreement with the numerical results presented here.

4.4.2 Scaling picture and differences between the bKPZ universality classes

We now argue heuristically that with the introduction of the wall just one new independent exponent arises. We suppose that the velocity of the interface in the growing phase follows $v \sim q - q_c$, which is in agreement with numerical results and an exact result presented in the last section. Since it is the time derivative of the mean height, which has the same scaling dimension

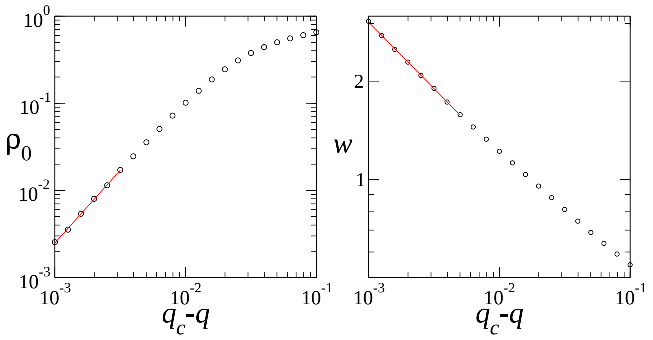

Figure 4.9: Off-critical simulations of the RSOSW model. Density of sites with height zero ρ_0 (left) and the interface width w (right) as functions of the distance from the critical point $q_c = 0.4295(1)$, with $p = 0.001$ and $L = 4096$.

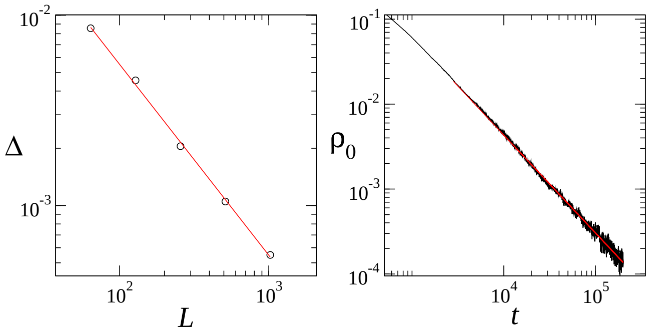

Figure 4.10: Left: Difference Δ between the finite-size critical point $q_c(L)$ and the extrapolated critical point $q_c(\infty) = 0.4295(3)$ as a function of L for $p = 0.001$. Right: ρ_0 as a function of t at the critical point $q_c = 0.4295(1)$, with $p = 0.001$, $L = 8192$ and 800 realizations.

as the interface width w, and $\xi_\parallel$ has the dimension of time, we expect that $w \sim (q - q_c)\xi_\parallel$. Combining this relation with (4.22), (4.24) and (4.27) we have the scaling relation

$$\nu_\perp = \frac{1}{z - \alpha}. \tag{4.82}$$

In this argument we combined relations valid above criticality ($v \sim q - q_c$) with relations valid below. However, one can see in table 4.1, where the exponents of the bKPZ and bEW universality classes are listed, that the scaling relation (4.82) leads to exponents in agreement with the numerical (bKPZ classes) and exact (bEW class) results. This may be explained as follows. Without a wall for $q < q_c$ the interface would have a negative velocity, going linearly to zero as a function of the distance from the critical line. It seems that, with the presence of the wall, quantities with the dimension of the mean height divided by quantities with dimension of time still go to zero linearly as criticality is approached. The scaling relation (4.82), was obtained for the first time in [99], for all dimensions, using a different argument.

With the scaling relation (4.82) and $z = \alpha/\gamma = \nu_\perp/\nu_\parallel$ we find that the critical exponents $\nu_\parallel$ and $\nu_\perp$ are determined by the scaling exponents. Therefore, there is only one independent (from the scaling exponents) critical exponent left, which is β.

All the above discussion should also be valid for the bKPZ+ universality class, the difference being that the new critical exponent β (or $\theta = \beta/\nu_\parallel$) has a different value. The best way to obtain the new critical exponent numerically is to perform time-dependent simulations using the SSW model, since in this model the critical point is known exactly. This was done in [112] and the estimated exponents are summarized in table 4.1.

The exponent β is bigger (smaller) than 1 for the bKPZ– (bKPZ+) universality class. This tell us that a typical interface configuration of the bKPZ– universality class at criticality is characterized by a smaller number of contact points with the substrate, in comparison to a bKPZ+ typical interface. In Fig. 4.11 we show typical interface configurations, obtained in [112] with

case	z	$\nu_\perp$	$\nu_\parallel$	ζ	θ	β
DP	1.58	1.10	1.73	0	0.159	0.276
bKPZ–	3/2	1	3/2	1/2	1.184(10)	1.776(15)
bEW	2	2/3	4/3	1/3	3/4	1
bKPZ+	3/2	1	3/2	1/2	0.228(5)	0.342(8)

Table 4.1: List of the critical exponents. Most of DP exponents in the first line come from [52], except for α and ζ which come from [121]. The bEW exponents come from the exact results presented in Sec. 3. The bKPZ exponents come the numerical results for the exponent θ obtained in [112] and the scaling relations presented here.

the SSW model at $p = 0$ ($\lambda > 0$) and $p = 1$ ($\lambda < 0$). For the bKPZ– case, a smaller number of contact points and larger detached regions (distance between two contact points) are observed.

Remarkably, the average distance between the contact points differs from the correlation length. More specifically, since the average distance of contact points $l(t)$ is proportional to $\rho_0^{-1}(t)$ and $\nu_\perp = 1$, we have that $l(t) > \xi_\perp(t)$ ($l(t) < \xi_\perp(t)$) for the bKPZ– (bKPZ+) class. The interplay of these two length scales leads to other differences between the bKPZ+ and bKPZ– universality classes, they are related to the distribution function of the distances between contact points and to the first depinning time probability distribution [112].

4.4.3 Wetting as a Contact Process with an external field

Let us now turn to the special case $p = 0$. Here the RSOSW model exhibits a very different dynamics, which was introduced in [120] and further analyzed in [119, 121]. This is a very particular case of the model, because for $p = 0$ once a layer is completely filled an evaporation on it becomes impossible.

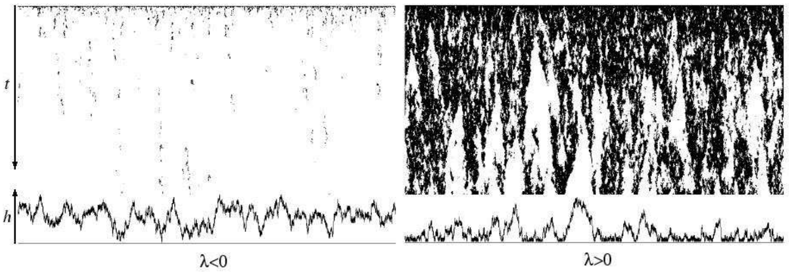

Figure 4.11: Upper row: typical spatio-temporal configuration of contact points with the substrate. Lower row: final interface configuration at $t = 5000$. The figures were obtained with numerical simulations of the SSW model at $p = 1$ ($\lambda < 0$) and $p = 0$ ($\lambda > 0$). The number of contact points in the $\lambda < 0$ case is clearly smaller. Figure taken from [112].

Hence, since the initial condition is a flat interface at height zero, the presence of the wall makes no difference.

It was shown in [120] that the phase transition at $p = 0$ belongs to the direct percolation (DP) universality class [48, 122], which is the most prominent universality class of nonequilibrium phase transitions into an absorbing state [49]. An explanation for this comes from the fact that the RSOSW model at $p = 0$ can be related to the contact process (CP)[52]. The CP is a well-known model in the DP universality class. It can viewed as a simple, and also simplistic, model for the propagation of a disease, where each site can be in two states: empty (healthy) or occupied by a particle (infected). Particles can create other particles at empty nearest neighbors sites (propagation of the disease) or die spontaneously (cure). If the system has no particles (no sick individuals) it is in the absorbing state and the dynamics ceases. A non-exact map between the CP and the RSOS at $p = 0$ model was proposed in [120], where sites with zero height are related to the infected individuals in the contact process. Hence, once the first layer is filled it is analogous to enter the absorbing state in CP, since no particles in this layer can be evaporated anymore and the height zero becomes inaccessible.

In [14] it was shown that the region in the phase diagram with $0 < p < 1$ can be interpreted as a DP process with an external field that destroys the transition. In the CP, an external field is introduced by allowing creation of particles at a certain rate. In thiscase there is no absorbing state anymore and the transition is lost. In the same way the non-zero p destabilizes the absorbing state in the RSOSW model, since even after the first layer is completely filled an evaporation on it is still possible. With this interpretation it is possible to predict the curvature of the phase transition line, Fig.4.3, and to calculate a crossover exponent from the DP to the bKPZ– universality class calculated (see [14] for details).

4.4.4 Numerical integration of the bKPZ equation

The MN equations can be integrated numerically very easily by using a method introduced in [123] to integrate Langevin equations with non-additive noise. The method consists of integrating the deterministic and stochastic parts of a discrete version of the Langevin equation separately in each time step.

We now explain this method for the MN1 equation in the case of an one-dimensional substrate. To this end we have to consider the spatially discrete version of equation (4.9), which reads

$$\frac{d}{dt}n_i = -an_i - bn_i^{s+1} - cn_i^{2s+1} + \sigma[n_{i+1} + n_{i-1} - 2n_i] + n_i\zeta_i, \tag{4.83}$$

where $n(x,t) \to n_i(t)$, $x \to i\delta x$ and we are using $\delta x = 1$. The algorithm evolves as follows. First a variable $n_i^*(t)$ is calculated from

$$n_i^*(t) = n_i(t) + \{-bn_i(t)^{s+1} - cn_i(t)^{2s+1} + \sigma[n_{i+1}(t) + n_{i-1}(t) - 2n_i(t)]\}dt, \tag{4.84}$$

which corresponds to one step of the integration, using the Euler method, of the deterministic part (without the linear term) of equation (4.83). After

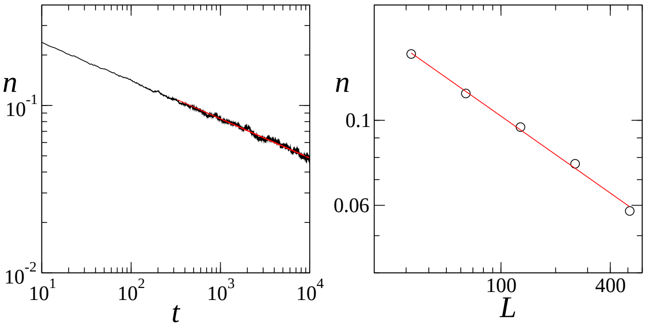

Figure 4.12: Numerical integration of equation (4.86). Left: time-dependent simulations with the order parameter $n = \langle m \rangle$ as a function of time at the critical point $a_c = 0.39025(25)$ for $L = 2048$, giving $\theta = 0.235(10)$. Right: finite-size simulations with the saturation value of n as a function of the system size L at the critical point, giving $\beta/\nu_\perp = 0.33(2)$. The values of the other parameters are $b = 1$, $c = 0$, $\sigma = 0.1$, $D = 1$, $s = 4$ and $dt = 0.1$.

that, $n_i(t + dt)$ is obtained with

$$n_i(t + dt) = n_i^*(t) \exp(-adt + \sqrt{Dt}\eta_i), \tag{4.85}$$

which is the solution of the one-variable Langevin equation constituted only of the stochastic part and the linear part of equation (4.83), where η_i is a random number coming from a Gaussian distribution with zero mean and unitary variance. The reason to add the linear term in the second step of the update scheme is that the stochastic part can still be solved exactly with it. Note that the term $-2\sigma n_i$, included in the first step, could instead be included in the second step. After all the L variables have been updated according to the above scheme a step dt is completed.

The numerical integration of the MN2 equation is more complicated because of the term $(\nabla n)^2/n$ [124]. In order to overcome this problem, Al Hammal et al. [125] considered a non-order parameter Langevin equation. Such an equation is obtained with the variable $m = 1/n$ that transforms the

MN2 equation (4.11) into:

$$\frac{\partial}{\partial t}m = am + bm^{1-s} + cm^{1-2s} + \sigma\nabla^2 m + m\zeta. \tag{4.86}$$

We integrated this equation numerically using the algorithm explained above. We performed time-dependent and finite-size simulations, obtaining $\theta = 0.235(10)$ and $\beta/\nu_\perp = 0.33(2)$ (see Fig. 4.12). The results are in agreement with the results obtained in [125] and the results presented in table 4.1. We note that changing the value of s does not change the critical behavior [125] (in Fig. 4.12 we used $s = 4$).

4.4.5 Numerical results for the attractive substrate case

As discussed in Sec. 2, in the bKPZ– case with an attractive force between the substrate and the interface there is a phase coexistence region if the attraction is strong enough and a depinning transition takes place at a new critical point (see Fig. 4.7).

This depinning transition was first observed to be first-order [109, 114]. Later Muñoz and Pastor-Satorras [107], with numerical integration of the MN1 equation, obtained exponents of the DP universality class. In Fig. 4.13 we present off-critical and time-dependent simulations for the RSOSW that agree with the findings from [107]. We used the values $p = 0.001$, where $q_c = 0.4295(1)$, and $q_0 = 0.39$ (which is smaller than q_0^*). We obtained the new critical point at $q_c^{(2)} = 0.4377(1)$, $\beta = 0.25(2)$ from off-critical simulations and $\theta = 0.159(5)$ from time-dependent simulations, both are in agreement with the DP exponents (see table 4.1). We note that DP exponents were also obtained for other microscopic models [110, 126]. Therefore, the observation of a first-order phase transition seems to be a transient effect.

Hinrichsen [127] argues about a possible connection between the pair contact process with diffusion (PCPD) and nonequilibrium wetting, pointing that the MN1 equation is equivalent to the Langevin equation for the PCPD [128]. There has been a long discussion about the universality class of the

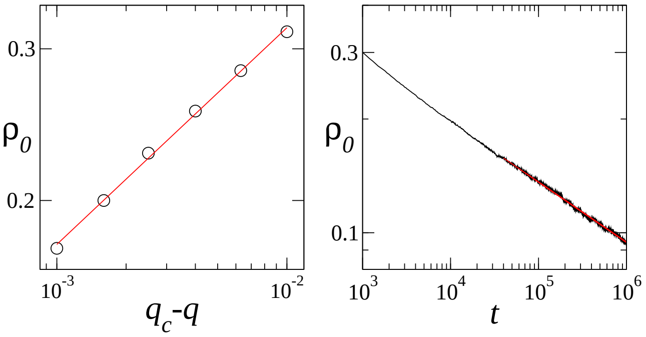

Figure 4.13: Simulations of the RSOSW model with an attractive force between the substrate and the interface. Left: off-critical simulations giving $\beta = 0.25(2)$. Right: time-dependent simulations giving $\theta = 0.159(10)$. Both exponents are in agreement with the DP exponents. The simulations were done at $p = 0.001$ and $q_0 = 0.39$, where $q_c = 0.4295(1)$ and $q_c^{(2)} = 0.4377(1)$.

PCPD [129], and it is still not clear if the PCPD model is in the DP universality class or if it is in a new universality class of models with an absorbing state. The result obtained in [107] would be in agreement with the PCPD being in the DP universality class, however, the continuum approach may be inadequate for PCPD [127].

Although the DP exponents were obtained in Fig. 4.13, the transition, that takes place with the parameters used there, is different from the transition at $p = 0$. To see this one can consider the survival probability $P_s(t)$, which is the probability that the system will not enter the absorbing state until time t. At $p = 0$ the survival probability can be less than one because once $\rho_0 = 0$ it will remain zero in the dynamics that follows. It decays to zero, in a power-law (exponential) way at (above) criticality and it reaches a saturation value after some transient below criticality. For $p \neq 0$ the survival probability is always one (in the moving and in the bound phases) because even if the first-layer is completely filled evaporation events on it are still possible. The Langevin equation related the RSOSW model at $p = 0$ is the

DP Langevin equation [109], where the noise term is multiplied by the square root of the field, and it cannot be obtained from the MN1 equation with a simple transformation of variables.

The tricritical point of the bKPZ– universality class was analyzed, with numerical integration of the MN1 equation and MC simulations of the SSW model, by Romera et al. [130]. They obtained $\gamma = 0.35(2)$, $z = 1.4(1)$, $\beta^{(2)} = 1.50(9)$, $\zeta^{(2)} = 0.9(1)$, $\theta^t = 0.49(2)$ and $\nu_{\parallel}^t = 2.0(2)$. As is the case of the bEW class, the critical exponents β^t, $\nu_{\perp}^t$ and $\nu_{\parallel}^t$ differ from the critical exponents of the bKPZ– class while the scaling exponents are in agreement with the KPZ values $\gamma = 1/3$ and $z = 3/2$. As far as we know, the critical behavior of the tricritical point of the bKPZ+ universality class was not yet analyzed.

We point out that the wetting transition can be envisaged as a contact process with long-range interactions, considering the contact points with the substrate as active sites and the detached part between two contact points as generating an effective long range interaction between them [131, 132, 133]. In the so-called $\sigma-$process [131], depending on the parameter controlling the long-range interactions the phase transition may be DP or first-order.

4.4.6 Extensions of the problem

Hitherto only short range interactions between the wall and the absorbed particles were considered. In order to study long range interactions one can take the potential

$$V(h) = \frac{b}{sh^s} + \frac{c}{lh^l}, \tag{4.87}$$

where the parameters b and c have the same function as they have in the short-range interaction potential (4.8) and $l > s$. Hammal et al. [134] studied complete wetting for the long range interactions case with numerical integration of the associated multiplicative noise equation, coming from the Cole-Hopf transformation of the bKPZ equation (4.6) with the potential

(4.87), and power counting arguments. The results are: for $s > 1$ the critical behavior is the same as the one obtained with short range interactions for the bKPZ– and bKPZ+ universality classes; for $s < 1$ mean field (in the sense that the noise is irrelevant) critical behavior holds. These results for long range interactions were also confirmed with a microscopic model in [134]. Another microscopic model with long range interactions was previously studied in [126], nevertheless, as pointed out in [103], it does not display a mechanism that produces surface tension (like the RSOS constraint for example) and, therefore, it is not clear if it corresponds to the bKPZ equation with the potential (4.87).

One relevant point in considering long range interactions is that it may play an important role in possible experimental realizations of nonequilibrium wetting. Another generalization of the problem, that can be central in an experiment, is to consider diffusion of single atoms in the interface. This generalization was studied in [135] using the RSOSW model with diffusion. In this new version of the model, another possible transition, taking place with rate D, is $h_i \to h_i - 1$ and $h_j \to h_j + 1$, where j is one of the nearest neighbors of i, before the transition $h_i > h_{i\pm1}$ and the final configuration respects the RSOS condition. It was found in [135] that for $p \neq 1$ diffusion can shift the critical line but the critical behavior is still the same and at $p = 1$ the critical behavior and the critical point do not change.

Another extension, which is not yet studied, is nonequilibrium wetting with disorder. In equilibrium wetting, the random substrate and also random bulk cases were studied, and new physical properties are born from these situations [92]. An open problem, in the equilibrium case, is what happens to critical wetting when a random substrate is considered [136, 137, 138].

4.5 Mean Field Approximations for microscopic models

In this section we present mean field approximations for the RSOSW and SSW models. We first write down the master equation for surface growth models and then apply simple and pair mean field approaches in order to solve it. The first mean field approximation, for microscopic models for nonequilibrium wetting, was introduced in [116]. The presentation here follows the works of Ginelli and Hinrichsen [111] for the SSW model and Barato and de Oliveira [13] for the RSOSW model. We also obtain some new results concerning pair mean field approach for the RSOSW model.

4.5.1 Master equation

A stochastic process with continuous time evolves according to the master equation (see [6]), such equation reads

$$\frac{d}{dt}P_\sigma(t) = \sum_{\sigma'\neq\sigma}\Big(P_{\sigma'}(t)w_{\sigma'\to\sigma} - P_\sigma(t)w_{\sigma\to\sigma'}\Big), \tag{4.88}$$

where $P_\sigma(t)$ is the probability of being in a configuration σ at time t and $w_{\sigma'\to\sigma}$ is the transition rate from the configuration σ' to the configuration σ. In the case of surface growth models with deposition and evaporation rates depending only on height of the target site and its nearest neighbors, the master equation becomes

$$\begin{aligned}\frac{d}{dt}P(h_1,h_2,...,t) = \sum_n\sum_{i=1}^{L}\{&w_n(h_{i-1},h_i-n,h_i+1)P(h_1,...,h_i-n,...,t)\\ &- w_n(h_{i-1},h_i,h_{i+1})P(h_1,...,h_i,...,t)\},\end{aligned} \tag{4.89}$$

where $w_n(h_{i-1},h_i-n,h_{i+1})$ is the rate for a transition from $(...,h_{i-1},h_i-n,h_{i+1},...)$ to $(...,h_{i-1},h_i,h_{i+1},...)$, L is the system size and we are considering an one-dimensional system with periodic boundary conditions.

Denoting $w_n(h_{i-1} = k, h_i = l, h_{i+1} = m)$ by $w_n(k, l, m)$ we have that for the RSOSW model, where the height changes by only $n = \pm 1$, the rates are:

$$w_+(k,k,k) = w_+(k+1,k,k) = w_+(k,k,k+1) = w_+(k+1,k,k+1) = q, \tag{4.90}$$

$$w_-(k,k+1,k) = w_-(k,k+1,k+1) = w_-(k+1,k+1,k) = 1, \tag{4.91}$$

and

$$w_-(k+1,k+1,k+1) = p. \tag{4.92}$$

On the other hand, for the SSW model they are non-zero only for $n = \pm 2$ and given by

$$w_{+2}(k,k-1,k) = p \tag{4.93}$$

and

$$w_{-2}(k,k+1,k) = 1 - p. \tag{4.94}$$

In the following we denote $P(k,l,m,t)w_n(k,l,m)$ by $J_n(k,l,m,t)$. The time evolution of the one-site probability distribution is obtained by summing over all heights but one in equation (4.89), which gives

$$\frac{d}{dt}P(l,t) = \sum_{k,m}\sum_n \{J_n(k,l-n,m,t) - J_n(k,l,m,t)\}, \tag{4.95}$$

For the the pair mean field approach (see below) we also need the time evolution of the two-site probability distribution, which is given by

$$\begin{aligned}\frac{d}{dt}P(k,l,t) = \sum_m\sum_n \{&J_n(m,k-n,l,t) + J_n(k,l-n,m,t)\\ &-J_n(m,k,l,t) - J_n(k,l,m,t)\}.\end{aligned} \tag{4.96}$$

The scaling exponents of the KPZ and EW universality classes are related to the interface width w. One can make the stronger assumption that the one-site probability distribution of these universality classes, for an infinite system and in the long time limit, is given by

$$P(h,t) = t^{-\gamma} f\left(\frac{h - vt}{t^\gamma}\right), \tag{4.97}$$

where $f(x)$ is a scaling function. Since in the calculations that follow we always consider an infinite system in the long time limit, when trying to solve the problem analytically, we use this ansatz for the one-site probability distribution at the wetting transition and in the moving phase.

The mean field approximations we apply to the RSOSW and SSW models in the following consist in approximating the probability distribution $P(h_1, h_2, ..., t)$ by a (simple or pair) factorized form so that the master equation becomes tractable. They are applied to one-dimensional models and expected to capture some features of them, they are not expected to become valid above some critical dimension.

4.5.2 The RSOSW model

Simple mean field approximation

In simple mean field, terms like $P(k, l, m, t)$ are approximated by their factorized form, i.e.,

$$P(k, l, m, t) = P(k, t)P(l, t)P(m, t). \tag{4.98}$$

Note that this approximation does not take the RSOS constraint into account. For example, the probability $P(k, k+2, k, t)$ is zero in the original problem and in the simple mean field approach it is simply given by $P(k, k+2, k, t) = P(k, t)^2 P(k+2, t)$.

With this approach the master equation for the one site probability distribution (4.95) for the RSOSW model acquires the following simpler form,

$$\begin{aligned}\frac{d}{dt}P_k = q(P_{k-1}^3 - P_k^3) + (1-2q)(P_k^2 P_{k+1} - P_{k-1}^2 P_k) + \\ (2-q)(P_k P_{k+1}^2 - P_{k-1} P_k^2) + p(P_{k+1}^3 - (1-\delta_{k,0})P_k^3),\end{aligned} \tag{4.99}$$

where P_k denotes the one-site probability distribution, $k \geq 0$ and $P_{-1} = 0$ (in order to account for the presence of the wall at height zero). The factor $(1 - \delta_{k,0})$ in the last term comes from the fact that evaporation at zero height is forbidden. The initial condition, corresponding to an initially flat interface, is $P_k = \delta_{k,0}$.

Below criticality we assume that P_k decays exponentially,

$$P_k = Ax^k, \tag{4.100}$$

where $A = 1 - x$ is a normalization constant and $x < 1$. This ansatz is valid below the critical line where the interface is bounded, while at criticality $x \to 1$. By substituting (4.100) in equation (4.99) we obtain

$$-px^3 + (q-2)x^2 + (2q-1)x + q = 0, \tag{4.101}$$

which, with $x = 1$, gives the critical line

$$q_c = \frac{1}{4}(p+3). \tag{4.102}$$

With the probability distribution (4.100) we have $P_0 = 1 - x$, $\langle h \rangle = \frac{x}{1-x}$ and $w = \frac{\sqrt{x}}{1-x}$. From equations (4.101) and (4.102), one can verify that near the critical line

$$x \approx 1 - \frac{2(q_c - q)}{2}. \tag{4.103}$$

Therefore,

$$P_0 \sim (q_c - q)^1, \qquad \langle h \rangle \sim (q_c - q)^{-1}, \qquad w \sim (q_c - q)^{-1}, \tag{4.104}$$

giving $\beta = 1$ and $\zeta = 1$.

In order to solve (4.99) at and above the critical line we take the continuum limit, where $P_k(t) \to P(h,t)$ and $h = k\delta$. In this limit, to second order in δ, equation (4.99) becomes

$$\partial_t P(h,t) = -12\delta(q - q_c)P^2\partial_h P + \delta^2(2q + 1 + 3p)\left(P(\partial_h P)^2 + \frac{1}{2}P^2\partial_h^2 P\right). \tag{4.105}$$

In the long time limit higher order terms are irrelevant even with $\delta = 1$. To see this one can carry out the calculation that follows with general δ and then verify it with the final result. Since we are interested in this limit we proceed with the calculations setting $\delta = 1$.

At the critical point the first term on the right hand side of the above equation vanishes, using the ansatz (4.97) we obtain consistency only if $\gamma = 1/4$ and $v = 0$. The differential equation for the scaling function is

$$f(x) + xf'(x) + 2(2q+1+3p)[2f(x)f'(x)^2 + f(x)^2 f''(x)] = 0, \qquad (4.106)$$

which has the solution $f(x) = \sqrt{1 - \frac{x^2}{2(2q+1+3p)}}$, giving

$$P(h,t) = \sqrt{t^{-1/2} - \frac{h^2}{2t(2q+1+3p)}}. \qquad (4.107)$$

Above the critical point only the first term in the right hand side of equation (4.105) matters, the second is irrelevant for $t \to \infty$. By following the same procedure as in the previous case, we obtain $\gamma = 1/3$, $v = 0$ and

$$f(x) + xf'(x) - 36(q - q_c)f(x)^2 f'(x) = 0, \qquad (4.108)$$

which has the solution $f(x) = \sqrt{x/12(q-q_c)}$, giving

$$P(h,t) = \sqrt{\frac{h}{12(q-q_c)t}}, \qquad (4.109)$$

for $q > q_c$.

Very surprising is the fact that with this very simple approximation we obtain the exact KPZ growth exponent $\gamma = 1/3$ above the critical line. However, we do not obtain the mean height growing linearly with time above criticality, i.e., $v = 0$ also for $q > q_c$. The next step is to perform an improved approximation, that satisfies the RSOS condition and gives $v > 0$ in the moving phase.

Pair mean field approximation

In the pair mean field approximation $P(k,l,m,t) = P(k,l,t)P(l,m,t)/P(l,t)$. This means that the probability distribution is approximated by a pair factorized form. Clearly, the present approach satisfies the RSOS condition.

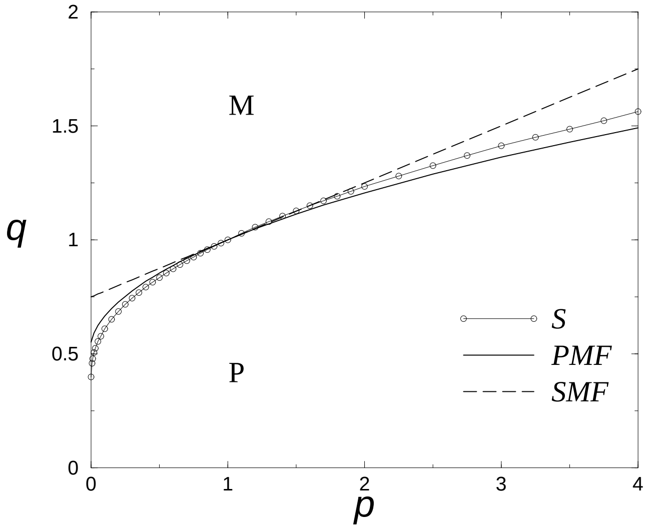

Figure 4.14: Comparison between the phase diagrams obtained with mean filed approximations, simple (SMF) and pair (PMF), and simulations (S) for the RSOSW model.

For the pair mean field we need the time evolution of one-site and two-site probability distributions. Because of the RSOS condition only $P_{k,k}$, $P_{k,k-1}$ and $P_{k,k+1}$ are non-zero. Therefore, we have four variables: the three two-site probability distributions and the one-site probability distribution P_k. They are not all independent, one obvious constraint is that $P_k = P_{k,k} + P_{k,k+1} + P_{k,k-1}$ and the other is $P_{k,k+1} = P_{k+1,k}$. The second comes from the facts that the transition rates are symmetric and we are considering periodic boundary conditions. Therefore, we are left with two independent sets of equations.

Applying the pair mean field to equation (4.96) we obtain

$$\begin{aligned}\frac{d}{dt}x_k &= 2q\left[\frac{y_{k-1}(y_{k-1}+x_{k-1})}{P_{k-1}} - \frac{x_k(x_k+y_k)}{P_k}\right]\\ &+2\left[\frac{y_k(y_k+x_{k+1})}{P_{k+1}} - \frac{x_k y_{k-1}}{P_k}\right] - 2p\frac{x_k^2}{P_k}(1-\delta_{k,0}),\end{aligned}\tag{4.110}$$

$$\frac{d}{dt}y_k = q\frac{x_k^2 - y_k^2}{P_k} - \frac{y_k^2}{P_{k+1}} + p\frac{x_{k+1}^2}{P_{k+1}},\tag{4.111}$$

where $x_k = P_{k,k}$ and $y_k = P_{k+1,k} = P_{k,k+1}$. The term $1 - \delta_{k,0}$ multiplying $2p\frac{x_k^2}{P_k}$ in the first equation comes again from the fact that evaporation events are forbidden at height zero and the initial condition is $x_k = \delta_{k,0}$ and $y_k = 0$ for all k.

The above equations were integrated numerically in [13], the results are in agreement with $\beta = 1$, $\zeta = 1/3$, the EW growth exponent $\gamma = 1/4$ at the critical line and the KPZ growth exponent $\gamma = 1/3$ above it. Moreover, with this improved approximation an interface growing linearly with time for $q > q_c$ is observed. The phase diagrams, coming from mean field, are compared to the one obtained with simulations in Fig. (4.14). One can see that the agreement with pair mean field is much better than with simple mean field.

Compared to the simple mean field the main improvements are: better agreement with simulations, when comparing the phase diagram and also observables (not shown here, see [13]), and an interface growing with a non-zero velocity in the moving phase. The exponent $\zeta = 1/3$ is different from the one obtained with simple mean field, which is $\zeta = 1$, while the others are the same (including the EW and KPZ growth exponents at and above criticality respectively).

An interesting feature of the pair mean field is that it becomes the exact solution of the model when $p = 1$. From equation (4.35), with the pair mean field approach, it follows that

$$q\frac{x_k}{P_k} = \frac{x_{k+1}}{P_{k+1}}, \qquad y_k^2 = x_k x_{k+1}, \tag{4.112}$$

which has the solution

$$\frac{x_k}{P_k} = \Lambda^{-1} q^k, \qquad \frac{y_k}{\sqrt{P_k P_{k+1}}} = \Lambda^{-1} q^{q+1/2}. \tag{4.113}$$

Equations (4.112) and (4.113), with the condition $P_k = x_k + y_k + y_{k-1}$, give

$$q^{k-1/2}\sqrt{P_{k-1}} + q^k\sqrt{P_k} + q^{k+1/2}\sqrt{P_{k+1}} = \Lambda\sqrt{P_k}. \tag{4.114}$$

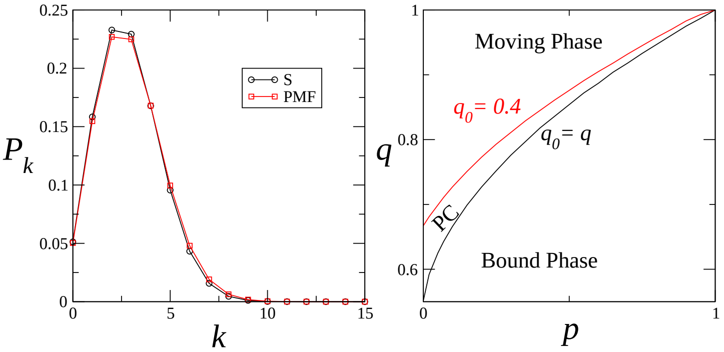

Figure 4.15: Pair mean field results. Left: comparison of the one site probability distribution obtained from pair mean field (PMF) and from simulations (S) at $q = 0.99$ and $t = 500$. Right: phase coexistence (PC) region at the $q \times p$ plane with $q_0 = 0.4$ obtained from numerical integration of the pair mean field equations.

This is equal to equation (4.49), with the components of the eigenvector, associated to the maximum eigenvalue Λ, given by $\phi_k = \sqrt{P_k}$.

The pair mean field becomes the exact solution at $p = 1$ and $q \leq 1$, because the probability distribution is pair-factorized in the stationary sate. This comes from the fact that the stationary probability distribution can be written as a product of transfer matrices. A natural question that arises is whether the time-dependent probability distribution is also pair-factorized. If this were the case, the solution of the pair mean field equations (4.110) and (4.111) would give the exact time-dependent probability distribution. In order to check this, we compare the one-site probability distribution obtained from simulations and numerical integration of (4.110) and (4.111) in Fig. 4.14. We see that they are in agreement, suggesting that the time-dependent probability distribution is indeed pair-factorized.

The case $q_0 \neq q$ can also be considered within the pair mean field approach. Equations (4.110) and (4.111), for $k = 0$ and $k = 1$, have to be modified to

$$\frac{d}{dt}x_0 = -2q_0\frac{x_0(x_0+y_0)}{P_0} + \text{evaporation part} \tag{4.115}$$

$$\frac{d}{dt}x_1 = 2q_0\frac{y_0(y_0+x_0)}{P_0} - 2q\frac{x_1(x_1+y_1)}{P_1} + \text{evaporation part} \tag{4.116}$$

$$\frac{d}{dt}y_0 = q_0\frac{x_0^2-y_0^2}{P_0} + \text{evaporation part}, \tag{4.117}$$

where the evaporation part corresponds to the terms of equation (4.110) and (4.111) that are not multiplied by q. By integrating these new equations we obtain the following results: For $q_0 < q_0^*$ the transition becomes first-order for $p \geq 1$ while for $p < 1$ a phase coexistence region (in the sense explained in Sec. 4.2) is observed, and the transition at the additional line $q_c^{(2)} > q_c$ seems to be first-order. In Fig. 4.15 we show the phase coexistence region in the $q \times p$ plane for $q_0 = 0.4$ obtained with numerical integration of the above equations. The results presented in Fig. 4.15 were not obtained elsewhere.

4.5.3 The SSW model

For the SSW model, with the pair mean field approach, we are left just with one independent set of equations. This happens because, in comparison to the RSOSW model, there are the same two constraints and not four but three variables (P_k, $P_{k,k+1}$ and $P_{k,k-1}$). We can define the height for an interface, satisfying the single-step constraint, in the following way. With every pair of sites with heights given by h_i, h_{i+1}, we associate a variable $h'_i = \min(h_i, h_{i+1})$, that can be viewed as defined in a point between the two sites. For example, the initial configuration, where $h_i = 0$ ($h_i = 1$) if i is even (odd), corresponds to $h'_i = 0$ for all i. In this way the two-site probability distribution $P_{k,k+1}$ can be viewed as an one-site probability distribution P_j, where $j = k$. In the calculations that follows we use this new one-site probability distribution.

The master equation for the (new) one-site probability distribution within pair mean field for the SSW model reads

$$\frac{d}{dt}P_j = p\left(\frac{P_{j-1}^2}{P_{j-1}+P_{j-2}} - \frac{P_j^2}{P_j+P_{j-1}}\right)$$
$$+(1-p)\left(\frac{P_{j+1}^2}{P_{j+1}+P_{j+2}} - \frac{P_j^2}{P_j+P_{j+1}}\right), \tag{4.118}$$

where the boundary conditions, to be specified below, depend on the velocity of the wall.

The above equation in the continuum limit reads

$$\partial_t P(h,t) = -\delta(p-1/2)\partial_h P + \delta^3\frac{(p-1/2)}{12}\left(3\frac{(\partial_h P)^3}{P^2} - 6\frac{\partial_h P\partial_h^2 P}{P} + 4\partial_h^3 P\right)+$$
$$\delta^4\left(\frac{(\partial_h P)^4}{4P^3} - 5\frac{(\partial_h P)^2\partial_h^2 P}{8P^2} + \frac{(\partial_h^2 P)^2}{4P} + \frac{\partial_h P\partial_h^3 P}{4P} - \frac{\partial_h^4 P}{8}\right) \tag{4.119}$$

where $h = j\delta$ and we went until order δ^4. As we did in the simple mean field for the RSOSW model we set $\delta = 1$, because one can show that higher order terms are irrelevant in the long time limit [111].

In order to solve equation (4.119) we apply the ansatz (4.97) to it. The first term produces a linear propagation of the interface, therefore

$$v = p - 1/2, \tag{4.120}$$

which is in agreement with equation (4.14). At $p = 1/2$ the first two terms on the right hand side of (4.119) vanish and a non-trivial equation is obtained only if $\gamma = 1/4$, giving the EW growth exponent in the equilibrium case. For $p \neq 1/2$ the third term on the right hand side of (4.119) is irrelevant in the long time limit and a non-trivial equation is obtained only if $\gamma = 1/3$, giving the KPZ growth exponent.

We proceed by presenting the resulting differential equations for the scaling function and their solutions for the cases $p = 1/2$, $p = 0$ and $p = 1$. In each case subtle boundary conditions have to be used in order to account for the moving substrate. Our aim is to calculate the exponent θ within this approximation for the bEW and bKPZ universality classes. To avoid confusion we denote the scaling function f and the critical exponent θ, for each value of p, by f_p and θ_p.

bEW case

For $p = 1/2$ the differential equation for the scaling function $f_{1/2}(x)$ is

$$(f_{1/2})^{-3}\Bigg[(f_{1/2})^4 - \frac{5}{2}f_{1/2}(f'_{1/2})^2 f''_{1/2} + (f_{1/2})^2\Bigg((f''_{1/2})^2 + f'_{1/2}f'''_{1/2}\Bigg) \\ +(f_{1/2})^3\Bigg(xf'_{1/2} - \frac{1}{2}f'''_{1/2}\Bigg) + (f'_{1/2})^4\Bigg] = 0, \quad (4.121)$$

where $x = ht^{-\gamma}$. Integrating it we get

$$2xf_{1/2} - \frac{(f'_{1/2})^3}{(f_{1/2})^2} + 2\frac{f'_{1/2}f''_{1/2}}{f_{1/2}} - f'''_{1/2} = 0. \quad (4.122)$$

We have to solve the above equation with the appropriate boundary conditions. At $p = 1/2$ the substrate is fixed at height zero, therefore, the evolution of the probability distribution P_j follows equation (4.118) for $j > 0$, while at zero height it follows

$$\frac{d}{dt}P_0 = -\frac{1}{2}P_0 + \frac{1}{2}\left(\frac{P_1^2}{P_1 + P_2}\right), \quad (4.123)$$

where the missing terms in the equation come from the fact that evaporation is forbidden at the substrate and $P_j = 0$ for $j < 0$. Now if we assume that the scaling function satisfies $f'(0) < \infty$ we have $P_j \approx t^{-1/4}f(0)$ for $j = 0, 1, 2$. Substituting this in the last equation, we see that it is valid only if $f(0) = 0$ (the left side of the equation is proportional to $t^{-5/4}$ and the right side is proportional to $t^{-1/4}$).

The solution of equation (4.122), satisfying the boundary condition $f(0) = 0$, is [111]

$$f_{1/2}(x) = \frac{2^{5/4}}{\sqrt{\pi}}x^2 \exp(-x^2/\sqrt{2}), \quad (4.124)$$

which gives the exponent $\theta_{1/2} = 3/4$.

bKPZ case

For $p \neq 1/2$ the differential equation becomes

$$(f_p)^{-2}\Bigg[8(f_p)^3 + 6v(f'_p)^3 - 12vf_pf'_pf''_p + 8(f_p)^2(xf'_p + vf'''_p)\Bigg] = 0, \quad (4.125)$$

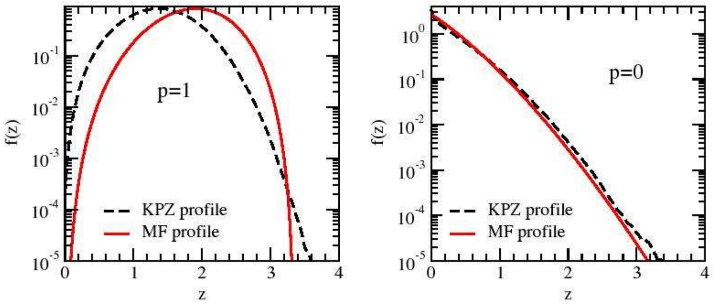

Figure 4.16: The scaling function $f(z)$ for the bKPZ– ($p = 1$) and the bKPZ+ ($p = 0$) universality classes, obtained from numerical simulations (dotted line) and mean field (MF) approach for the SSW model. Figure taken from [111].

where $x = (h - vt)t^{-\gamma}$.

Obtaining the suitable boundary conditions for the cases $p = 0$ and $p = 1$ accounting for a moving wall is more involved. With an argument similar to the one presented above it is possible to show that $f_1(0) = 0$ and $f_0(0) \neq 0$ [111]. With these boundary conditions the solutions of equation (4.125), that are physically suitable, are [111]:

$$p = 1: \qquad f_1(x) \propto \begin{cases} \left[Ai\left(\frac{-x}{2^{1/3}}\right) - 3^{-1/2} Bi\left(\frac{-x}{2^{1/3}}\right) \right]^4 & \text{if } 0 \leq x < x_0 \\ 0 & \text{if } x_0 \leq x < \infty \end{cases} \tag{4.126}$$

and

$$p = 0: \qquad f_0(x) \propto Ai\left(\frac{x}{2^{1/3}}\right)^4, \tag{4.127}$$

where $Ai(x)$ and $Bi(x)$ are Airy functions and $x_0 \approx 3.32426$. The scaling function (4.126) gives the exponent $\theta_1 = 4/3$ for the bKPZ– case and (4.127) $\theta_0 = 1/3$ for the bKPZ+ case. They are different from the exponents obtained from numerical simulations (see table 4.1).

Although the mean field theory does not predict the correct value of the critical exponent θ in the nonequilibrium cases, it does predict differences between the bKPZ+ and bKPZ– universality classes. For the bKPZ– (bKPZ+) an exponent bigger (smaller) than the equilibrium exponent $\theta_{1/2} = 3/4$ is obtained. Moreover, as shown in Fig 4.16, the scaling functions given in equations (4.126) and (4.127)are qualitatively similar to the scaling functions obtained from numerical simulations.

With this mean field approach the one-site probability distribution for the free interface case can also be obtained, in this case the differential equations for the scaling functions have to be solved with different boundary conditions [111]. In [139], several exact results were obtained for the free interface case with the polynuclear growth model, which is in the KPZ universality class. A very important question is whether, with the methods used in [139], the bounded interface case can also be treated, allowing one to compute the exponent θ for the bKPZ universality classes exactly.

4.6 Nonequilibrium wetting in higher dimensions

We now turn to nonequilibrium wetting in higher dimensions. First we present a mean field approach to the MN equations, which yields a qualitative picture of what happens above the critical dimension. Then we discuss the critical behavior that is expected in higher dimensions using power counting and renormalization group arguments.

4.6.1 Mean field for the continuum model

The mean field approximation to the MN equations is done in the following way [140]. The first step is to approach the discrete Laplacian by

$$\nabla^2 n_i = \frac{1}{2d}\sum_j (n_j - n_i) \approx \langle n\rangle - n_i, \qquad (4.128)$$

where the sum runs over all nearest neighbors and this approximation is expected to become valid above some critical dimension. In the MN1 case the resulting equation reads

$$\frac{d}{dt}n = -an - bn^{s+1} - cn^{2s+1} + \sigma(n - \langle n \rangle) + n\zeta. \tag{4.129}$$

The associated Fokker-Planck equation [7, 6] is

$$\frac{\partial}{\partial t}P(n, \langle n \rangle, t) = -\frac{\partial}{\partial n}\{[-(a - D/2)n - bn^{s+1} - cn^{2s+1} + \sigma(n - \langle n \rangle)]P(n, \langle n \rangle, t)\} + \frac{D}{2}\frac{\partial^2}{\partial n^2}[n^2 P(n, \langle n \rangle, t)]. \tag{4.130}$$

Solving the above equation in the stationary state we obtain

$$P_s(n, \langle n \rangle) \propto n^{2(a-\sigma)/D-1} \exp\left(-\frac{2b}{Ds}n^s - \frac{c}{Ds}n^{2s} - \frac{2\sigma\langle n \rangle}{nD} \right), \tag{4.131}$$

where $P_s(n, \langle n \rangle)$ is the probability distribution in the stationary sate. Finally the critical behavior of the order parameter $\langle n \rangle$ is obtained with the self-consistency condition

$$\langle n \rangle = \frac{\int_0^\infty nP_s(n, \langle n \rangle)dn}{\int_0^\infty P_s(n, \langle n \rangle)dn}. \tag{4.132}$$

For the MN2 case we consider the non-order parameter Langevin equation (4.86) together with the approximation (4.128). The solution of the corresponding Fokker-Planck equation is

$$P_s(m, \langle m \rangle) \propto m^{2(a-\sigma)/D-1} \exp\left(-\frac{2b}{Ds}m^{-s} - \frac{c}{Ds}m^{-2s} - \frac{2\sigma\langle m \rangle}{mD} \right). \tag{4.133}$$

Using the mean field approach introduced we now consider complete wetting, therefore, we set $c = 0$ and b constant and positive. In the calculations below, for the MN2 case we follow [125] and for the MN1 case we follow [141, 142].

For the MN2 case, the self-consistency condition (4.132) with the probability distribution (4.133) leads to the following equation,

$$\langle m \rangle = \frac{I_1(\langle m \rangle)}{I_0(\langle m \rangle)}, \tag{4.134}$$

where

$$I_k(y)=\int_0^{\infty} dx x^{k+2(a-\sigma)/D-1}\exp\biggl(-\frac{2b}{Ds}x^{-s}-\frac{2\sigma y}{xD}\biggr). \tag{4.135}$$

We want to calculate the exponent β, defined by $\langle m\rangle\sim(a_c-a)^{-\beta}$ (m is a non-order parameter). We can write $I_k(y)$ as

$$I_k(y)=\biggl(\frac{2\sigma y}{D}\biggr)^{k+2(a-\sigma)/D}\int_0^{\infty} dz z^{-1-k-2(a-\sigma)/D}e^{-z}\exp\biggl[-\frac{2b}{Ds}\biggl(\frac{Dz}{2\sigma y}\biggr)^{s}\biggr] \tag{4.136}$$

where $z=\frac{2\sigma y}{Dx}$. At criticality $\langle m\rangle\to\infty$, we are interested in the asymptotic form of $I_k(y)$, with $y\to\infty$. In this limit

$$I_k(y)\approx\biggl(\frac{2\sigma y}{D}\biggr)^{k+2(a-\sigma)/D}\Gamma(-2a/D+2\sigma/D-k)$$
$$-\biggl(\frac{2\sigma y}{D}\biggr)^{k+2(a-\sigma)/D-s}\frac{2b}{Ds}\Gamma(-2a/D+2\sigma/D-k+s), \tag{4.137}$$

where the term $\exp\biggl[-\frac{2b}{Ds}\biggl(\frac{Dz}{2\sigma y}\biggr)^{s}\biggr]$ was expanded to first order in $(z/y)^s$. The above asymptotic form for $I_k(y)$ and equation (4.134) lead to [125]

$$\langle m\rangle\sim(-D/2-a)^{-1/s}, \tag{4.138}$$

which gives $\beta=1/s$ and $a_c=-D/2$.

Using (4.131) and (4.132) the resulting equation for the MN1 case is [141, 142]

$$\langle n\rangle=\frac{J_1(\langle n\rangle)}{J_0(\langle n\rangle)}, \tag{4.139}$$

where

$$J_k(y)=\int_0^{\infty} dx x^{k+2(a-\sigma)/D-1}\exp\biggl(-\frac{2b}{Ds}x^{s}-\frac{2\sigma y}{xD}\biggr). \tag{4.140}$$

It can be shown that, for $y\to 0$, [141, 142]

$$J_k(y)\approx A_k+B_k y^{2(a-\sigma)/D+k}+C_k y^{2(a-\sigma)/D+k+s}, \tag{4.141}$$

leading to

$$\langle n\rangle\sim(D/2-a)^{\max[1/s,D/2\sigma]} \tag{4.142}$$

where max indicates the maximum. This shows that for the MN1 case we have a more complex critical behavior: a weak-noise regime, where $D < 2\sigma/s$ and $\beta = 1/s$, and a strong-noise regime, where $D > 2\sigma/s$ and $\beta = D/2\sigma$. With the asymptotic form (4.141) one can also calculate the critical exponents related to higher order moments $\langle n^k \rangle = J_k(\langle n \rangle)/J_{k-1}(\langle n \rangle)$. The strong-noise regime can be further divided into two regimes that are different with respect to the critical behavior of higher order moments [142].

Critical wetting can be studied with the same kind of procedure, as done by de los Santos et al. [143]. In critical wetting, for the MN2 case just one regime is found with the critical exponent being independent of the noise strength, while for the MN1 case weak and strong noise regimes are found. Moreover, with the present mean field approximation, phase coexistence for the bKPZ– universality class, when the attraction between the substrate and the interface is strong enough, is observed [144, 115].

We point out that in contrast to the method presented above a simpler approach would be consider the one-variable case by taking out the Laplacian. The one-variable MN1 equation was solved exactly in [145]. It has a rich scaling behavior, nevertheless it does not display the strong noise regime. One interesting feature of the one-variable approximation is that it allows one to clarify essential differences between the MN1 and the DP Langevin equations [146].

4.6.2 Scaling analysis

Given a Langevin equation we can define the partition function Z by summing over all configurations and realizations of noise that satisfy it. In the case of the MN1 equation (4.9) with the potential (4.10) and $c = 0$ it reads

$$Z \propto \int DnD\zeta P[\zeta]\delta\left(\frac{\partial}{\partial t}n + an + bn^s - \nabla^2 n - n\zeta\right), \tag{4.143}$$

where

$$P[\zeta] \propto \exp(\zeta^2/2D) \tag{4.144}$$

and $\int DnD\zeta$ denotes a functional integration. With the introduction of a response field $\tilde{n}$ one can integrate out the noise [63], resulting in the following equation,

$$Z \propto \int DnD\tilde{n} \exp\Big(- S[n,\tilde{n}]\Big), \tag{4.145}$$

with the action $S[n,\tilde{n}]$ given by

$$S[n,\tilde{n}] = \int d^dx dt \left[\frac{D}{2}\tilde{n}^2 n^2 - \tilde{n}\left(\frac{\partial}{\partial t}n + an + bn^p - \nabla^2 n\right)\right], \tag{4.146}$$

where, for simplicity, we set $\sigma = 1$. Preforming naive power counting in this action we obtain

$$[n] + [\tilde{n}] = -d \qquad \text{and} \qquad [D] = d - 2, \tag{4.147}$$

where $[x]$ represents the dimension of the quantity x in units of length. Therefore, the critical dimension, above which the noise becomes irrelevant, is $d_c = 2$. It is known that the response field $\tilde{n}$ scales as the survival probability [74]. In the case of the bKPZ– universality class the survival probability is always one, therefore the dimension of the response field $\tilde{n}$ is zero, giving $[n] = d$. Power counting at the critical dimension $d_c = 2$ gives

$$\beta = 1, \qquad \nu_\perp = 1/2, \qquad \nu_\| = 1. \tag{4.148}$$

Using standard methods [147] one can perform a perturbative expansion with the action (4.146) and then obtain the renormalization group flow diagram for the MN1 equation. The calculations of which we shall discuss some important points below can be found in [102]. Since the term proportional to b goes to zero in the moving phase, the bKPZ equation is equivalent to the KPZ equation in the moving phase. The flow diagram is similar to the well-known KPZ one [148]: above the critical dimension $d_c = 2$ there is a weak-noise attractive fixed point, where $D = 0$, and a strong-noise repulsive fixed point. If the noise strength is smaller then a certain threshold the flow runs to the weak noise fixed point and the critical exponents are given by

(4.148). On the other hand, if it is larger the flow runs to infinity and the critical behavior is not accessible through perturbation theory. Therefore the situation is similar to the one obtained with the mean field approximation. This was verified with numerical integration of the MN1 equation for $d = 3$ in [140].

Another important point about the perturbative expansion is that changing s, the hardness of the wall, does not introduce new divergences and therefore it is not expected to affect the critical behavior [102]. This is in agreement with numerical results and different from the mean field result that predicts an exponent depending on s in the weak noise regime.

The critical behavior at the critical dimension $d = 2$ cannot be determined by perturbation theory. This is a very important case because in experimental situations the substrate is usually two-dimensional. The critical exponents θ (or β) of the bKPZ universality classes in two dimensions are not known.

The renormalization group flow equations can be derived in an alternative way without writing down the action, but direct from the Langevin equation. For the MN1 equation this can be found in [104] and for the KPZ equation in [20].

4.7 Final remarks

Just as the KPZ equation represents a robust universality class of nonequilibrium growing free interfaces, the bKPZ equation is expected to represent a robust universality class of nonequilibrium growing interfaces in the presence of wall. While equilibrium wetting transitions can be studied with the bEW equation, nonequilibrium wetting transitions are described by the bKPZ equation. Below we point out what we consider the main open problems in nonequilibrium wetting.

With the introduction of the wall critical exponents arise, just one of them is independent while the others can be determined from scaling relations and the KPZ scaling exponents. An important open problem in nonequilibrium wetting is the exact calculation of the exponent θ for the bKPZ universality classes. While an exact solution for the free interface case, for a specific microscopic model in the KPZ universality class, is known [139], no exact solution is known for the bounded case. As we showed here within a mean field approximation for the SSW model the exponent θ and the one-site probability distributions for the bKPZ universality classes can be determined analytically but they differ from the numerical results obtained for the full model.

As pointed out, extensions of the problem that were already considered involve long-range interactions between the substrate and the absorbed particles and the study of the RSOSW model with diffusion of particles. What has not benn studied so far is nonequilibrium wetting with disorder, which can be very relevant in an experimental situation. It may be also relevant in possible experimental realizations to consider nonequilibrium wetting on a two-dimensional substrate. The critical exponents of the bKPZ universality class in $d = 2$ were not yet determined. Performing Monte Carlo simulations with microscopic models or numerical integration of the Langevin equation at $d = 2$ is a trivial task, but the main problem is to find some approximative method that can support the results obtained with simulations.

The main challenge, in what we defined here as nonequilibrium wetting, is to observe the predicted critical behavior experimentally. Any growing interface in the presence of a wall and under nonequilibrium conditions is, in principle, a potential candidate for an experimental realization of the bKPZ universality classes. Following the discussion in [103] good candidates may come from crystal growth and synchronization transitions in extended one-dimensional systems.

Chapter 5

Entropy production and fluctuation relations

5.1 Introduction

For some Markov processes it is possible to associate an entropy with a single stochastic path [149]. Consider a realization that starts at a configuration (or state) C_0 at time $t = T_0$, jumps from C_{i-1} to C_i at time τ_i until it reaches the state C_N and stays at C_N until, at least, time T. The variation of the external medium entropy during the time interval $\Delta T = T - T_0$ is defined by [149]

$$\Delta S_m = \sum_{i=1}^{N} \ln \frac{w_{C_{i-1} \to C_i}}{w_{C_i \to C_{i-1}}}, \tag{5.1}$$

where $w_{C \to C'}$ is the transition rate from the state C to the state C'. On the other hand, the definition of the variation of the system entropy is

$$\Delta S_{sys} = \ln \frac{P(C_0, T_0)}{P(C_N, T)}, \tag{5.2}$$

where $P(C, t)$ is the probability of being in the state C at time t. The variation of the total entropy is just $\Delta S_{tot} = \Delta S_m + \Delta S_{sys}$. We are considering continuous time Markov processes following the master equation,

$$\partial_t P(C,t) = \sum_{C' \neq C} \Big(P(C',t) w_{C' \to C} - P(C,t) w_{C \to C'} \Big). \tag{5.3}$$

In order for the definition of ΔS_m to be valid the Markov process has to be such that all transitions are reversible, i.e., if $w_{C \to C'} \neq 0$ then $w_{C' \to C} \neq 0$, for all pair of states C and C'. The entropy production of the medium $\dot{s}_m(t)$ is defined by

$$\Delta S_m = \int_{T_0}^{T} \dot{s}_m(t) dt. \tag{5.4}$$

From equation (5.1), the (ensemble) average entropy production of the medium is [149, 150]

$$\langle \dot{s}_m(t) \rangle = \sum_{C,C'} \ln \frac{w_{C \to C'}}{w_{C' \to C}} P(C,t) w_{C \to C'}. \tag{5.5}$$

In the same way one has that, the average entropy production of the system is

$$\langle \dot{s}_{sys}(t) \rangle = \sum_{C,C'} \ln \frac{P(C,t)}{P(C',t)} P(C,t) w_{C \to C'}. \tag{5.6}$$

The total entropy production is just the sum of the system and the medium entropy production. As we will see, $\langle \dot{s}_{tot}(t) \rangle$ is always positive and in the stationary state the average entropy production of the system goes to zero. Only when detailed balance is fulfilled $\langle \dot{s}_{tot} \rangle$, the average total entropy production in the stationary state, is exactly zero. Therefore a positive entropy production is a characteristic of nonequilibrium stationary states.

The fluctuation relation [151, 152, 153, 154, 155, 156, 157, 158] constrains the probability distribution of the variation of total entropy $P(\Delta S_{tot} = X)$ during a time interval ΔT in the following way:

$$\ln \left(\frac{P(\Delta S_{tot} = X)}{P(\Delta S_{tot} = -X)} \right) = X. \tag{5.7}$$

For this relation to be valid one has to start the measure of the entropy variation at a time T_0 such that the stationary state has already been reached in order. Another fluctuation relation, valid in the limit $\Delta T \to \infty$, is

$$\ln\left(\frac{P(\Delta S_m = X)}{P(\Delta S_m = -X)}\right) = X, \tag{5.8}$$

where in this case the initial time T_0 can be chosen freely (the probability distribution $P(C, T_0)$ does not have to be the stationary one). An additional restriction, in comparison to the finite time fluctuation relation (5.7), is that the number of states has to be finite (see below).

Large deviation theory [159, 160, 161] deals with exponentially decaying probabilities. In equilibrium statistical mechanics when preforming Legendre transforms to calculate different thermodynamic potentials, one is using results of large deviation theory, which is the appropriate mathematical theory for equilibrium statistical mechanics [161]. It is possible to perform such calculations because in equilibrium the probability distribution of states is known. Such general large deviation principles are not available in nonequilibrium, where the distribution of sates is generally not known. In this sense fluctuation relations are of conceptual interest: they are a fairly general statement that implies, as we will show, a symmetry of the large deviation function associated with the probability distribution of entropy.

In this chapter we study the entropy production and the asymptotic fluctuation relation (5.8) for a microscopic surface growth model in the Kardar-Parisi-Zhang [96] (KPZ) universality class. The KPZ equation reads

$$\partial_t h(x,t) = v + \nu\nabla^2 h(x,t) + (\lambda/2)(\nabla h(x,t))^2 + \eta(x,t), \tag{5.9}$$

where x denotes the position on a $d-$dimensional interface (we will be dealing only with the $d = 1$ case), $h(x,t)$ represents the height of the interface and $\eta(x,t)$ is a Gaussian white noise. The Laplacian term is related to surface tension, v is the velocity of the interface at zero slope and the non-linear term is the lowest order term that breakdown the up-down symmetry ($h(x,t) \to -h(x,t)$) [20, 95]. We expect that a nonequilibrium stationary state of a KPZ interface is characterized by v and λ. Since a nonequilibrium stationary state has a positive entropy production, we would like to study how the entropy production is a function of v and λ. We will work with a microscopic model in the KPZ universality class, the restricted solid on solid (RSOS) model, which was used in the context of nonequilibrium wetting in chapter 4. The reason for this choice is that the RSOS model has a rich phase diagram and we can perform analytical calculations (exact and approximative). Also, we shall see that within the RSOS model entropy and height are quantities that are closed related, and we will study the large deviation function associated with the height in order to see if it has a symmetry like the fluctuation relation (5.8). Another point we look at, using numerical simulations of the RSOS model, is finite-size (of the time interval) effects for the asymptotic fluctuation relation (5.8).

In the following section we present a discussion about the entropy production. After that, we prove the fluctuation relations (5.7) and (5.8) in Sec. 5.3. In Sec. 5.4 we define the RSOS model and the quantities we want to calculate. Sec. 5.5 contains analytical calculations of the average entropy production in the stationary state, in order to analyze how it is a function of v and λ. The asymptotic fluctuation relation for a KPZ interface is discussed in Sec. 5.6. We conclude in Sec. 5.7. None of these new results have been published so far.

5.2 Entropy production

We are considering continuos time Markov processes with reversible transition rates(if $w_{C\to C'}\neq 0$ then $w_{C'\to C}\neq 0$), which is a sufficient condition to guarantee ergodicity. Therefore we have a unique stationary state solution $P(C)=\lim_{t\to\infty}P(C,t)$. According to (5.3) the stationary state probability distribution obeys

$$\sum_{C'\neq C}\Big(P(C')w_{C'\to C}-P(C)w_{C\to C'}\Big)=0. \tag{5.10}$$

Defining the probability current

$$K_{C'\to C}(t) = w_{C'\to C}P(C',t) - w_{C\to C'}P(C,t), \tag{5.11}$$

we find that in the stationary state the sum of all currents following to and leaving a state adds up to zero:

$$\sum_{C'\neq C} K_{C'\to C} = 0. \tag{5.12}$$

If the transition rates are such that detailed balance holds, then all $K_{C'\to C} = 0$ and the stationary probability distribution is the equilibrium probability distribution $P^{eq}(C)$. Otherwise, if we have a nonequilibrium stationary state, $K_{C\to C'}$ may be non-zero. Zia and Schmittmann [162] postulated that a nonequilibrium stationary state can be characterized by the stationary state probability distribution $P(C)$ and the stationary state probability current $K_{C\to C'}$, in the following sense. The term $W_{C\to C'} = w_{C\to C'}P(C)$ can be divided into a symmetric and an antisymmetric part, that is:

$$W_{C\to C'} = W^a_{C\to C'} + W^s_{C\to C'}, \tag{5.13}$$

where $W^a_{C\to C'} = (W_{C\to C'} - W_{C'\to C})/2$ and $W^s_{C\to C'} = (W_{C\to C'} + W_{C'\to C})/2$. In this way the probability current becomes,

$$K_{C\to C'} = 2W^a_{C\to C'}. \tag{5.14}$$

Therefore, since a nonequilibrium stationary state is characterized by $P(C)$ and $K_{C\to C'}$, by varying the transition rates in such a way that only the symmetric term $W^s_{C\to C'}$ changes, the nonequilibrium stationary state remains the same. Note that from the fact that $W_{C\to C'}$ is positive, the symmetric part has to fulfill the relation

$$W^s_{C\to C'} \geq \frac{1}{2}K_{C\to C'}. \tag{5.15}$$

From (5.6) the entropy production of the system can be written as

$$\dot{s}_{sys} = \frac{1}{2}\sum_{C,C'} K_{C\to C'}(t)\ln\frac{P(C,t)}{P(C',t)}. \tag{5.16}$$

Writing this expression in the form

$$\dot{s}_{sys} = \frac{1}{2}\sum_{C,C'} K_{C\to C'}(t)\ln P(C,t) - \frac{1}{2}\sum_{C,C'} K_{C\to C'}(t)\ln P(C',t), \tag{5.17}$$

one immediately sees from (5.12) that the entropy production of the system is zero in the stationary state ($\dot{s}_m = \dot{s}_{tot}$). From (5.5) and (5.6), the total entropy production is given by

$$\dot{s}_{tot}(t) = \frac{1}{2}\sum_{C,C'} K_{C\to C'}(t)\ln\frac{W_{C\to C'}}{W_{C'\to C}}. \tag{5.18}$$

From this last equation and the definition of $K_{C\to C'}$ (5.11), it becomes apparent that the total entropy production is always positive. When detailed balance is fulfilled the total entropy production in the stationary state is zero and it is otherwise (when we have a nonequilibrium stationary state) positive, therefore, we expect that it can somehow quantifies how far a nonequilibrium stationary state is from equilibrium. From(5.13) and (5.18), the total entropy production in the stationary state can be written as

$$\dot{s}_{tot} = \frac{1}{2}\sum_{C,C'} K_{C\to C'}\ln\frac{W^s_{C\to C'} + W^a_{C\to C'}}{W^s_{C'\to C} + W^a_{C'\to C}}. \tag{5.19}$$

Therefore, by varying the transition rates such that only $W^s_{C\to C'}$ is varied, we see that the same nonequilibrium stationary state can have different values of $\dot{s}_{tot}$. Moreover, different stationary states may have the same entropy production.

5.3 Fluctuation relations

In this section we prove the finite time (5.7) and the asymptotic (5.8) fluctuation relations, mainly following [157]. Below we obtain two fundamental results that we use to derive them.

A time-integrated current is defined by

$$J = \sum_{k=1}^{N} \theta_{C_{k-1}\to C_k}, \tag{5.20}$$

where $\theta_{C\to C'} = -\theta_{C'\to C}$. As in the introduction we consider a stochastic path that starts at C_0 at time T_0, jumps from $C_{k-1} \to C_k$ at time τ_k until a state C_N is reached and stays at C_N, at least, until time T. Note that the time interval $\Delta T = T - T_0$ is fixed while the number of jumps N may be different for different realizations. J is a random variable that depends on the specific stochastic path. Let us introduce the joint probability $P_J(C,T)$ of being at a state C at time T with time-integrate current J. The Laplace transform of it is

$$\tilde{P}_s(C,T) = \sum_J P_J(C,T)\exp(-sJ). \tag{5.21}$$

From the master equation (5.3), follows

$$\begin{aligned}
&\frac{d}{dT}\tilde{P}_s(C,T) = \\
&= \sum_{C'}\sum_J P_{J-\theta_{C'\to C}}(C',T) w_{C'\to C}\exp[-s(J-\theta_{C'\to C}] - \tilde{P}_s(C,T)\sum_{C'} w_{C\to C'} \\
&= \sum_{C'}\sum_J P_J(C',T)\exp(-sJ)\exp(-s\theta_{C'\to C}) w_{C'\to C} - \tilde{P}_s(C,T)\sum_{C'} w_{C\to C'} \\
&= -\sum_{C'} \tilde{H}_{CC'}(s)\tilde{P}_s(C',T) \qquad (5.22)
\end{aligned}$$

where

$$\begin{aligned}
\tilde{H}_{CC'}(s) = -w_{C'\to C}\exp(-s\theta_{C'\to C}) \qquad & \text{if } C \neq C' \\
= \sum_{C''} w_{C\to C''} \qquad & \text{if } C = C' \qquad (5.23)
\end{aligned}$$

Note that the time evolution matrix $\tilde{H}(s)$ is not a stochastic matrix, meaning that the sum of all elements in a column is not zero.

In the quantum-hamiltonian formalism the master equation (5.3) is written in the from

$$\frac{d}{dt}|P(t)\rangle = -H|P(t)\rangle, \tag{5.24}$$

where $|P(t)\rangle = \sum_C P(C,t)|C\rangle$ and $|C\rangle$ is a basis vector corresponding to the state C. The element CC' of the matrix H is given by $H_{CC'} = -w_{C'\to C}$ if

$C \neq C'$ and $H_{CC} = \sum_{C'' \neq C} w_{C'' \to C}$. In this formalism the average of some observable $B(t)$ reads

$$\langle B(t) \rangle = \langle 1 | B(t) | P(t) \rangle \tag{5.25}$$

where $\langle 1 | = \sum_C \langle C |$. In addition, the solution of equation (5.24) is formally written as $|P(t)\rangle = \exp(-Ht)|P_0\rangle$. With the quantum-hamiltonian formalism and the fact that the time evolution operator for $\tilde{P}_s(C,T)$ is (5.23), the generating function of the time integrated current can be written in the form

$$\langle \exp(-sJ) \rangle = \langle 1 | \exp(-\tilde{H}(s)\Delta T) | P(T_0) \rangle. \tag{5.26}$$

Since the time-integrated current is zero at T_0, we have $|\tilde{P}_s(T_0)\rangle = |P(T_0)\rangle$. Relation (5.26) is the first fundamental result to prove the fluctuation relations (5.7) and (5.8).

The elements CC', with $C \neq C'$, of the transposed matrix $\tilde{H}^T(s)$ are given by

$$\tilde{H}^T_{CC'}(s) = -w_{C \to C'} \exp(-s\theta_{C \to C'}). \tag{5.27}$$

If $\theta_{C \to C'} = \ln(w_{C \to C'}/w_{C' \to C})$ we have

$$\tilde{H}^T_{CC'}(s) = -w_{C' \to C} \exp(-(1-s)\theta_{C' \to C}) = \tilde{H}(1-s)_{CC'}. \tag{5.28}$$

Since the diagonal elements are independent of s, it follows that, for $\theta_{C \to C'} = \ln(w_{C \to C'}/w_{C' \to C})$,

$$\tilde{H}^T(s) = \tilde{H}(1-s), \tag{5.29}$$

which is the second fundamental result. Note that for $\theta_{C \to C'} = \ln(w_{C \to C'}/w_{C' \to C})$ the current J is just ΔS_m

5.3.1 Finite time fluctuation relation

We now consider a stochastic process such that the transition rates depend on time. We also consider forward and backward rates that are related by

$$w^B_{C \to C'}(t) = w^F_{C \to C'}(T-t). \tag{5.30}$$

We consider that the forward process starts with the probability distribution $P(C,T_0)$ and has the transition rates $w^F(t)$, while the backward process starts with the probability distribution $P(C,T)$ and has the backward transition rates $w^B(t)$. We are interested in the following (trajectory dependent) functional

$$R = \ln\left(\frac{P(C_0,T_0)}{P(C_N,T)}\prod_{i=1}^{N}\frac{w^F_{C_{i-1}\to C_i}(\tau_i)}{w^F_{C_i\to C_{i-1}}(\tau_i)}\right). \tag{5.31}$$

Note that the above functional is a sum of a time-integrated current term and a boundary term, which is the logarithm of $P(C_0,T_0)/P(C_N,T)$. Using relation (5.30), it can be written in the form

$$R = \ln\left(\frac{P(C_0,T_0)w_{C_0\to C_1}(\tau_1)w_{C_1\to C_2}(\tau_2)...w_{C_{N-1}\to C_N}(\tau_N)}{P(C_N,T)w_{C_{N-1}\to C_N}(T-\tau_N)...w_{C_2\to C_1}(T-\tau_2)w_{C_1\to C_0}(T-\tau_1)}\right). \tag{5.32}$$

Now the interpretation of R is clear: It is the logarithm of the probability of realizing the trajectory $C_0 \to C_1 \to ... \to C_N$ in the forward process divided by the probability of the inverse trajectory in the backward process. If one considers the backward process the same functional is given by

$$R = \ln\left(\frac{\sum_{i=1}^{N} w^B_{C_{i-1}\to C_i}(\tau_i)P(C_N,T)}{\sum_{i=1}^{N} w^B_{C_i\to C_{i-1}}(\tau_i)P(C_0,T_0)}\right). \tag{5.33}$$

The fluctuation relations will arise from a relation between the generating function of R in the backward and in the forward processes.

From (5.26) we have

$$\begin{aligned}\langle\exp(-sR)\rangle_F &= \langle 1|P_T^s\exp\left(\sum_{i=1}^{N}\tilde{H}(s,\tau_i)\right)P_{T_0}^{-s}|P(T_0)\rangle\\ &= \langle P(T_0)|P_{T_0}^{-s}\exp\left(\sum_{i=1}^{N}\tilde{H}^T(s,T-\tau_i)\right)P_T^s|1\rangle,\end{aligned} \tag{5.34}$$

where the subscript F (B) stands for forward (backward) and P_T is a diagonal matrix with elements $P(C,T)$. Note that since the transition rates depend on time, the term $\exp(-\tilde{H}(s)\Delta T)$ in (5.26) is modified to $\exp(\sum_{i=1}^{N}\tilde{H}(s,\tau_i))$.

Using (5.29) we obtain

$$\begin{aligned}\langle \exp(-sR)\rangle_F &= \langle P(T_0)|P_{T_0}^{-s} \exp\left(\sum_{i=1}^{N} \tilde{H}(1-s, T-\tau_i)\right) P_T^{s}|1\rangle \\ &= \langle 1|P_{T_0}^{(1-s)} \exp\left(\sum_{i=1}^{N} \tilde{H}(1-s, T-\tau_i)\right) P_T^{-(1-s)}|P(T)\rangle. \qquad (5.35)\end{aligned}$$

The last equality shows that

$$\langle \exp(-sR)\rangle_F = \langle \exp(-(1-s)R)\rangle_B. \qquad (5.36)$$

From this relation one can derive several fluctuation relations, e. g., the Jarzynski [163] and Crooks [164] relations (see [157]). Denoting by $P_F(R = X)$ ($P_B(R = X)$) the probability that the functional R has the value X in the forward (backward) process, relation (5.36) can be written in the form

$$\sum_X P_F(R = X)\exp(-sX) = \sum_X P_B(R = X)\exp(-(1-s)X). \qquad (5.37)$$

Since the above relation has to be true for all s, we can conclude

$$\frac{P_B(R = -X)}{P_F(R = X)} = \exp(-X). \qquad (5.38)$$

Considering time independent transition rates and choosing T_0 such that the system has already reached the stationary state ($P(C, T_0) = P(C, T) = P(C)$) the last relation becomes the finite time fluctuation relation (5.7).

5.3.2 Asymptotic fluctuation relation

In the expression for the total entropy one can see that the medium entropy $\sum_{k=1}^{N} \ln(w_{C_{k-1}\to C_k}/w_{C_k\to C_{k-1}})$ is a time-integrated current and the system entropy $\ln[P(C, T_0)/P(C, T)]$ is the boundary term. Therefore, the medium entropy grows linearly with ΔT, while the system entropy remains the same as ΔT is increased. Naively, one expects the boundary term to become irrelevant in the limit $\Delta T \to \infty$ and, therefore, the asymptotic fluctuation relation (5.8) should hold. In order for this to be true the number of states

C has to be finite. Heuristically, if the number of states is infinite, there may be highly improbable states that can generate divergences in the boundary term $\ln[P(C,T_0)/P(C,T)]$, making it relevant also in the limit $\Delta T \to \infty$ (see [157, 165] for a comprehensive discussion). In the following we prove the asymptotic fluctuation relation (5.8) in a more precise way.

We consider the time-averaged current $j = J/\Delta T$ and denote by $P(j = x)$ the probability that $j = x$. The large deviation function $I(x)$, associated to this probability distribution is defined by [161]

$$I(x) = -\lim_{\Delta T \to \infty} \frac{1}{\Delta T} \ln P(j = x). \tag{5.39}$$

One can show that the function

$$\hat{I}(s) = -\lim_{\Delta T \to \infty} \frac{1}{\Delta T} \ln\langle \exp(-Js)\rangle, \tag{5.40}$$

is the Legendre transform of the large deviation function, i.e.,

$$I(x) = \max_s \{\hat{I}(s) - sx\}. \tag{5.41}$$

From (5.26), the generating function can be written in form

$$\begin{aligned} \langle \exp(-sJ)\rangle &= \sum_i \langle 1|\phi_i\rangle\langle\phi_i|P(T_0)\rangle \exp(-\epsilon_i(s)\Delta T) \\ &\approx \langle 1|\phi_0\rangle\langle\phi_0|P(T_0)\rangle \exp(-\epsilon_0(s)\Delta T), \end{aligned} \tag{5.42}$$

where $\epsilon_i(s)$ and $|\phi_i\rangle$ are the eigenvalues and eigenvectors of $\tilde{H}(s)$. Therefore, from the definition of $\hat{I}(s)$ (5.40), we conclude: the function $\hat{I}(s)$ is given by the lowest eigenvalue $\epsilon_0(s)$. In this part enters the fact that the number of states has to be finite; if we have an infinite state space the identification of the function $\hat{I}$ with the lowest eigenvalue may not be valid [165]. We consider a time-integrated current J of the form (5.20), such that it is possible to find a quantity E defined by

$$w_{C\to C'} = w^{eq}_{C\to C'} \exp(E\theta_{C\to C'}/2), \tag{5.43}$$

where $w^{eq}_{C\to C'}$ are the equilibrium transition rates. Combining $P^{eq}(C)w^{eq}_{C\to C'} = P^{eq}(C')w^{eq}_{C'\to C}$ and (5.29) yelds

$$\tilde{H}^T(s) = P_{eq}^{-1}\tilde{H}(E-s)P_{eq}, \tag{5.44}$$

where P_{eq} is a diagonal matrix with element $P^{eq}(C)$. Because of the last relation the eigenvalues of $\tilde{H}(s)$ and $\tilde{H}(E-s)$ are identical. Therefore, assuming (5.42) to be valid,

$$\hat{I}(s) = \hat{I}(E-s). \tag{5.45}$$

Since $\hat{I}(s)$ is the Legendre transform of the large deviation function $I(x)$ equation (5.41) implies that

$$I(x) - I(-x) = Ex. \tag{5.46}$$

This is a bit more general than the asymptotic fluctuation relation (5.7), that corresponds to $E = 1$.

5.4 The RSOS model

The microscopic realization of the KPZ equation we consider in this chapter is the RSOS model, which is defined as follows. To each site i of a one-dimensional discrete lattice of size L a random variable h_i is attached. This random variable can take any integer value and it is interpreted as the interface height at site i. The possible interface configurations are such that

$$h_{i+1} - h_i = 0, \pm 1, \tag{5.47}$$

where we assume periodic boundary condition, i.e. $h_{L+1} = h_1$. This is called the RSOS restriction and it creates an effective surface tension. The model evolves by random sequential updates in the following way. A site i is randomly chosen and a particle can be deposited or evaporated with rates that depend on the heights of site i and it's nearest neighbors. Defining the variable $u = h_{i-1} + h_{i+1} - 2h_i$, the possible microscopic transitions together with their respective rates are [117]:

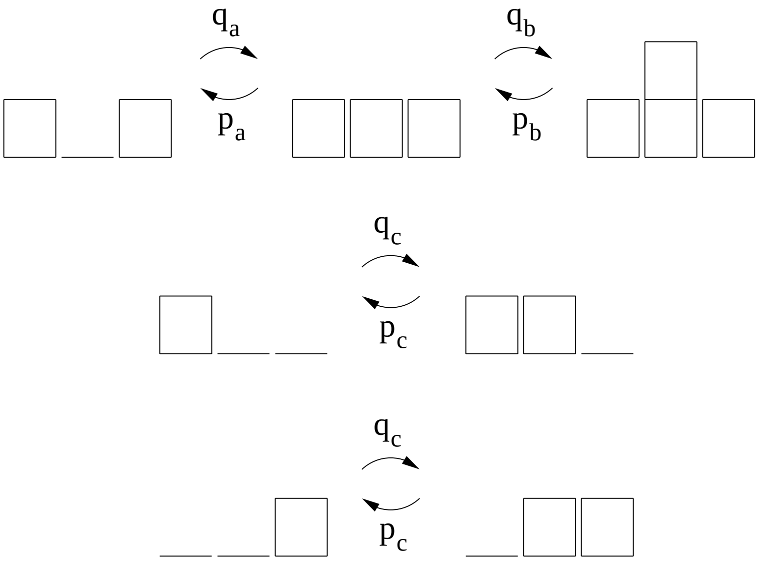

Figure 5.1: Deposition and evaporation rates for the RSOS model.

(a) if $u = 0$ deposition with rate q_b and evaporation with rate p_a,

(b) if $u = -2$ deposition with rate q_a ,

(c) if $u = 2$ evaporation with rate p_b,

(d) if $u = -1$ deposition with rate q_c,

(e) if $u = 1$ evaporation with rate p_c.

where deposition (evaporation) means $h_i \to h_i + 1$ ($h_i \to h_i - 1$). Note that u commonly take the values $u = 0, \pm 1, \pm 2$ because of the RSOS restriction. The transition rules are represented in Fig. 5.1. We had already introduced the RSOS model in chapter 4 in the study of nonequilibrium wetting. The difference between the model considered in chapter 4 and the present RSOS model is the presence of a hard-wall at zero height. In what follows we will be dealing with the medium entropy exclusively. Therefore, we will refer to it as entropy, dropping the subscript m.

Considering the limit $L \to \infty$ and assuming translational invariance the time evolution of the one-site height probability distribution $P(h_i, t)$ can be written as

$$\frac{d}{dt}P(h_i,t)=\sum_{l=\pm1}\Big(w_l(h_{i-1},h_i-l,h_{i+1})P(h_{i-1},h_i-l,h_{i+1},t)$$
$$-w_l(h_{i-1},h_i,h_{i+1})P(h_{i-1},h_i,h_{i+1},t)\Big), \qquad (5.48)$$

where the transition rates $w_n(h_{i-1},h_i,h_{i+1})$ are given above (for example $w_+(h,h-1,h)=q_a$ and $w_-(h,h+1,h)=p_b$). Two quantities we want to calculate are the velocity of the interface v and the ensemble averaged entropy production, that from now on we denote by $\dot{s}$ without the brackets. Using (5.48), they can be written in the following forms:

$$v(t)=\frac{d}{dt}\langle h_i\rangle=\sum_{h_i}h_i\frac{d}{dt}P(h_i,t)$$
$$=\sum_{h_{i-1},h_i,h_{i+1}}\sum_{l=\pm1}lw_l(h_{i-1},h_i,h_{i+1})P(h_{i-1},h_i,h_{i+1},t) \qquad (5.49)$$

and, using (5.5),

$$\dot{s}(t)=\sum_{h_{i-1},h_i,h_{i+1}}\sum_{l=\pm1}\ln\left(\frac{w_l(h_{i-1},h_i,h_{i+1})}{w_{-l}(h_{i-1},h_i-l,h_{i+1})}\right)w_l(h_{i-1},h_i,h_{i+1})P(h_{i-1},h_i,h_{i+1},t), \qquad (5.50)$$

The RSOS model can be viewed as model of charges $\sigma_i=h_{i+1}-h_i$ jumping on a lattice. In terms of these variables the transition rates of the RSOS model are:

$$\begin{aligned}
-+ &\rightarrow 00 && \text{with rate } q_a\\
00 &\rightarrow -+ && \text{with rate } p_a\\
00 &\rightarrow +- && \text{with rate } q_b\\
+- &\rightarrow 00 && \text{with rate } p_b.\\
0+ &\rightarrow +0 && \text{with rate } q_c\\
+0 &\rightarrow 0+ && \text{with rate } p_c\\
-0 &\rightarrow 0- && \text{with rate } q_c\\
0- &\rightarrow -0 && \text{with rate } p_c.
\end{aligned} \qquad (5.51)$$

This description in terms of charges is very convenient for the calculations that we shall perform. The velocity and the entropy production in the stationary state, in terms of the charges variables, are written in the form

$$v = (q_b - p_a)\langle 00\rangle + q_a\langle -+\rangle - p_b\langle +-\rangle + q_c(\langle 0+\rangle + \langle -0\rangle) - p_c(\langle +0\rangle + \langle 0-\rangle), \tag{5.52}$$

and

$$\begin{aligned} \dot{s} = (q_b \ln \frac{q_b}{p_b} - p_a \ln \frac{q_a}{p_a})\langle 00\rangle + q_a \ln \frac{q_a}{p_a}\langle -+\rangle - p_b \ln \frac{q_b}{p_b}\langle +-\rangle \\ +q_c \ln \frac{q_c}{p_c}(\langle 0+\rangle + \langle -0\rangle) - p_c \ln \frac{q_c}{p_c}(\langle +0\rangle + \langle 0-\rangle), \end{aligned} \tag{5.53}$$

where $\langle \sigma\sigma'\rangle$ is the density of the pair $\sigma\sigma'$ at nearest neighbor sites in the stationary state. The above formulas can be derived from (5.49) and (5.50). They are easily obtained from the transition rules (5.51).

The interface slope m is defined by

$$m = \sum_{i=1}^{L} \sigma_i. \tag{5.54}$$

Since we consider periodic boundary conditions the total number of positive charges is equal to the number of negative charges in any configuration and, therefore $m = 0$. One way of introducing a non-zero interface slope in the RSOS model is to change the RSOS restriction between sites L and 1 so that $h_L - h_1 = M, M\pm 1$. In this case the interface slope is given by $m = M/(L-1)$. It can be shown that the λ term in the KPZ equation can be defined for a microscopic model. It is related to how the velocity depends on the interface slope in the following way [20],

$$v(m) = v + (\lambda/2)m^2. \tag{5.55}$$

One can show that detailed balance is fulfilled for the RSOS model only if $q_a/p_a = q_b/p_b = q_c/p_c = C$, where C is a constant [117]. In this case v and λ are equal to zero. Otherwise, at least one of the two quantities are non-zero. Therefore we suppose that a nonequilibrium stationary state is characterized by v and λ, this means that it is characterized by the interface velocity and by how the velocity depends on the interface slope. In the next section we calculate the entropy production, the velocity and the parameter λ defined above. We are interested in investigating how the entropy production is a function of these two quantities. From the discussion in Sec. 5.2 we expect it to increase as the absolute values of v and λ increase, as we go away from the detailed balance condition. We note that there is meaning in talking about the RSOS model stationary state if one is considering quantities that become time-independent in the long time limit, like v and λ. Other relevant observables like the interface width are not stationary, but they are not under consideration here.

Another important quantity, used in the calculations below, is the density of charges, which is given by

$$\rho = \sum_{i=1}^{L} \sigma_i^2. \tag{5.56}$$

From the transition rules (5.51) we see that the time evolution of the density of charges is given by

$$\frac{d}{dt}\rho(t) = (q_b + p_a)\langle 00\rangle - q_a\langle -+\rangle - p_b\langle +-\rangle. \tag{5.57}$$

As we show next, in the limit $L \to \infty$, it is possible to find the density of charges in the stationary state ρ and then calculate v, λ and $\dot{s}$.

5.5 Calculation of the entropy production

5.5.1 Solving the RSOS model

Here we describe the method, introduced by Neergaard and den Nijs [117], to solve the RSOS model. It is the same method used in 4.3.4 to calculate the interface velocity in the RSOS model. The description here is more complete and we also calculate other quantities. First we assume that the probability of a certain configuration in the stationary state depends on two variables: the total number of charges (divided by two for later convenience)

$$N = \sum_j \sigma_j^2/2 \tag{5.58}$$

and on the electrostatic energy

$$E = \sum_j j\sigma_j. \tag{5.59}$$

With this ansatz the (unnormalized) probability of a state can be written in the simple form

$$f(N,E) = x^N y^E, \tag{5.60}$$

where $x \leq 1$ and $y \leq 1$. From the transition rules (5.51) the master equation is given by,

$$\begin{aligned}
&n_{+-}[q_b f(N-1,E+1) - p_b f(N,E)] + n_{-+}[p_a f(N-1,E-1) - q_a f(N,E)] \\
&+ n_{00}[q_a f(N+1,E+1) + p_b f(N+1,E-1) - (q_b+p_a) f(N,E)] \\
&+ (n_{0-} + n_{+0})[q_c f(N,E-1) - p_c f(N,E)] \\
&+ (n_{-0} + n_{0+})[p_c f(N,E+1) - q_c f(N,E)] = 0
\end{aligned} \tag{5.61}$$

where $n_{\sigma\sigma'}$ is the probability of finding a pair $\sigma\sigma'$ of nearest neighbors sites in a configuration with N charges and electrostatic energy E. Using the relation $n_\sigma = \sum_{\sigma'} n_{\sigma\sigma'}$ for $\sigma = 1$ and $\sigma = -1$, where $n_\sigma = N/L$ if $\sigma = \pm 1$ and $n_\sigma = 1 - 2N/L$ if $\sigma = 0$, one arrives at the equation

$$n_{0-} + n_{+0} + 2n_{+-} = n_{-0} + n_{0+} + 2n_{-+}. \tag{5.62}$$

With this constraint there are four independent variables in equation (5.61), namely n_{00}, n_{+-}, $n{-+}$ and $(n_{0-} + n_{+0} + 2n_{+-})$. Hence, equation (5.61) is satisfied only if all the coefficients multiplying these variables are equal to zero. From the term multiplying $(n_{0-} + n_{+0} + 2n_{+-})$ we get the condition

$$(q_c - p_c y^{-1})(1-y) = 0. \tag{5.63}$$

The first solution of this equation is $y = q_c/p_c$, which, with the other constraints, leads to the fulfillment of detailed balance (see [117]). The interesting case corresponds to $y = 1$, where the lattice configurations become independent of the electrostatic energy, depending only on the total number of charges. Within this solution, the coefficient in front of n_{00} gives

$$x = \frac{q_b + p_a}{q_a + p_b}. \tag{5.64}$$

On the other hand the coefficients of n_{+-} and n_{-+} lead to the same relation, namely

$$q_c - p_c = \frac{q_b q_a - p_a p_b}{2(q_b + p_a)}. \tag{5.65}$$

Therefore, in the region of the phase space where the constraint (5.65) is satisfied the probability of a configuration with M charges in system of size L in the stationary state is given by

$$P(N) = Z_{N,L}^{-1} x^N \tag{5.66}$$

where

$$Z_{N,L} = \sum_{N=0}^{L/2} \frac{L!}{N!N!(L-2N)!} x^N \tag{5.67}$$

is the partition function and x is given by (5.64). In the large L limit the sum in (5.67) is dominated by its maximum and the density of charges is given by

$$\rho = \frac{2}{2 + x^{-1/2}}. \tag{5.68}$$

From (5.66), we also have

$$\langle \sigma\sigma' \rangle = \langle \sigma \rangle \langle \sigma' \rangle + o(1/L), \tag{5.69}$$

and, therefore, in the limit $L \to \infty$ the term $\langle \sigma\sigma' \rangle$ factorizes.

In the case of non-zero interface slope we have

$$\langle + \rangle = \frac{\rho + m}{2} \tag{5.70}$$

and

$$\langle - \rangle = \frac{\rho - m}{2}. \tag{5.71}$$

From these two equations and supposing that $\langle \sigma\sigma' \rangle$ factorizes we obtain: from (5.52),

$$v(m) = (q_b - p_a)(1 - \rho(m))^2 + \frac{1}{4}(q_a - p_b)(\rho(m)^2 - m^2) + (q_c - p_c)(1 - \rho(m))\rho(m); \tag{5.72}$$

from (5.57),

$$(q_b + p_a)(1 - \rho(m))^2 - \frac{1}{4}(q_a + p_b)(\rho(m)^2 - m^2) = 0. \tag{5.73}$$

The last equation implies

$$m^{-1}\frac{d}{dm}\rho(m) = [\rho + 4\frac{(q_b + p_a)}{q_a + p_b}(1 - \rho)]^{-1}. \tag{5.74}$$

Note that the function $m^{-1}\frac{d}{dm}\rho(m)$ at $m = 0$ becomes just $x^{-1/2}/2$, where x is given by (5.64). From (5.55) we get $\lambda = m^{-1}\frac{d}{dm}v(m)$ at $m = 0$. This relation combined with equations (5.72) and (5.74) gives

$$\lambda = \frac{x^{-1/2}}{4}[(q_a - p_b)\rho - 4(q_b - p_a)(1 - \rho) + 2(q_c - p_c)(1 - 2\rho)] - \frac{(q_a - p_b)}{2} \tag{5.75}$$

One can obtain the same expression for λ by deriving the deterministic part of the KPZ equation for the RSOS model [117]. Finally, from (5.53), with $m = 0$ the entropy production is given by

$$\dot{s} = (q_a \ln\frac{q_a}{p_a} - p_b \ln\frac{q_b}{p_b})\frac{\rho^2}{4} + (q_b \ln\frac{q_b}{p_b} - p_a \ln\frac{q_a}{p_a})(1 - \rho)^2 + (q_c - p_c)\ln\frac{q_c}{p_c}\rho(1 - \rho) \tag{5.76}$$

Hence, we have obtained the quantities v, $\dot{s}$ and λ as a function of the density of charges in the stationary state ρ, assuming factorization of $\langle \sigma\sigma' \rangle$. As we showed, this is the case if (5.65) holds and in the limit $L \to \infty$, where the density of charges is given by (5.68). Next we present the exact results.

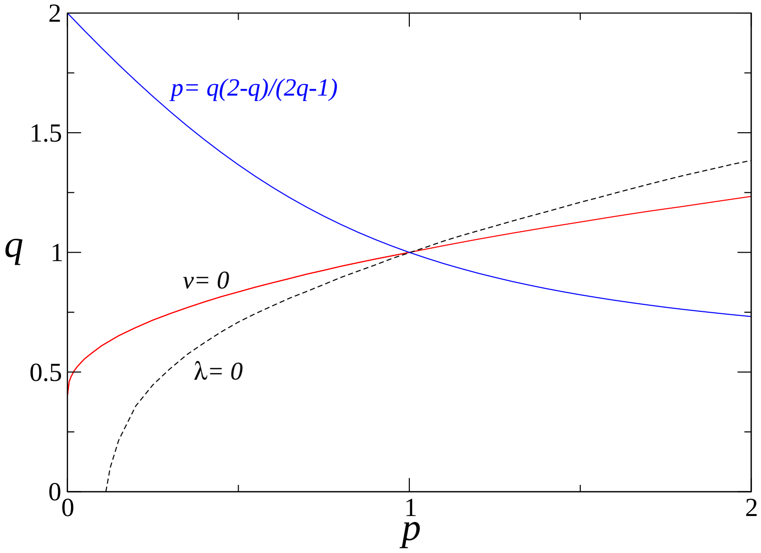

Figure 5.2: Phase diagram of the RSOS model, obtained from numerical simulations

5.5.2 Exact results

In order to work with a smaller number of control parameters we now consider a more specific version of the RSOS model where [100]

$$q_a = q_b = q_c = q \qquad p_a = p \qquad p_b = p_c = 1. \tag{5.77}$$

Unless stated explicitly, we will consider these transition rates throughout the whole chapter. In Fig. 5.2 we show the phase diagram of this model obtained from simulations. We show the lines $v = 0$ and $\lambda = 0$, note that these lines cross at $q = 1$ and $p = 1$, where detailed balance holds.

From equation (5.65), we see that the method we have in hands applies only along the line $p = q(2-q)/(2q-1)$ shown in Fig. 5.2. On this line, at $q = 1$ we have equilibrium and we expect the entropy production to be zero at $q = 1$ and grow as q increases (decreases) for $q > 1$ ($q < 1$). Using (5.68) the density of charges in the stationary state is

$$\rho = \frac{2}{2 + \sqrt{(2q-1)/q}}. \tag{5.78}$$

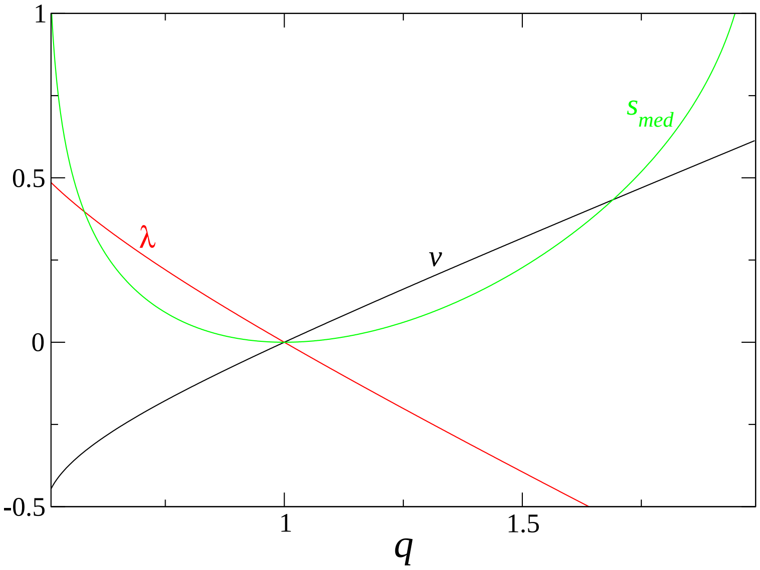

Figure 5.3: The quantities v, λ and $\dot{s}$ as a function of q, given by equations (5.79), (5.80) and (5.81), respectively. Note that the entropy production grows with the distance from equilibrium ($q = 1$).

With this equation and from (5.72), (5.75) and (5.76), the velocity, λ and the entropy production are given by

$$v = (q-1)\rho, \tag{5.79}$$

$$\lambda = -(q-1)\frac{\rho}{4q(1-\rho)}[1 + 6q - \rho(2q+1)], \tag{5.80}$$

and

$$\dot{s} = (q-1)\left(\frac{\rho^2}{2}\ln\frac{2q-1}{2-q} + \frac{\rho}{2}(2-\rho)\ln q\right). \tag{5.81}$$

In Fig 5.3 we plot the three quantities as a function of q. We see that the entropy production is always positive and it grows as the distance from the equilibrium point $q = 1$ increases. The velocity and λ have opposite sings and as their absolute values increase as the entropy production increases. This is in agreement with the idea that the entropy production gives a measure of how far the system is from equilibrium.

5.5.3 Approximative results

In order to access the whole phase diagram $q \times p$ we use the following approximation. We assume the method, that applies only in the case $p = q(2-q)/(2q-1)$, to be valid everywhere. That is, we assume that the probability distribution of a configuration is determined only by its total number of charges. Within this approximation from (5.64) and (5.68) we obtain, in the limit $L \to \infty$,

$$\rho = 2/(2 + x^{-1/2}), \tag{5.82}$$

with

$$x = (q + p)/(q + 1). \tag{5.83}$$

We can calculate v, λ and $\dot{s}$ in the same way as we did before, i.e., using (5.72), (5.75) and (5.76). This is like a mean field approximation that assumes the probability distribution of charges to be simple factorized (as we showed this is directly related to the fact that the probability distribution of a state depends only on ρ), and it is equivalent to an approximation that supposes that the distribution of heights is pair-factorized [13] (see previous chapter).

Within this approximation we first find the lines $v = 0$ and $\lambda = 0$. The root of the equation $v = 0$ is

$$p = -q + q^2 + q^3. \tag{5.84}$$

Furthermore the roots of the equation $\lambda = 0$, are

$$p = (-3 - q + 5q^2 + q^3 \pm \sqrt{5 + 10q - 9q^2 - 20q^3 + 3q^4 + 10q^5 + q^6})/8. \tag{5.85}$$

For $p > 1$ ($p < 1$) the root with physical meaning is the one with the plus (minus) sign. In Fig. 5.4 we show the lines $v = 0$ and $\lambda = 0$. As one can see they have the same concavity, in comparison to the lines obtained with simulations (Fig. 5.2) and, as expected since we did an approximation, they do not coincide with the lines obtained from simulations. If we fix p the entropy production has a minimum at a certain value of q. In Fig. 5.4

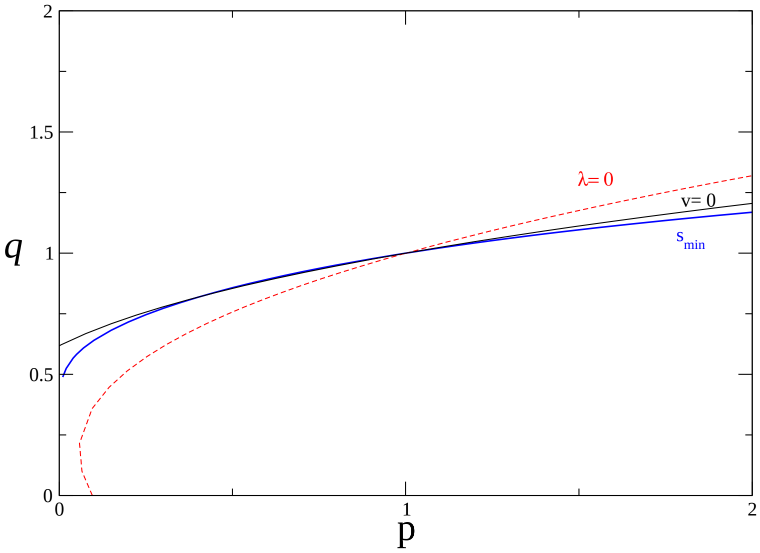

Figure 5.4: Approximated phase diagram. We show the lines $v = 0$, $\lambda = 0$ and the line corresponding to the minimum of the entropy production, denoted by $\dot{s}_{min}$, obtained with the mean field approximation. $v = 0$ is given by (5.84), $\lambda = 0$ is given by (5.85)and the line $\dot{s}_{min}$ is obtained numerically.

we also plot the line where the entropy production is minimum, we do not have an analytical expression for this line. The minimum of the entropy production does not coincide with the line $v = 0$, nevertheless, it is near it. Therefore, the entropy production strongly depends on v and it also depends on λ. With simulations the same situation is obtained. This approximation provides a very good qualitative picture.

In principle we can find q and p as functions of v and λ and then obtain $\dot{s}$ as a function of v and λ. However, in general, a analytical expression cannot be found. An exception is the $v = 0$ line, where we can find the entropy production as a function of λ in the following way. From (5.75), (5.82) and (5.83), at the $v = 0$ line ($p = -q + q^2 + q^3$), we find

$$\lambda = (q - 1)/q. \tag{5.86}$$

Note that for large q we have $\lambda \to 1$ and, therefore, on this line $\lambda < 1$.There is also a lower bound, corresponding to $(p = 0, q = (\sqrt{5}-1)/2)$, where $\lambda = -(\sqrt{5}-1)/2 \approx -0.618$. Finally, from (5.76) we have

$$\dot{s} = -\frac{\lambda}{(\lambda-3)^2}\ln\left(\frac{(\lambda-1)^3}{\lambda^2-\lambda-1}\right). \tag{5.87}$$

where the above relation is valid for $-(\sqrt{5}-1)/2 < \lambda < 1$. As expected, the entropy production is zero at $\lambda = 0$ and grows as the absolute value of λ grows. The distance from equilibrium increases as we go away from $q = 1$, therefore it is reasonable that for $q \to 0$ and $q \to \infty$ the entropy production diverges. It is clear that this is the case by considering the upper and lower bonds of λ discussed above.

Summarizing, our calculations show that the entropy production is a function of v and λ, the parameters that characterize the nonequilibrium stationary state of a KPZ interface. The results are all in agreement with the idea that the entropy production gives a measure of the distance from equilibrium, since it increases as we go away from the equilibrium point. As we shall see next, the way how the entropy production varies with v and λ depends on the microscopic model under consideration.

5.5.4 Different transition rates

We now consider the model defined by the parameters $q_a = wA$, $p_a = A$, $q_b = wB$, $p_b = B$, $q_c = w$ and $p_c = 1$. We choose $A = 2Bw/(B(1+w)-2)$ so that equation (5.65) is satisfied and, therefore exact results can be obtained. The positivity of the transition rates requires $B > 2/(1+w)$. With these transition rates the entropy production is just $\dot{s} = v\ln w$. Proceeding in the same way as we did above we can calculate v and λ. In this case the lines $\lambda = 0$ and $v = 0$ coincide and are given by $w = 1$. It is possible to vary w and B in such way that the velocity is kept fixed while λ varies . Since $\dot{s} = v\ln w$, this shows that in the present case the entropy production is independent of λ. Therefore, the way how $\dot{s}$ depends on v and λ is not robust in the sense that it depends on the specific transition rates we choose. Considering the discussion presented in the end of Sec. 5.2, where we showed that the same nonequilibrium stationary state can have different values of entropy production and that different nonequilibrium stationary states can have the same value of entropy production, this non-robustness is not surprising.

5.6 Fluctuation relation for a KPZ interface

5.6.1 Finite size effects on the asymptotic fluctuation relation

Here we test numerically how the asymptotic fluctuation relation (5.8) is obeyed for finite ΔT. In Fig. 5.5 we plot the function

$$f(X) = \ln \frac{P(\Delta S_m = X)}{P(\Delta S_m = -X)} \tag{5.88}$$

for the usual RSOS model and also for a different version of it, where $|h_i - h_{i-1}| \leq 5$ for different values of ΔT. Note that in the second case there is a bigger number of states. What can be seen in Fig. 5.5 is that finite size (of the time interval) effects become stronger when the number of states is bigger. This can be explained in the following way. With a bigger number of states the rare states will have a very low probability making the term $\ln(P(C,T_0) - P(C,T))$ (the system entropy) more relevant. We chose a small system size $L = 16$ for the simulations because for smaller systems the fluctuations in the entropy are stronger and, therefore, one has access to a lager interval in X. Note that in the limit $L \to \infty$ the entropy becomes a macroscopic quantity making the fluctuation relation meaningless.

In [166] a correction to the relation (5.8) for finite times was proposed, where $f(X) = X$ for small enough values of X and then it saturates at $2\langle \Delta S_m \rangle$. This finite size correction was also found to hold for other models in [167]. Therefore it is of interest to know by which systems it is obeyed.

In order to see stronger finite size effects we consider a bound KPZ interface that has an infinite number of states. If one forbids evaporation in

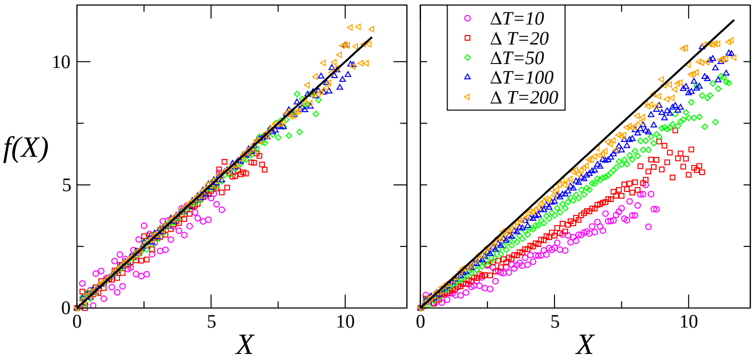

Figure 5.5: Asymptotic fluctuation relation for the RSOS model. We plot the function $f(X)$, defined in (5.88), for the usual RSOS model, on the right, and, on the left, a RSOS model where the difference of two neighbors heights is less or equal to five. The system size is $L = 16$ and the transition rates are $(p = 0.5, q = 0.8)$

the RSOS model at the layer $h_i = 0$ we have a RSOS model with a wall and the following happens. If the parameters q and p are such that the velocity is positive after some transient the interface grows with the same velocity as if the wall was not present. Otherwise, if the velocity is negative, the interface stays bounded fluctuating close to the wall. In this case a new type of physical behavior arises (see previous chapter), but we are not interested in that here, we are just interested in testing the asymptotic fluctuation relation (5.8). There is an infinite number of states, because the mapping onto a charge problem cannot be made anymore. One has to know where is the zero height, at which evaporation is forbidden. In Fig. 5.6 we can see that the finite size effects in this case are much stronger and the saturation value of $f(X)$ is in agreement with $2\langle\Delta S_m\rangle$.

5.6.2 Fluctuation relations for the height

For $p = 1$ the entropy is just the height multiplied by $\ln q$. Therefore, in the line $p = 1$, the large deviation function associated to the probability

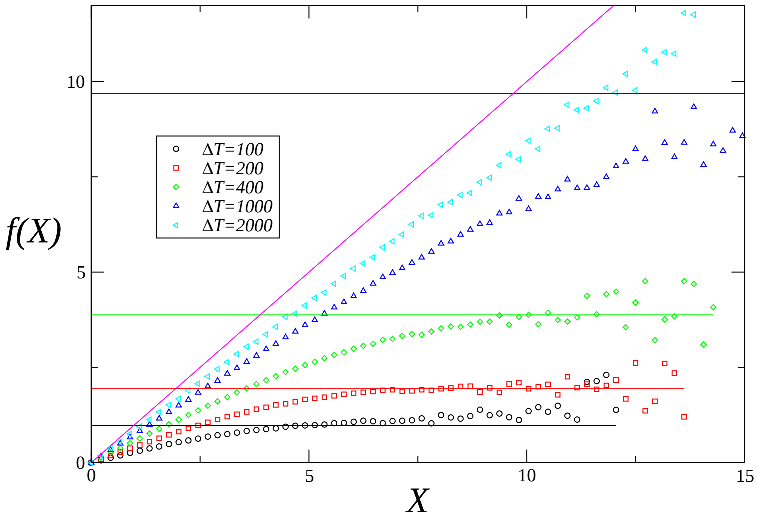

Figure 5.6: Asymptotic fluctuation relation for the RSOS model with a wall. In this case evaporation at the bottom layer is forbidden and the number of states is infinite (see text). The horizontal lines represent the value $2\langle\Delta S_m\rangle$, and they are in good agreement with the saturation values on $f(X)$, defined in (5.88). Also, the system size is $L = 16$ and the transition rates are $(p = 0.5, q = 0.8)$

distribution of the height variation has the symmetry (5.46), with $E = \ln q$. On the other hand, for $p \neq 1$ we cannot find an E satisfying (5.43). Therefore, we do not know if the large deviation function of the height variation having the symmetry (5.46) is a general feature of KPZ interfaces or if it holds only when very specific transition rates are chosen (the line $p = 1$ in the present case). If two time-integrated currents are considered a relation more general than (5.46) can be found [157, 168]. In the following we show this fluctuation relation and apply it to the RSOS model.

We consider two time-integrated currents, $J^{(1)} = \sum_{k=1}^{N} \theta^{(1)}_{C_{k-1}\to C_k}$ and $J^{(2)} = \sum_{k=1}^{N} \theta^{(2)}_{C_{k-1}\to C_k}$. If one can find quantities E_1 and E_2 such that

$$\frac{w_{C\to C'}}{w_{C'\to C}} = \frac{w^{eq}_{C\to C'}}{w^{eq}_{C'\to C}} \exp(E^{(1)}\theta^{(1)}_{C\to C'} + E^{(2)}\theta^{(2)}_{C\to C'}), \tag{5.89}$$

then similarly to (5.44) we have

$$\tilde{H}^T(s_1, s_2) = P_{eq}^{-1}\tilde{H}(E_1 - s_1, E_2 - s_2)P_{eq}, \tag{5.90}$$

where the non-diagonal terms are given by

$$\tilde{H}(s_1.s_2)_{C'C} = -w_{C\to C'} \exp(-s_1\theta^{(1)}_{C\to C'} - s_1\theta^{(2)}_{C\to C'}). \tag{5.91}$$

In the same way we obtained (5.46), the last equation implies

$$I(x, y) - I(-x, -y) = E^{(1)}x + E^{(2)}y, \tag{5.92}$$

where

$$I(x, y) = -\lim_{\Delta T\to\infty} \frac{1}{\Delta T} P(j^{(1)} = x, j^{(2)} = y). \tag{5.93}$$

As it will become clear later when applying the above result to the RSOS model, this relation for the joint probability distributions is valid for more time-integrated currents.

The time-integrated currents ΔH_q and ΔH_{qp} are defined in the following way. During a simulation, if a deposition event occurs, such that the evaporation of the newly deposited particles would take place with rate

1 (p), then $\Delta H_q \to \Delta H_q + 1$ ($\Delta H_{qp} \to \Delta H_{qp} + 1$). If an evaporation event occurs, such that it takes place at rate 1 (p), then $\Delta H_q \to \Delta H_q - 1$ ($\Delta H_{qp} \to \Delta H_{qp} - 1$). Therefore we find that $\Delta H = \Delta H_q + \Delta H_{qp}$ and $\Delta S_m = \ln(q)\Delta H_q + \ln(q/p)\Delta H_{qp}$. Using all these time-integrated currents, fluctuation relations including the height as one of the two currents can be found. From (5.92) we have:

$$\begin{aligned} \ln\left(\frac{P(\Delta H = X, \Delta H_q = Y)}{P(\Delta H = -X, \Delta H_q = -Y)}\right) &= X\ln q - Y\ln p, \\ \ln\left(\frac{P(\Delta H = X, \Delta H_{qp} = Y)}{P(\Delta H = -X, \Delta H_{qp} = -Y)}\right) &= X\ln\frac{q}{p} + Y\ln p. \end{aligned} \tag{5.94}$$

The height appears explicitly in these relations and they are valid in the entire phase diagram. Therefore, it is possible to find fluctuation relations for the height if a second time-integrated current is considered. A fluctuation relation including only the height is very desirable, since the height is a quantity that can be measured experimentally (unlike ΔH_q, ΔH_{qp} and ΔS_m).

5.6.3 Small systems

In order to obtain information about the large deviation function associated with the probability distribution of the variation of height we consider a system with three sites and calculate its Legendre transform explicitly. Because of the periodic boundary conditions and the conservation of the total charge, in a three-site system, there are seven possible states. They are: 1) 000; 2) $0+-$; 3) $-0+$; 4) $+-0$; 5) $0-+$; 6) $+0-$; 7) $-+0$. Using this labeling of states, the matrix $-\tilde{H}(s)$, defined in (5.23), is given by

$$\begin{pmatrix} -3(q+p) & \mathrm{e}^{s} & \mathrm{e}^{s} & \mathrm{e}^{s} & q\mathrm{e}^{-s} & q\mathrm{e}^{-s} & q\mathrm{e}^{-s} \\ q\mathrm{e}^{-s} & -2q-1 & 0 & 0 & 0 & \mathrm{e}^{s} & \mathrm{e}^{s} \\ q\mathrm{e}^{-s} & 0 & -2q-1 & 0 & \mathrm{e}^{s} & 0 & \mathrm{e}^{s} \\ q\mathrm{e}^{-s} & 0 & 0 & -2q-1 & \mathrm{e}^{s} & \mathrm{e}^{s} & 0 \\ p\mathrm{e}^{s} & 0 & q\mathrm{e}^{-s} & q\mathrm{e}^{-s} & -2-q & 0 & 0 \\ p\mathrm{e}^{s} & q\mathrm{e}^{-s} & 0 & q\mathrm{e}^{-s} & 0 & -2-q & 0 \\ p\mathrm{e}^{s} & q\mathrm{e}^{-s} & q\mathrm{e}^{-s} & 0 & 0 & 0 & -2-q \end{pmatrix} \tag{5.95}$$

As we showed, (5.40) and (5.42) imply that the Legendre transform of the large deviation function $\hat{I}(s)$ is given by the minimum eigenvalue of the matrix $\tilde{H}(s)$. Analogously to (5.44), one can show that

$$\tilde{H}^{T}(s) = P^{-1}\tilde{H}(E-s)P, \tag{5.96}$$

where $E = \frac{3\ln q - \ln p}{3}$ and P is a diagonal matrix with the elements $P_{1,1} = 1$, $P_{2,2} = P_{3,3} = P_{4,4} = p^{1/3}$ and $P_{5,5} = P_{6,6} = P_{7,7} = p^{2/3}$. Therefore, for the three-site system we find that

$$\hat{I}(s) = \hat{I}(\frac{3\ln q - \ln p}{3} - s). \tag{5.97}$$

The large deviation function (and its Legendre transform) associated to the height variation is symmetric. The explicit form of $\hat{I}(s)$ can be obtained by doing some algebra. Making the translation $s \to s + \frac{3\ln q - \ln p}{6}$ the maximum of $\hat{I}(s)$ is placed at $s = 0$ and $\hat{I}(s)$ is given by,

$$\begin{aligned} \hat{I}(s) = 2q + p + 1 - 18^{-1/3}\Big(-9f(s) + 3^{1/2}\sqrt{-4B^{3} + 27(f(s))^{2}}\Big)^{1/3} \\ -\frac{2^{1/3}}{3^{1/3}}B\Big(-9f(s) + 3^{1/2}\sqrt{-4B^{3} + 27(f(s))^{2}}\Big)^{-1/3} \end{aligned} \tag{5.98}$$

where $A = (p-1)(2p^{2} + (q-1)q + p(6q-1))$, $B = 1 + 3(p-1)p + 5q + 6pq + q^{2}$ and $f(s) = A - 12q^{3/2}p^{1/2}\cosh(3s)$.

In a system with four sites there are nineteen states, therefore in order to calculate $\hat{I}(s)$ one has to find the minimum eigenvalue of 19×19 matrix. We cannot find $\hat{I}(s)$ explicitly in this case. Moreover, for $L = 4$ it is not possible to find a diagonal matrix P such that $\tilde{H}^T(s) = P^{-1}\tilde{H}(E - s)P$. This would imply that all eigenvalues $\epsilon(s)$ of the matrix have the symmetry $\epsilon(s) = \epsilon(E - s)$, but by calculating them numerically we see that this is not the case. We can calculate the minimum eigenvalue numerically and it turns out that it is symmetric. Nevertheless, the value of E, such that $\hat{I}(s) = \hat{I}(E - s)$ differs from $\frac{3\ln q - \ln p}{3}$, which was found for $L = 3$. For example, at $q = p = 1/2$ for $L = 3$ we have $E = 2\ln(2)/3 \approx 0.462$ and for $L = 4$ we have $E \approx 0.474$.

The Legendre transform of the large deviation function (of the current of particles) divided by the system size L was found to be extensive in the simple symmetric exclusion process [169]. In Fig. 5.7 we plot $\hat{I}(s)/L$ for the cases $L = 3, 4, 5, 6$, at $q = p = 1/2$. In this plot we changed the variable s so that the maximum of $\hat{I}(s)$ is at $s = 0$, that is, $s \to s + E/2$. Surprisingly, the centered $\hat{I}(s)/L$ looks extensive with system size, although the values of E are different for different values of L.

5.7 Conclusion

In this chapter we have studied the entropy production and fluctuation relations for the RSOS model, which is in the KPZ universality class. We calculated the entropy production, the velocity and λ in a line of the two-dimensional phase diagram of the RSOS model exactly. Assuming that the nonequilibrium stationary state of the RSOS model is characterized by v and λ, such that the distance from equilibrium ($\lambda = 0$ and $v = 0$) increases as the modulus of these quantities increase our calculations are in agreement with the idea that the entropy production gives a measure of the distance from equilibrium.

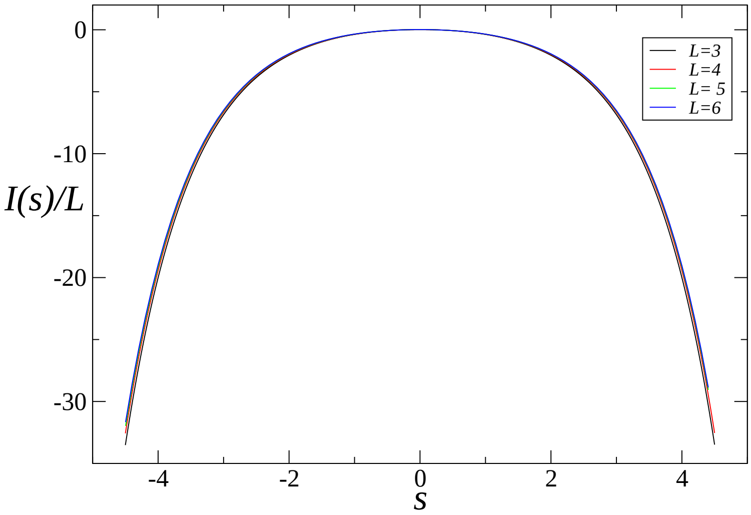

Figure 5.7: The centered Legendre transform (see text) of the large deviation function associated with the variation of height $\hat{I}(s)$ for the RSOS model with $L = 3$ and $L = 4$. The deposition and evaporation rates are $q = p = 1/2$

The exact solution we applied works only along the line $p = 2(2-q)/(2q-1)$. In order to obtain analytical results for the entire phase diagram we considered a mean field approximation. Using this approximation we obtained analytical expressions for the lines $v = 0$ and $\lambda = 0$. Although they do not coincide with the lines coming from simulations they are very close and the curvature of the lines is the same. Furthermore, we calculated the entropy production as a function of λ at the line $v = 0$, it was found that $\dot{s}$ grows as we go away from $\lambda = 0$, again in agreement with the idea that the entropy production gives a measure of the distance form citicality.

While v and λ (the way the interface velocity depends on the interface slope) are physically meaningful quantities, in the sense that they could be measure in an experiment this is not the case for the entropy production $\dot{s}$. Albeit we were able to obtain how $\dot{s}$ varies with v and λ we showed that the way the entropy production is a function of these quantities is not robust, depending on the specific microscopic model one is dealing with.

We studied finite size effects in the asymptotic fluctuation relation (5.8) using the RSOS model. We showed that the finite size effects become stronger as the number of states is increased and, in addition, that the saturation values of $f(X)$ defined in (5.88), is at $2\langle\Delta S_m\rangle$ in agreement with [166, 167]. We also obtained fluctuation relations for the height considering a second time-integrated current.

Considering very small systems we calculated the Legendre transform of the large deviation function associated to the height. As we showed a fluctuation relation for the height holds only when $p = 1$, because in this case the height is just the entropy multiplied by a constant, namely $\ln q$. For $p \neq 1$ the large deviation function associated to the height probability distribution is still symmetric but the value of E ($\hat{I}(s) = \hat{I}(E - s)$) varies with system size.

Finally, we would like to point out that the fluctuation relation is very general, in the sense that it is valid for any Markov process such that if $w_{C\to C'} \neq 0$ then $w_{C'\to C} \neq 0$. On the other hand, it is also very specific in the sense that it is valid only for the entropy (or a constant multiplying it). In the present example we showed that there is no fluctuation relation for the height.

Chapter 6

Conclusion and perspectives

In this thesis we have investigated various fundamental aspects of nonequilibrium statistical physics such as phase transitions and the role of fluctuations, as well as possible applications. To this end we have focused on specific topics, namely, pulsed laser deposition, boundary induced phase transitions into an absorbing state, nonequilibrium wetting, entropy production as well as fluctuation relations. In the following we summarize our main results and point out some perspectives of future work.

Concerning pulsed laser deposition, we have analyzed rate equations and the anomalous scaling of the nucleation density. First we considered a simple set of rate equations, where the islands are treated as point-like objects. The equations were solved exactly in the limit of strong and temporally separate pulses. Since this approximation does not take the fractal dimension of the islands into account it was not possible to faithfully reproduce the crossover from MBE to PLD. This problem was overcome with a second improved set of rate equations which accounts for the dimension of the islands by incorporating their fractality in an effective way. Moreover, we showed that these improved equations lead to results which are in excellent agreement with simulations. Revisiting a previously introduced concept of logarithmic scaling of the nucleation density we observed small violations in the corresponding data collapses for intermediate coverages with a systematic drift, indicating that logarithmic scaling may be a good approximation for pulse intensities in computer simulations and experiments but probably it is not asymptotically valid in the limit $I \to 0$. As an alternative suggestion, we have proposed that the nucleation density, for a fixed value of the coverage, varies with I as a power law and that the exponent varies with the coverage. This suggestion is supported by numerical simulations and leads to numerical results which are more accurate than the data collapses obtained on the basis of logarithmic scaling.

The model for pulsed laser deposition considered here does not take transient mobility of adatoms into account, and we think that this is a severe deficiency. Transient mobility was shown to have great influence in the growth kinetics [26, 27, 28], and it is one of the reasons leading to a better layer by layer growth of PLD when compared to MBE. It would be interesting to propose a model suitable for Monte Carlo simulations that incorporates transient mobility. This could be done as follows. First, as shown in [26, 28], one has to change how islands of different sizes compete for the monomers in an appropriate way. In the model for PLD studied here this can be achieved by changing the way how sites are chosen during the deposition of a pulse. As a second essential ingredient the model has to incorporate a process for the dissociation of monomers from small islands, since, as shown in [28], for pulsed deposition coarsening occurs mainly trough an Ostwald ripening mechanism.

As a second main result of this thesis we introduced a new universality class of nonequilibrium phase transitions into an absorbing state in chapter 3. It is probably the simplest universality class of phase transition into an absorbing state because the transition is generated by the special dynamics of only a single site at the boundary. It was shown that the model corresponds to a zero-dimensional limit of DP with Lévy flights in time and some of the critical exponents can be determined exactly using field theoretical methods.

By relating this model to a $0+1$-dimensional non-Markovian process we also showed that in nonequilibrium systems with temporal long-range interactions a phase transition can take place even in zero dimensions.

A nice aspect of this new universality class is its simple field theory. The parameter κ, which controls the non-locality in time, plays a similar role as the dimension in the field theory for DP, since for $\kappa < \kappa_c = 1/3$ mean field behavior sets in. Unlike the dimension, κ can be varied continuously in a simulation, allowing us to approach the mean field level continuously. Therefore, it would be interesting to perform an ϵ-expansion to two-loop order and to obtain the critical exponents using non-perturbative renormalization group approach methods and then compare the results with the exponents obtained from numerical simulations.

Another critical phenomenon induced by the presence of a surface occurs in nonequilibrium growth process on an inert substrate, referred to as nonequilibrium wetting. In this framework nonequilibrium wetting is described by the KPZ equation with a potential that accounts for a wall. In the same way as the KPZ equation represents a robust universality class of nonequilibrium growing free interfaces, the so-called bound KPZ (bKPZ) equation is expected to represent a robust universality class of nonequilibrium growing interfaces in the presence of wall. In chapter 4 we demonstrate the very rich phenomenology of the bKPZ equation and investigate several microscopic models in the bKPZ universality class. We would like to mention that recently the critical exponents of the bKPZ– universality class in two dimensions have been obtained with numerical simulations in [170]. This is important because it is likely that an experimental realization of nonequilibrium wetting will take place on a two-dimensional system. In fact, in what we defined here as nonequilibrium wetting, the main challenge is to observe the predicted critical behavior experimentally.

From a more fundamental perspective, we studied entropy production and fluctuation relations in chapter 5. Studying KPZ type growth with the

RSOS model we were able to characterize the distance from equilibrium by calculating the interface velocity and its dependence on the interface tilt. We calculated the entropy production exactly along a specific line of the phase diagram and with a mean field approximation in the whole phase diagram. With both methods we confirmed that the entropy production grows with the distance from equilibrium. In some cases, we could also obtain the entropy production as a function of v and λ, which are the physically meaningful quantities. However, as we showed, the formulas are not robust, i.e. they depend on the microscopic model under consideration.

The last part of this thesis was concerned with fluctuation relations. Using again the RSOS model we studied finite size effects in the asymptotic fluctuation relation, obtaining results in agreement with a modified fluctuation relation that takes finite size effects into account. The fluctuation relation is a symmetry in the large deviation function (and its Legendre transform) associated with the variation of entropy during a fixed time interval. Due to a similarity between entropy and height within the RSOS model we investigated the Legendre transform of the large deviation function associated with the variation of height. We derived fluctuation relations for the height by considering the joint probability of two time-integrated currents. Moreover, we calculated the Legendre transform of the large deviation function associated with the height exactly for a three-site model and found that it is symmetric. At $p = 1$, the height is just the entropy multiplied by $\ln(q)$, meaning that the probability distribution of the height variation is constrained through a fluctuation relation. However, for $p \neq 1$ the relation between height and entropy is more complicated and there is no fluctuation relation for the height. Nevertheless, the Legendre transform of the large deviation function is symmetric (and $\hat{I}(s)/L$ seems to be extensive) for $L = 3, 4$, and the position of the maximum (given by $E/2$) was found to vary with the system size. Therefore it is possible that a more general statement about the symmetry of the large deviation function of other time-integrated currents, different from the entropy, exists.

Bibliography

[1] L. D. Landau and E. M. Lifshitz, *Course of Theoretical Physics* (Pergamon Press, New York, 1993), Vol. 5.

[2] R. K. Pathria, *Statistical Mechanics* (Oxford Press, Boston, 1996).

[3] L. D. Landau and E. M. Lifshitz, *Course of Theoretical Physics* (Pergamon Press, New York, 1993), Vol. 1.

[4] W. Feller, *Probability Theory and its Applications* (New York, Wiley, 1968).

[5] R. J. Baxter, *Exactly Solvable Models in Statistical Mechanics* (New York, Academic Press, 1982).

[6] N. G. Van Kampen, *Stochastic Processes in Physics and Chemistry* (Amsterdam, North-Holland, 1981).

[7] C. W. Gardiner, *Handbook of Stochastic Methods* (Berlin, Springer Verlag, 1985).

[8] A. C. Barato, H. Hinrichsen, and D. E. Wolf, Phys. Rev. E **77**, 041607 (2008).

[9] A. C. Barato and H. Hinrichsen, Phys. Rev. Lett. **100**, 165701 (2008).

[10] A. C. Barato and H. Hinrichsen , J. Stat. Mech., P02020 (2009).

[11] A. C. Barato, J. A. Bonachela, C. E. Fiore, H. Hinrichsen, and M. A. Muñoz, Phys. Rev. E **79**, 041130 (2009).

[12] A. C. Barato, J. Stat. Phys. **138**, 728 (2010).

[13] A. C. Barato and M. J. de Oliveira, J. Phys. A **40**, 8205 (2007).

[14] A. C. Barato, H. Hinrichsen, M. J. de Oliveira, Phys. Rev. E **77**, 011101 (2008).

[15] D. B. Chrisey and G. K. Hubler, *Pulsed Laser Deposition of Thin Films* (John Wiley, New York, 1994).

[16] J. Shen, Z. Gai, and J. Kirschner, Surf. Sci. Rep. **52**, 163 (2004).

[17] T. A. Witten and L. M. Sander, Phys. Rev. Lett. **47**, 1400 (1981).

[18] P. Meakin, in *Phase Transitions and Critical Phenomena*, edited by C. Domb and J.L. Lebowitz (Academic Press, London, 1986), Vol. 12, p. 335.

[19] L. Tang, J. Phys. (Paris) I **3**, 935 (1993).

[20] A.-L. Barabási and H. E. Stanley, *Fractal Concepts in Surface Growth* (Cambridge Univ. Press, Cambridge-UK, 1995).

[21] B. Hinnemann, H. Hinrichsen, and D. E. Wolf, Phys. Rev. Lett. **87**, 135701 (2001); B. Hinnemann, H. Hinrichsen, and D. E. Wolf, Phys. Rev. E **67**, 011602 (2003).

[22] H. Brune, Surf. Sci. Rep. **31**, 121 (1998).

[23] P. Jensen and B. Niemeyer, Surf. Sci. **384**, L823 (1997); N. Combe, and P. Jensen, Phys. Rev. B **57**, 15553 (1998).

[24] P. M. Lam, S. J. Liu, and C. H. Woo, Phys. Rev. B **66**, 045408 (2002).

[25] S. B. Lee, Phys. Rev. E **67**, 012601 (2003).

[26] E. Vasco, New J. Phys. **8**, 253 (2006).

[27] E. Vasco and J. L. Sacedon, Phys. Rev. Lett. **98**, 036104 (2007).

[28] E. Vasco, C. Polop, and J. L. Sacedon, Phys. Rev. Lett. **100**, 016102 (2008).

[29] J.A. Venables, Philos. Mag. **27**, 697 (1973); J.A. Venables, G.D.T. Spiller and M. Hanbücken, Rep. Prog. Phys. **47**, 399 (1984).

[30] G. S. Bales, and D. C. Chrzan, Phys. Rev. B **50**, 6057 (1994).

[31] L. Sittler and H. Hinrichsen, J. Phys. A **35**, 10 531 (2002).

[32] J. G. Amar, F. Family, and P. M. Lam, Phys. Rev. B **50**, 8781 (1994).

[33] G. Ehrlich and F. G. Hudda, J. Chem. Phys. **44**, 1039 (1966).

[34] R. L. Schwoebel and E. J. Shipsey, J. Appl. Phys. **37**, 3682 (1966).

[35] M. Strikovski and J. H. Miller, Appl. Phys. Lett. **73**, 1733 (1998).

[36] E. Vasco and C. Zaldo, J. Phys. Condens. Matter **16**, 8201 (2004).

[37] N. V. Brillianov and P. L. Krapivsky, J. Phys. A **24**, 4787 (1991).

[38] P. L. Krapivsky, private communication (2008).

[39] P. Meakin, A. Coniglio, H. E. Stanley, and T. A. Witten, Phys. Rev. A **34**, 3325 (1986).

[40] L. P. Kadanoff, S. R. Nagel, L. Wu, and S. M. Zhou, Phys. Rev. A **39**, 6524 (1989).

[41] C. Tebaldi, M. De Menech, and A. L. Stella, Phys. Rev. Lett. **83**, 3952 (1999).

[42] X-Z. Wu, L. P. Kadanoff, A. Libchaber, and M. Sano, Phys. Rev. Lett. **64**, 2140 (1990).

[43] M. Henkel and G. M. Schütz, Physica A **206**, 187 (1994).

[44] J. Krug, Phys. Rev. Lett. **67**, 1882 (1991).

[45] G. M. Schütz, in *Phase Transitions and Critical Phenomena*, edited by C. Domb and J. L. Lebowitz, (Academic Press, New York, 2000), Vol. 19.

[46] V. Popkov, L. Santen, A. Schadschneider, and G. M. Schütz, J. Phys. A: Math. Gen. **34**, L45 (2001).

[47] B. Derrida, M. R. Evans, V. Hakim, and V. Pasquier, J. Phys. A: Math. Gen. **26**, 1493 (1993).

[48] H. Hinrichsen, Adv. Phys. **49**, 815 (2000).

[49] G. Ódor, Rev. Mod. Phys. **76**, 663 (2004); *Universality in nonequilibrium lattice systems*, (Wrold Scientific, Singapore, 2008).

[50] S. Lübeck, Int. J. Mod. Phys. B **18**, 3977 (2004).

[51] K. A. Takeuchi, M. Kuroda, H. Chaté, and M. Sano, Phys. Rev. Lett. **99**, 234503 (2007); Phys. Rev. E **80**, 051116 (2009).

[52] J. Marro and R. Dickman, *Nonequilibrium phase transitions in lattice models* (Cambridge University Press, Cambridge, UK, 1999).

[53] C. Kaiser and L. Turban, J. Phys. A: Math. Gen. **27**, L579 (1994).

[54] C. Kaiser and L. Turban, J. Phys. A: Math. Gen. **28**, 351 (1995).

[55] H. Hinrichsen and H. M. Koduvely, Eur. Phys. J. B **5**, 257 (1998).

[56] P. Fröjdh , M. Howard, and K. Lauritsen, J. Phys. A **31**, 2311 (1998).

[57] P. Fröjdh , M. Howard, and K. Lauritsen, Int. J. Mod. Phys. **B15**, 1761 (2001).

[58] O. Deloubrière and F. van Wijland, Phys. Rev. E. **65**, 046104 (2002).

[59] S. R. Broadbent and J. M. Hammersley, Proc. Cambridge Phil. Soc. **53**, 629 (1957).

[60] D. Stauffer and A. Aharony, *Introduction to Percolation Theory* (Taylor and Francis, London, 1992).

[61] Fisher, M. E., and J. W. Essam, J. Math. Phys. **2**, 609 (1961).

[62] T. Tomé e M.J. de Oliveira, *Dinâmica Estocástica e Irreversibilidade*, (Edusp, São Paulo, 2001).

[63] H.-K. Janssen, Z. Phys. B, **23** 377 (1976); Z. Phys. B, **42** 151 (1981).

[64] P. Grassberger, Z. Phys. B **47**, 365 (1982).

[65] T. E. Harris, Ann. Probab. **2**, 969 (1974).

[66] F. van Wijland, Phys. Rev. E. **63**, 022101 (2001).

[67] M. Doi, J. Phys. A: Math. Gen. **9**, 1465 (1976).

[68] L. Peliti, J. Phys. **46**, 1469 (1985).

[69] U. C. Täuber, M. Howard, and B. P. Vollmayr-Lee, J. Phys. A: Math. Gen. **38**, 79 (2005).

[70] P. A. Martin and F. Rothen, *Many-body Problems and Quantum Field Theory* (Springer, Heidelberg, 2004).

[71] M. Moshe, Phys. Rep. C **37**, 255 (1978).

[72] P. Grassberger and A. de la Torre, Ann. Phys. (New York) **122**, 373 (1979).

[73] G. Huber, M. H. Jensen and K. Sneppen, Phys. Rev. E. **52**, 2133 (1995).

[74] M. A. Muñoz, G. Grinstein and Y. Tu, Phys. Rev. E. **56**, 5101 (1997).

[75] M. E. Fisher, Rev. Mod. Phys. **46**, 597 (1975).

[76] J.J. Binney, N.J. Dowrick, A.J. Fisher, and M.E.J. Newman, *The Theory of Critical Phenomena: An Introduction to the Renormalization Group* (Oxford Science, Oxford, 1995).

[77] H. K. Janssen and U. Täuber, Ann. Phys. NY **315**, 147 (2005).

[78] H. C. Fogedby, Phys. Rev. E. **50**, 1657 (1994).

[79] K. B. Oldham and J. Spanier, *The Fractional Calculus* (Academic Press, New York, 1974).

[80] K.S. Miller and B. Ross, *An Introduction to the Fractional Calculus and Fractional Differential Equations* (John Wiley and Sons, New York, 1993).

[81] A. Vespignani, R. Dickman, M. A. Muñoz, and S. Zapperi, Phys. Rev. E **62**, 4564 (2000). R. Dickman, M. A. Muñoz, A. Vespignani, and S. Zapperi, Braz. J. of Physics **30**, 27 (2000).

[82] H. Taitelbaum, Z. Koza, T. Yanir and G. H. Weiss, Physica A **266**, 280 (1999).

[83] K. E. P. Sugden and M. R. Evans, J. Stat. Mech. (2007) 11013.

[84] F. Baumann, M. Henkel, M. Pleimling, and J. Richert, J. Phys. A **38**, 6623 (2005).

[85] S. Redner,*A guide to first passage Processes* (Cambridge University Press, Cambridge, UK, 2001).

[86] H. Hinrichsen, J. Stat. Mech. (2007) 07066.

[87] J. W. Cahn, J. Chem. Phys. **66**, 3667 (1977).

[88] D. B. Abraham, Phys. Rev. Lett. **44**, 1165 (1980).

[89] J.M.J. van Leeuwen and H.J. Hilhorst, Physica A **107**, 318 (1981).

[90] T. W. Burkhart, J. Phys. A **14**, L63 (1981).

[91] D. B. Abraham and E. R. Smith, J. Stat. Phys. **43**, 621 (1986).

[92] S. Dietrich, in *Phase Transitions and Critical Phenomena*, edited by C. Domb and J.L. Lebowitz (Academic Press, London, 1986), Vol. 12, p. 1.

[93] R. Lipowsky, J. Phys. A **18**, L585 (1985).

[94] S. F. Edwards and D. R. Wilkinson, Proc. R. Soc. London **381**, 17 (1982).

[95] J. Krug, Adv. Phys. **46**, 139 (1997).

[96] M. Kardar, G. Parisi and Y.-C. Zhang, Phys. Rev. Lett **56**, 889 (1986).

[97] P. G. de Gennes, Rev. Mode. Phys. **57**, 827 (1985).

[98] P. G. Sullivan and M.M. Telo da Gama, in *Fluid Interfacial Phenomena*, edited by C.A. Croxton (Wiley, New York, 198).

[99] Y. Tu, G. Grinstein, and M.A. Muñoz, Phys. Rev. Lett. **78**, 274 (1997).

[100] H. Hinrichsen, R. Livi, D. Mukamel, and A. Politi, Phys. Rev. Lett. **79**, 2710 (1997).

[101] M. A. Muñoz and T. Hwa, Europhys. Lett. **41**, 147 (1998).

[102] M. A. Muñoz, in *Advances in Condensed Matter and Statistical Mechanichs*, edited by E. Korutcheva and R. Cuerno (Nova Science, New York, 2004), p. 37.

[103] F. de los Santos and M. M. Telo da Gama, Trends in Stat. Phys. **4**, 61 (2004).

[104] G. Grinstein, M.A. Muñoz, and Y. Tu, Pys. Rev. Lett. **76**, 4376 (1996).

[105] A.S. Pikovsky and J. Kurths, Phys. Rev. E **63**, 898 (1994).

[106] V. Ahlers and A. Pikovsky, Phys. Rev. Lett. **88**, 254101 (2002).

[107] M.A. Muñoz and R. Pastor-Satorras, Phys. Rev. Lett. **90**, 204101 (2003).

[108] T. J. Newman and A. J. Bray, J. Phys. A **29**, 7917 (1996).

[109] H. Hinrichsen, R. Livi, D. Mukamel and A. Politi, Phys. Rev. E **61**, R1032 (2000).

[110] F. Ginelli, V. Ahlers, D. Mukamel, A. Pikovsky, A. Politi and A. Torcini, Phys. Rev. E **68**, 065102 (2003).

[111] F. Ginelli and H. Hinrichsen, J. Phys. A **37**, 11085 (2004).

[112] T. Kissinger, A. Kotowicz, O. Kurz, F. Ginelli, and H. Hinrichsen, J. Stat. Mech.: Theor. Exp., P06002 (2005).

[113] F. Family and T. Vicsek, J. Phys. A **18**, L75 (1985).

[114] F. de los Santos, M.M. Telo da Gama, and M.A. Muñoz, Europhys. Lett. **57**, 803 (2002).

[115] F. de los Santos, M.M. Telo da Gama, and M.A. Muñoz, Phys. Rev. E **67**, 021607 (2003).

[116] H. Hinrichsen, R. Livi, D. Mukamel and A. Politi, Phys. Rev. E **68**, 041606 (2003).

[117] J. Neergaard and M. den Nijs, J. Phys. A **30**, 1935 (1997).

[118] M. E. Fisher, J. Stat. Phys. **34**, 667 (1984).

[119] U. Alon, M. Evans, H. Hinrichsen, and D. Mukamel, Phys. Rev. E **57**, 4997 (1998).

[120] U. Alon, M. Evans, H. Hinrichsen, and D. Mukamel, Phys. Rev. Lett. **76**, 2746 (1996).

[121] H. Hinrichsen, Phys. Rev. E **67**, 16110 (2003).

[122] M. Henkel, H. Hinrichsen, and S. Lübeck, *Nonequilibrium phase transitions*, vol. 1 (Springer, Berlin, Germany, 2008).

[123] I. Dornic, H. Chaté, and M.A. Muñoz, Phys. Rev. Lett. **94**, 100601 (2005).

[124] M.A. Muñoz, F. de los Santos, and A. Achahbar , Braz. J. Phys. **33**, 443 (2003).

[125] O. Al Hammal, F. de los Santos, and M.A. Muñoz, J. Stat. Mech. P10013 (2005).

[126] A. Lipowsky and M. Droz, Phys. Rev. E **68**, 056119 (2003).

[127] H. Hinrichsen, arXiv:cond-mat/0302831, (2003).

[128] M. J. Howard and U. C. Täuber, J. Phys. A **30**, 7721 (1997).

[129] M. Henkel and H. Hinrichsen, J. Phys. A **37**, R117-R159 (2004).

[130] E. Romera, F. de los Santos, O. Al Hammal, and M.A. Muñoz, Phys. Rev. E **76**, 011116 (2008).

[131] F. Ginelli, H. Hinrichsen, R. Livi, D. Mukamel, and A. Politi, Phys. Rev. E **71**, 026121 (2005).

[132] F. Ginelli, H. Hinrichsen, R. Livi, D. Mukamel, and A. Torcini, J. Stat. Mech., P08008 (2006).

[133] H. Hinrichsen, J. Stat. Mech., P07006 (2007).

[134] O. Al Hammal, F. de los Santos, M. A. Muñoz, and M. M. Telo da Gama, Phys. Rev. E **74**, 011121 (2006).

[135] S. Rossner and H. Hinrichsen, Phys. Rev. E **74**, 041607 (2006).

[136] G. Forgacs, J. M. Luck, Th. M. Nieuwehuizen, and H. Orland, J. Stat. Phys. **51**, 29 (1988).

[137] B. Derrida, V. Hakim, and J. Vannimenus, J. Stat. Phys. **66**, 1189 (1992).

[138] D. M. Gangardt and S. K. Nechaev, J. Stat. Phys. **130**, 483 (2008).

[139] M. Prähofer and H. Spohn, Phys. Rev. Lett., **84** 4882 (2000); Physica A **279**, 342 (2000);J. Stat. Phys., **108** 1071 (2002);J. Stat. Phys., **115** 255 (2004).

[140] W. Genovese and M.A. Muñoz, Phys. Rev. E. **60**, 1377 (1999).

[141] T. Birner, K. Lippert, R. Müller, A. Kühnel, and U. Behn, Phys. Rev. E. **65**, 046110 (2002).

[142] M.A. Muñoz, F. Colaiori, and C. Castellano, Phys. Rev. E. **72**, 056102 (2005).

[143] F. de los Santos, E. Romera, O. Al Hammal, and M.A. Muñoz, Phys. Rev. E **75**, 031105 (2007).

[144] L. Giada and M. Marsili, Phys. Rev. E **62**, 6015 (2000).

[145] R. Graham and A. Schenzle, Phys. Rev. A **20**, 1628 (1982).

[146] M.A. Muñoz, Phys. Rev. E. **57**, 1377 (1998).

[147] J. Zinn-Justin, *Quantum Field Theory and Critical Phenomena*, (Oxford Science, Oxford, 1989).

[148] K. J. Wiese, J. Stat. Phys. **93**, 143 (1998).

[149] U. Seifert, Phys. Rev. Lett. **95**, 040602 (2005).

[150] J. Schnakenberg, Rev. Mod. Phys. **48**, 571 (1976).

[151] D. J. Evans, E. G. D. Cohen, and G. P. Morriss, Phys. Rev. Lett. **71**, 2401 (1993).

[152] D. J. Evans and D. J. Searles, Phys. Rev. E **50**, 1645 (1994).

[153] G. Gallavotti and E. G. D. Cohen, Phys. Rev. Lett. **74**, 2694 (1995).

[154] J. Kurchan, J. Phys. A: Math. Gen. **31**, 3719 (1998).

[155] J. L. Lebowitz and H. Spohn, J. Stat. Phys. **95**, 333 (1999).

[156] C. Maes, J. Stat. Phys. **95**, 367 (1999).

[157] R. J. Harris and G. M. Schütz G M, J. Stat. Mech. P07020 (2007).

[158] J. Kurchan, J. Stat. Mech. P07005 (2007)

[159] R. S. Ellis, *Entropy, Large Deviations, and Statistical Mechanics* (Springer, New York, 1985).

[160] F. den Hollander, *Large Deviations* (Field Institute Monographs, Providence, RI, 2000).

[161] H. Touchette, Phys. Rep. **478**, 1-69 (2009).

[162] R. Zia and B. Schmittmann, J. Stat. Mech. P07012 (2007).

[163] C. Jarzynski, Phys. Rev. Lett. **78**, 2690 (1997).

[164] G. E. Crooks, Phys. Rev. E **60**, 2721 (1999).

[165] A. Rákos and R. J. Harris, J. Stat. Mech. P05005 (2008).

[166] R. van Zon and E. G. D. Cohen, Phys. Rev. Lett. **91**, 110601 (2003).

[167] A. Puglisi, L. Rondoni and A. Vulpiani, J. Stat. Mech. P08010 (2006).

[168] C. Maes and K. Netocny, Europhys. Lett. **82**, 30003 (2008).

[169] V. Lecomte and J. Tailleur, J. Stat. Mech. P03004 (2007).

[170] F. Ginelli, M. Cencini, and A. Torcini, J. Stat. Mech. P12018 (2009).